STRUCTURAL ORGANIZATION AND MECHANISMS OF COOPERATIVITY IN THE N-TERMINAL DOMAINS OF THE HUMAN CU-ATPASES

By

Erik S. LeShane

A DISSERTATION

Presented to the Department of Molecular and Medical Genetics
and the Oregon Health & Science University
School of Medicine
in partial fulfillment of
the requirements for the degree of

Doctor of Philosophy

September, 2010

School of Medicine
Oregon Health & Science University

CERTIFICATE OF APPROVAL

This is to certify that the Ph.D. dissertation of

Erik LeShane

has been approved

Dr. Ninian Blackburn/ Chair

Dr. David Farrens

Dr. Ujwal Shinde

Dr. David Koeller

Dr. Svetlana Lutsenko

TABLE OF CONTENTS

List of Figures

Abbreviations

A-Domain – Actuator Domain (for P-Type ATPase)

aa – amino acid

AA – Atomic Absorption

ACN - Acetonitrile

AEBSF - 4-(2-Aminoethyl)benzenesulfonyl fluoride

ALS – Amyotrophic Lateral Sclerosis

ATP – Adenosine Tri-Phosphate

CBP – Chitin Binding Protein

CD – Circular Dichroism

CNS – Central Nervous System

CPM – 7-diethylamino-3-(4'-maleimidylphenyl)-4-methylcoumarin

CSF – Cerebrospinal Fluid

Cu-ATPases – Human copper transporting ATPases ATP7A and ATP7B

DDP - Cisplatin (cis-diamminedichloridoplatinum)

DTT - Dithiothreitol

ER – Endoplasmic Reticulum

ETIC – Endemic Tyrolean Childhood Cirrhosis

EXAFS – Extended X-ray Absorption Fine Structure

GPI - Glycosilphosphatidylinositol

GSH – Glutathione (Reduced)

ICC – Indian Childhood Cirrhosis

ICP-MS - Inductively Coupled Plasma Mass Spectrometry

ICT – Idiopathic Copper Toxicosis

LEC – Long-Evans Cinnamon (rat strain)

MBD – Metal Binding Domain

MBP – Maltose Binding Protein

MBS – Metal Binding Site

MD – Molecular Dynamics

MMTSB – Multiscales Modeling Tools for Structural Biology

Mo - Mottled

MRI – Magentic Resonance Imaging

MS/MS – Tandem Mass Spectrometry

N-ATP7A – N-Terminal Domain of ATP7A

N-ATP7B – N-Terminal Domain of ATP7B

N-Domain – Nucleotide Binding Domain (for P-Type ATPase)

N-Terminal – Amino Terminal

NAMD – Nanoscale Molecular Dynamics (Software package)

NMR – Nuclear Magnetic Resonance

OHS – Occipital Horn Syndrome

P-Domain - Phosphorylation Domain (for P-Type ATPase)

PAGE – Poly-Acrylamide Gel Electrophoresis

PCR – Polymerase Chain Reaction

PDB – Protein Data Bank

RCSB – Research Collaboratory for Structural Biology

RMSD – Root Mean Square Deviation

SDS – Sodium Dodecyl Sulfate

TCEP – Tris-Carboxyethyl Phosphine

TGN – Trans-golgi network

TIP3P – Three-site explicit water model (computational)

TM – Transmembrane segment

TPCK – Tosyl Phenylalanyl Chloromethyl Ketone

Tris - Tris(hydroxymethyl)aminomethane

WT – Wild Type

Acknowledgements

It is true that no scientist works alone, and this work would not be possible without the contributions of numerous individuals. First and foremost, I have to thank my mentor and advisor, Dr. Svetlana Lutsenko, for her support, patience and collaboration throughout my time in graduate school. The members of the Lutsenko lab and metal ion program project grant over the years have served as excellent friends and collaborators.

I also want to acknowledge the members of my dissertation advisory committee, Drs. David Farrens, David Koeller, and Ujwal Shinde, for their help and guidance. In particular, Dr. Shinde has helped us generate countless ideas through his molecular models.

I have to thank my family, especially my parents, as well as the tremendous network of friends who have made this journey enjoyable.

This work has been supported by the NIH Grant R01 DK071865 and the NIH training Grant 5-T32-HL007781.

Abstract

Copper is an essential trace element used as a cofactor by numerous enzymes in the catalysis of electron transfer reactions. The reactivity of copper necessitates strict homeostatic mechanisms to maintain necessary concentrations while also preventing toxicity. The disruption of copper homeostasis can be seen in the severe genetic diseases Menkes Disease and Wilson's Disease. The diseases are caused by mutations in the copper-transporting ATPases ATP7A and ATP7B, respectively. ATP7A and ATP7B are P-Type ATPases that both feature six N-Terminal metal binding domains (MBDs) that sense cytosolic copper concentrations through interactions with the copper chaperone ATOX1 and regulate ATPase activity and localization accordingly. The mechanism by which the N-Termini integrate and relay this information is poorly understood. The research presented here uses biochemical and computational techniques to characterize the organization and roles of the individual MBDs within the N-Terminal domains of the Cu-ATPases.

We present evidence that the N-Terminal MBDs of ATP7B (N-ATP7B) are organized into a close-packed structure that allows for minor structural perturbations, such as copper binding to the CxxC motif of an MBD, to result in significant domain reorganization. This close packing can also be disrupted by the mutation of the CxxC motifs of MBDs 2,3,4 or 6 to AxxA. For MBD2 and MBD3, this mutation is also accompanied by an increased susceptibility of the domain to oxidation. However, when both MBD2 and 3 are mutated in tandem, the domain retains normal redox activity,

suggesting the two MBDs work in concert. In contrast to the AxxA substitutions, when the CxxC of MBD2 is mutated to SxxS, N-ATP7B retains the conformation and reduction state of the wild-type protein, suggesting that hydrogen bonding plays a role in inter-MBD communication. MBD2 has been previously shown to be the primary site of copper transfer from ATOX1. Our data suggests that the organization of the MBDs in the Apo state favors transfer to MBD2, while MBD4 and MBD6 are likely to receive copper as downstream targets.

The chaperone Atox1 transfers copper to N-ATP7A and N-ATP7B through the formation of heterodimers with individual MBDs. We show that ATOX1 is capable of transferring copper to all six MBDs of both N-Terminal domains, but that N-ATP7B can be fully metallated with a significantly lower concentration of Cu-ATOX1. ATOX1 may fully metallate N-ATP7B with repeat exposures at lower concentrations, and shows preferential target MBDs within both N-Termini. N-ATP7A shows reduced mobility upon copper transfer, but unlike N-ATP7B, does not show an altered proteolysis pattern with increased copper bound. These data suggest the two N-Terminal domains have different structural responses to copper binding, with N-ATP7B possessing a degree of cooperativity not seen for N-ATP7A. This cooperativity may be altered by the Wilson's disease causing mutants G85V and G591D, as they both show alterations in the concentration dependence of copper transfer from Cu-ATOX1.

Cooperativity and reorganization are likely to be mediated by the inter-MBD loop regions. These loops contain sequences necessary for inter-domain and inter-protein

interactions that regulate ATPase activity and trafficking. Our data suggests that copper transfer to N-ATP7B triggers a sequential set of conformational changes resulting in differential exposure of key loop residues. This mechanism provides the basis for copper dependent regulation of ATP7B.

Chapter 1

Introduction

I. Copper in Human Physiology: Uses and Physiological Regulation

Copper is an essential trace element required for numerous cellular functions in all organisms. The redox potential of this transition element allows for copper to exist as Cu(I) or Cu(II). This reactivity lends copper to be a cofactor in catalyzing oxidation-reduction reactions. However, the ease with which copper donates or accepts electrons requires copper to be kept under strict homeostatic control in order to prevent unwanted and potentially damaging reactions.

Mammalian metabolic pathways involve numerous copper dependent enzymes. Ceruloplasmin is a copper dependent ferroxidase that facilitates cellular export of iron (1). Ceruloplasmin deficiency can lead to the accumulation of iron deposits in brain, liver and pancreas (2). Cytochrome C Oxidase uses copper as part of the final stages in the electron transport chain (3). Dopamine ß-hydroxlase and tyrosinase use a copper cofactor in the production of catecholamine and melanin, respectively (4, 5). Lysyl oxidase is essential for proper cross-linking of collagen in connective tissue (6), while superoxide dismutase utilizes copper and zinc in the detoxification of free radicals (7).

Dietary or genetic copper deficiency manifests as deficits in these enzymes and their products, resulting in systemic tissue and organ damage. Mice kept on copper deficient diets develop cardiac hypertrophy, leading to heart failure (8, 9). Ruminant animals that graze in copper deficient environs are a risk for lordosis (swayback) (10). In humans, copper deficiency is a rare but serious disorder, most notably in the genetic syndrome

Menkes Disease (11). Patients undergoing gastric bypass surgery are at risk for deficiency, as are individuals who take chronic high-level zinc supplements (12), as both of these treatments greatly decrease systemic copper absorption.

In excess however, copper can be toxic to cells, owing to its ability to induce oxidation of proteins and lipids, as well as facilitate DNA damage. The profound effects of copper overload can be seen in Wilson's disease, which presents with significant tissue damage (13). High cellular copper levels are also common in several neurodegenerative diseases, such as Alzheimer's disease, Parkinson's disease, prion disease and Amyotrophic Lateral Sclerosis (ALS), all of which are plaque-associated neurodegenerative disorders that present with increased deposits of copper (and often other metals such as zinc) in neurons (14, 15).

Adults have a recommended daily intake of 0.9 mg of dietary copper, and typically acquire nearly twice this amount with a balanced western diet (16). Thus, a careful balance must be struck between retaining sufficient copper while simultaneously removing excess. Copper is absorbed in the gastro-intestinal tract, primarily by enterocytes, which then facilitate copper entry into the bloodstream (17). Once there, copper is thought to bind to alpha-2-macroglobulins, histidine, serum albumin, glutathione, or other molecules that allow copper to circulate to other organs (18).

Among the major destinations for dietary copper is the liver, which acts as the central organ for redistribution and removal of excess copper. Hepatocytes produce and secrete

ceruloplasmin back into the bloodstream (19). Each molecule of ceruloplasmin can bind six copper atoms, and this ferroxidase is the major copper-binding protein in the serum (20). Excess copper is removed through excretion into the bile, where it is then discharged from the body via fecal matter (21).

Copper is also excreted through the kidney, as well as the mammary gland in lactating women. Considerably less copper is removed through the urine than the bile (22). However, copper levels in the kidney are quite high (23), suggesting a significant (but currently unknown) role for copper in maintaining renal function. Copper excreted into the milk through the mammary gland is at least partially bound to ceruloplasmin (18). High copper levels in milk underscore its essential role in development.

Copper also plays an essential role in the brain, particularly during development where it plays an essential role in neurite outgrowth (24) and myelination (25). The choroid plexus appears to be the key center for copper redistribution within the brain (26), but the distribution mechanism, as well as the methods of copper transport across the blood-brain and blood-cerebrospinal fluid barriers, is poorly understood. Ceruloplasmin is too large to cross the blood brain barrier requiring the brain to produces its own supply of the molecule (27). However, the ceruloplasmin produced in brain astrocytes is GPI linked (28), and hence unlikely to transport copper between cells or across the blood-CSF barrier. Mice heterozygous for mutations in the plasma membrane copper transporter Ctr1 show significantly lowered levels of copper in the brain (29), suggesting the

involvement of this transporter, but it is not clear how the serum copper carriers would donate copper for this type of transport into the brain.

II. Cellular Physiology of Copper Homeostasis

II-a. Copper Uptake Transporters

Cells require a tightly regulated homeostatic mechanism to maintain adequate cellular copper concentrations while simultaneously preventing toxic levels of accumulation. In yeast, it has been estimated that little to no copper exists as a free cation in the cytosol (30). Rather, copper is constantly bound, and transferred from one molecule to another. This system requires a network of membrane transporters, cytosolic chaperones and small molecules to direct copper to cellular compartments where it can either be utilized or removed from the cell (Fig 1.1).

Copper primarily enters the cell through the high-affinity membrane transporter CTR1 (31). CTR1 is ubiquitously expressed in human tissues, and while not associated with any known human genetic disease, Ctr1 knockout is embryonic lethal in mice (29). CTR1 exists at the cell surface in a homo-trimer subject to N-linked glycosylation (32). While the transporter appears to be passive, the actual mechanism of translocation is not well characterized. CTR1 has been observed at both the plasma membrane and in intracellular vesicles (33), suggesting the transporter could facilitate copper entry by functioning as a channel or through a process of binding and internalization.

Internalization to vesicles may also be used as a method of regulating CTR1 activity, as transcription and translation of the transporter are not rapidly downregulated in response to elevated copper (34).

A second copper transporter, CTR2, is highly homologous to CTR1, but is a lower-affinity transporter (35). CTR2 function is poorly characterized, but it has been shown to be predominantly located in vesicular compartments (including late endosomes and lysosomes) (36, 37). The divalent metal transporter DMT1 is also capable of transporting copper (38), and is expressed in numerous tissue types where copper regulation is critical, such as the intestine, kidney, placenta and brain (39). To what extent these two transporters contribute to copper transport remains to be seen.

II-b. Metallochaperones

Copper entering the cell is directed to target proteins and compartments by a unique class of proteins known as metallochaperones (Fig 1.1). There is some evidence that the chaperones can directly receive copper from CTR1 (40), though this interaction may not be essential for copper entry to the cytosol. The chaperone CCS delivers copper to SOD1 (41). SOD1 can acquire copper in the absence of CCS, but the process is less efficient (42). The chaperone COX17 is involved in directing copper to mitochondria for eventual incorporation into Cytochrome C Oxidase (43). This process involves numerous mitochondrial chaperones and may involve multiple copper transfers (44). COX2 has

been shown to be highly dependent on COX17 for copper acquisition, while COX1 appears to have an alternate mechanism (45).

ATOX1 is a 7,400 Da cytosolic protein capable of binding a single copper atom between two Cys residues (46) (See Fig 1.6 and additional biochemical descriptions below). The chaperone delivers copper to the copper transporting ATPases ATP7A and ATP7B, which regulate copper entry to the biosynthetic pathway as well as removal of copper from the cell. In the absence of ATOX1, cells retain each of these functions, but are markedly less efficient in both capacities. *Atox1* -/- mice fail to thrive, and display many of the symptoms of copper deficiency (47), suggesting that copper dependent enzymes are not sufficiently metallated without the chaperone directing the metal to the ATPases. There is some evidence indicating that ATOX1 has an additional function in regulating transcription in a copper dependent manner (48). It is also of note that the name ATOX1 derives from "Anti-oxidant" after the homolog in yeast (ATX1), which was shown to suppress toxicity from reactive oxygen species when expressed in SOD1 deficient cells (49). It is not known whether this is due strictly to proper targeting of copper, or if the chaperone has other roles in managing cellular oxidation. Considering ATOX1 regulates both Cu-ATPases, little is known about the differences in functional interactions between the chaperone and its targets. In Chapter 3, we explore whether ATOX1 uses common delivery mechanisms for ATP7A and ATP7B, as well as the consequences of ATOX1 mediated copper transfer for these ATPases.

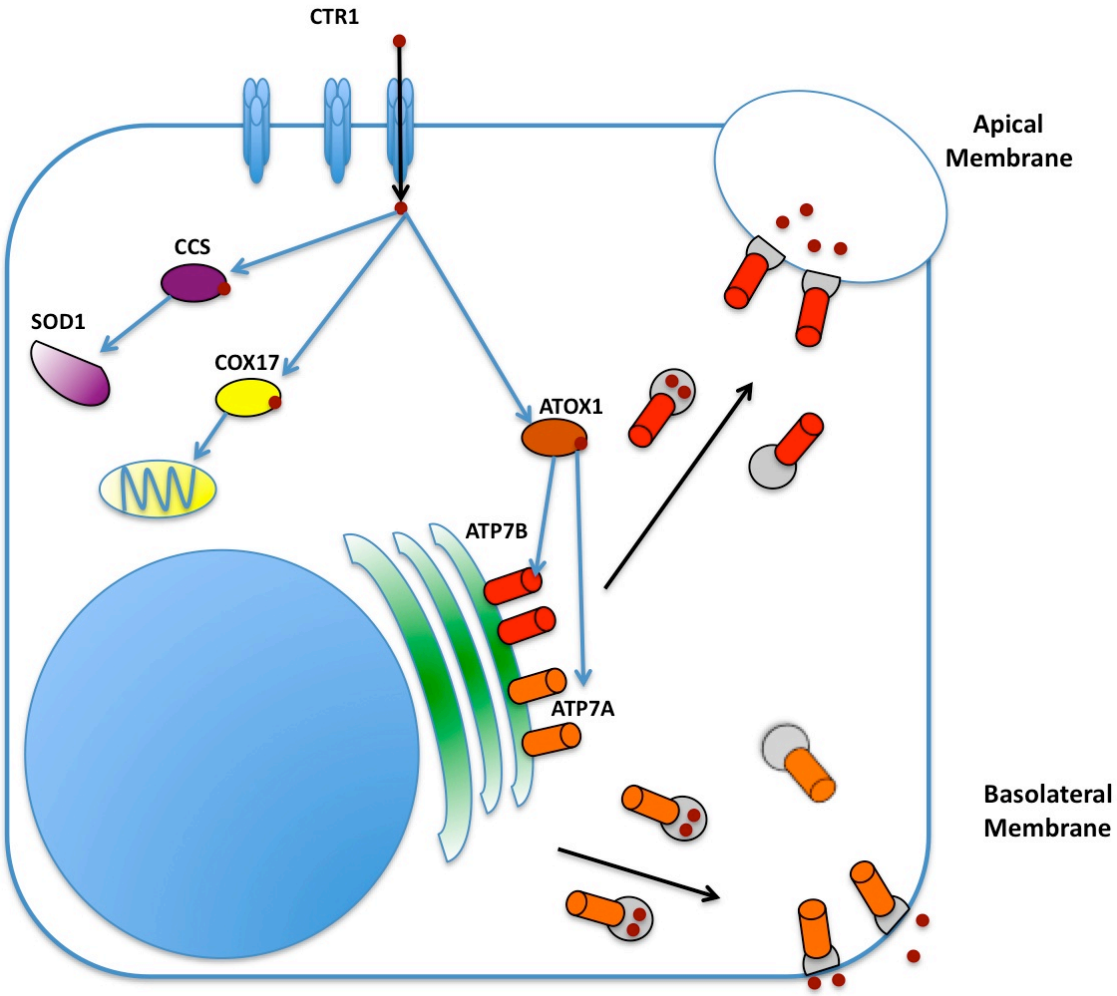

Figure 1.1. Cellular copper physiology and distribution. Cartoon of a cell showing key copper transport proteins. Copper enters the cell primarily through CTR1, where it is bound by metallochaperones CCS, COX17 and ATOX1 and directed to specific cellular compartments. ATOX1 delivers copper to the Cu-ATPases ATP7A and ATP7B, which reside in the TGN under basal conditions where they facilitate copper entry into the biosynthetic pathway. At high copper concentrations, ATP7A and ATP7B may relocalize to vesicles that traffic to the basolateral and apical membranes, respectively, allowing for copper to be removed into the extracellular lumen.

II-c. The Copper Transporting ATPases

Under basal copper levels, ATP7A and ATP7B are localized to the Trans-Golgi network (TGN) where they can transport copper into the lumen of the Golgi for incorporation by copper-dependent enzymes (50) (Fig 1.1). ATOX1 interacts with the copper binding N-Terminal domain (Described further below; also Fig 1.6), transferring copper and stimulating catalytic activity of Cu-ATPases (51). It is not clear whether the ATPases transfer copper directly to target proteins in the Golgi. However there does appear to be some ATPase-target preference; for example, Ceruloplasmin is expressed in hepatocytes and glial cells, where only ATP7B is expressed (19, 27). Likewise, tyrosinase and peptidylglycine α-amidating monooxygenase (PAM) have been specifically shown to have reduced activity in the absence of ATP7A (52, 53). While ATP7B and ATP7A may have some overlapping functions, they are clearly not redundant. The biochemical basis for their specialization is not well defined. In Chapter 3, we explore their differences in copper acquisition from ATOX1 and how their mechanisms for copper sensing may impart differences in function. In the Appendix, we explore how these functions may be utilized in a therapeutic manner.

When copper levels increase, ATP7A and ATP7B are both capable of trafficking out of the TGN and into vesicles where they can sequester excess copper for removal from the cell (50, 54). These vesicles can then fuse with the plasma membrane, jettisoning copper before being recycled into endosomal compartments. The ATPases can return to the TGN when cytosolic copper levels have decreased.

The mechanism for vesicle budding and ATPase trafficking is poorly understood. Copper appears to induce ATPase association with cellular trafficking machinery such as dynactin (55), as well as the adapter molecule COMMD1 (56). These interactions may be predicated on conformational changes in the ATPase that occur upon copper binding (57). Additionally, ATP7A and ATP7B undergo kinase-mediated phosphorylation in response to copper; this modification also correlates with changes in cellular localization (58, 59). While the identity of this kinase is unknown, it is notable that ATP7A has been shown to relocate in response to changes in both Ca+ and hormone concentrations (60, 61), suggesting a potential role for cell signaling mechanisms in the regulation of trafficking.

In polarized cells, it is apparent that ATP7A and ATP7B traffic to specific membranes – the basolateral and apical, respectively (50). ATP7B trafficking is best characterized in hepatocytes, in which the apical membrane borders on the bile duct, where excreted copper can be removed through the feces (62). ATP7A trafficking to the basolateral membrane is particularly important in the intestine (17), kidney (63) and mammary gland (61), where copper needs to be excreted into specific extracellular lumens. In tissues where both ATPases are expressed, this allows copper export to be directed to either membrane. However, in renal cells, for example, ATP7B does not traffic out of the TGN at all (63) perhaps due to tissue-specific splicing. The very N-Terminus of ATP7B has been shown to be critical for proper trafficking (64), and the splicing out of the first exon may give rise to a strictly TGN-localized version of ATP7B.

II-d. Genetic Organization and Expression Patterns of ATP7A and ATP7B

ATP7A and ATP7B derive from common ancestral copper transporters; many lower organisms employ a single Cu-ATPase (65). As such, the two genes and proteins are quite similar, yet possessing some key differences that dictate some distinction in function. The *ATP7A* gene contains 23 exons spanning nearly 140 kb of genomic DNA (66); *ATP7B* is 21 exons in length (67). Most differences in genetic organization lie in the 5' exons, with the last 70% of the two genes being highly similar. Both genes show some propensity for alternative splicing (68). *ATP7B*, in particular gives rise to a truncated version of ATP7B expressed in the pineal gland (69). The regulation of transcription and splicing of these two genes is poorly understood.

ATP7A is expressed in nearly all adult human tissues, with the notable exception of the liver, which only expresses ATP7B (Fig 1.2). ATP7B is not as ubiquitous as ATP7A, but is found in many tissues, including the brain, kidney, lung, placenta and mammary gland. Although some cells express both ATP7A and ATP7B, *in situ* hybridization has shown that in tissues such as the brain, while both Cu-ATPases are present, they are expressed in different cell types (27). Analysis of mouse tissue has shown that expression patterns change throughout development (70). ATP7A can be detected in the liver at early gestation, after which is gradually downregulated. ATP7B is expressed in the CNS, liver and heart at early gestation, prior to being upregulated in other tissues. ATP7A is expressed at high levels in the developing brain, particularly the choroid plexus (71), and appears to play an essential role in neurite outgrowth (24).

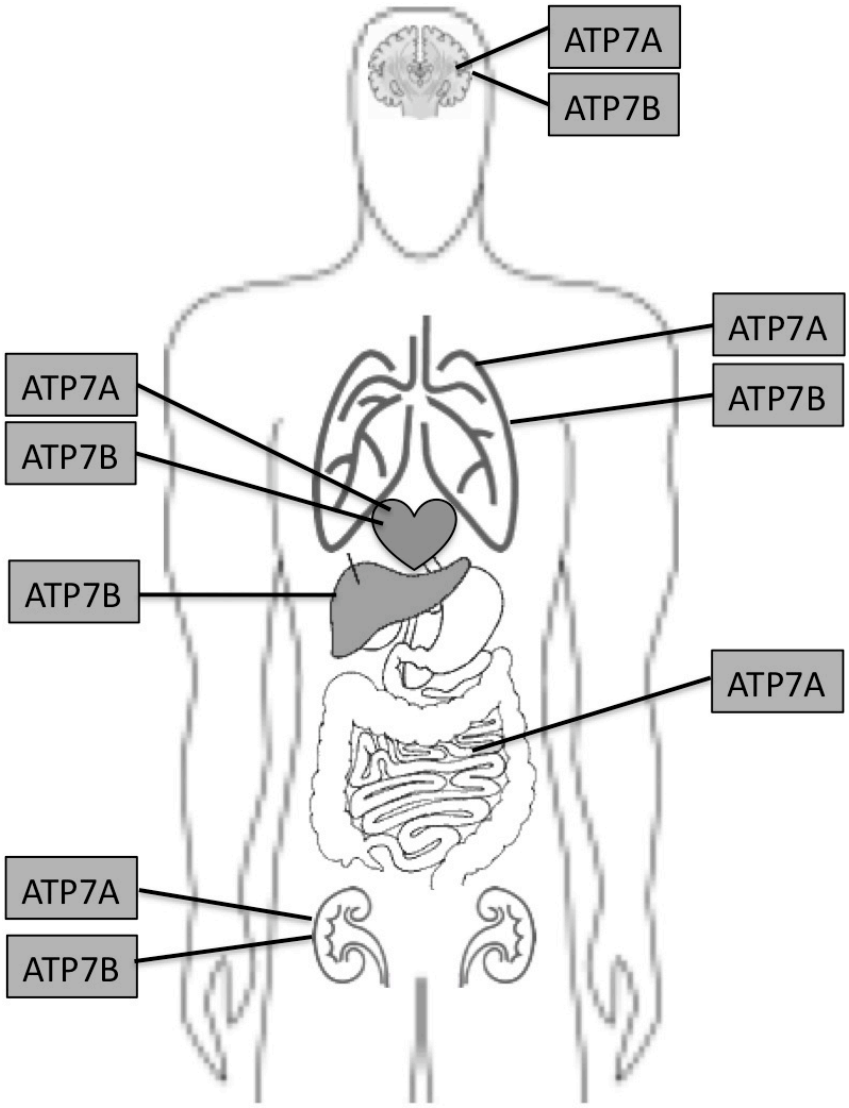

Figure 1.2. Expression of Cu-ATPases in human tissues. Dietary copper is absorbed through the intestine, where ATP7A is expressed, and redistributed in the liver, where ATP7B is expressed. Many tissue types that require strict copper regulation express both Cu-ATPases including the brain, heart, lungs and kidneys. Menkes Disease (ATP7A) and Wilson's Disease (ATP7B) show distinct phenotypes of copper deficiency and copper overload, respectively, due in large part to the differences in distribution of the two Cu-ATPases and their non-redundant functionalities.

III. Copper and its Role in Human Disease

III-a. Menkes Disease

Menkes disease is an X-linked recessive disorder caused by mutations to the copper transporting ATPase ATP7A, located at Xq12-q13 (72). The disease manifests as inherent copper deficiency, with symptoms related to loss of function of copper-dependent enzymes. Menkes disease has a prevalence of 1:100,000; patients with the most severe form of the disease have a life expectancy of less than five years (73).

Classical Menkes disease is characterized by severe neurological defects (including mental retardation and seizures), growth retardation, hypopigmentation, laxity of connective tissue, and "kinky hair" (74). The deficit in ATP7A function is primarily manifested as disrupting copper entry to the biosynthetic pathway, the outcome of which is a deficit in cupro-enzyme function. Specific enzyme deficits correlate with disease symptoms; Cytochrome C Oxidase (hypothermia, muscle weakness), lysyl oxidase (connective tissue laxity), and tyrosinase (hypopigmentation) are some examples. Menkes disease can present in the classical form or a mild form (with less severe neurological defects). Occipital-Horn Syndrome (OHS) is also caused by mutations in ATP7A, and shows many of the same features as Menkes disease, but typically with very mild or absent neurological defects (75). Over 200 mutations in ATP7A have been identified that lead to either Menkes disease or OHS. Insertions, deletions, missense, nonsense and splice site mutations are equally represented, though very few missense

mutations are found within the first seven exons of the gene (76). While there is some broad genotype-phenotype correlation (truncation mutations are more associated with classic Menkes Disease, splice-site mutations are more represented in OHS), there is considerable overlap, with some mutations found throughout the spectrum of disease presentation.

Treatment options are limited to attempts at improving systemic copper levels, typically through subcutaneous copper-histidine injections, bypassing the intestinal uptake pathway (77). Treatment starting in early infancy has been successful at extending lifespan into adolescence, though patients still suffer neurological and circulatory abnormalities, due to the essential nature of copper in early development (78). Patients with milder forms of the disease typically have a better long-term outcome. New treatment methods will be needed to improve efficiency at delivering copper to the brain, as well as replacing ATP7A function within cells.

The “mottled” (Mo) mouse has naturally occurring mutations in Atp7a, the mouse homolog of ATP7A (79). Mice with the Mo phenotype range in severity from embryonic lethal to long-term viable (particularly the “brindled” mouse) (80). Disease severity in the Mo mice does correlate strongly with mutation, with the brindled mice genotype being a conserved 2-aa deletion in the actuator domain of ATP7A (81). The resulting protein does not relocalize in response to elevated copper (82). Recently, a zebrafish model, “calamity”, has been identified with a splice site mutation in atp7a, the zebrafish homolog of ATP7A, resulting in a complete inactivation of the protein (83). Both

zebrafish and mouse models promise to be important in studying disease progression, particularly in parsing the roles of ATP7A and copper in development.

III-b. Wilson's Disease

Wilson's disease is an autosomal recessive disorder caused by mutations to the copper transporting ATPase ATP7B, located at 13q14.3-q21.1 (66). The disease is characterized by progressive accumulation of copper, primarily in the liver, with symptoms resulting from the toxic buildup of excess copper. Some patients also develop a severe neurological phenotype. Wilson's disease has a prevalence of approximately 1:30,000 individuals (84), though this is higher in some isolated populations, including 1 in 7,000 individuals in Sardinia (85), and up to 1 in 5,400 individuals in Hong Kong Han Chinese (86).

The primary manifestation of this disease is the intracellular accumulation of copper in hepatocytes. This buildup leads to hepatitis and liver cirrhosis, while leaving patients at a higher risk for some forms of liver cancer (87). Patients have a marked decrease of serum ceruloplasmin and increased urinary copper (86). These changes are commonly used as diagnostic tools. Not all patients develop the neurological phenotype, but those that do may develop seizures or Parkinson-like features, as well as psychiatric problems (88). Patients with this phenotype develop copper deposits in the cornea, visible as Kayser-Fleischer rings (89), and in the basal ganglia, visible with MRI (90). Kidney

disease is also quite common in Wilson's disease patients, many of whom have altered calcium reuptake, leading to hypercalciuria and nephrocalcinosis (91).

Early diagnosis and treatment are extremely important to effectively managing symptoms. Treatment is predicated on removing excess copper, as well as reducing copper intake and absorption (92). Removing excess copper is primarily accomplished with the use of copper chelators, such as penicillamine or trientine. Reducing copper intake can be accomplished by restricting the diet to limit copper-rich foods along with inhibiting copper absorption with zinc supplements. Zinc ingestion stimulates expression of metallothionien, which acts as a copper chelator in the intestine. If hepatic symptoms have progressed to the point of liver failure, liver transplantation is extremely effective (93). Liver transplantation may be effective in reversing neurological symptoms in some cases (94) but is dependent on the degree of disease progression (95).

Over 300 disease-causing mutations have been found in ATP7B. Mutations can be found throughout the gene; most are missense in nature. The most common are H1069Q (especially in Europe and N. America) and R778L (southeast Asia) (96). In general, patients with truncation mutations present with symptoms earlier than do those with base-pair substitution mutations resulting in a partially functional protein (97), though there is some heterogeneity in disease severity in patients with the same mutation. Similarly, no genotype-phenotype correlation has been found relating to the presentation or severity of neurological symptoms.

Numerous animal models have been characterized that display Wilson's Disease characteristics. The well-characterized Atp7b -/- mouse features progressive hepatic copper build-up, as well as other Wilson's Disease characteristics such as reduced circulating holo-ceruloplasmin. This model has allowed for further study of the molecular pathogenesis of Wilson's Disease, showing alterations in hepatic lipid metabolism (98) as well as changes in gene expression in other affected tissues (27, 99). Both the Long-Evans-Cinnamon (LEC) rat and the toxic-milk mouse also display characteristics similar to Wilson's Disease, and derive from mutations in their respective ATP7B homolog. The LEC rat has a ~900 bp deletion at the 3' end of Atp7b (100), while the toxic-milk mouse has a single-base substitution in Atp7b (101). These models are essential for studying the molecular pathogenesis of disease progression, while also providing a platform for testing new forms of therapy. A naturally occurring form of canine copper-toxicosis results in dogs with similar liver pathology, but the mutation has been mapped to a separate gene, COMMD1 (102). In humans, the COMMD1 gene product interacts with ATP7B, and may be essential for vesicular targeting of the ATPase (103) as well as protein stabilization (56). A correlation between COMMD1 polymorphisms and Wilson's Disease phenotype has yet to be found (104, 105).

III-c. Other copper-disease associations

In addition to Wilson's Disease, another class of disorders presents with a similar phenotype. Indian childhood cirrhosis (ICC) (106), endemic Tyrolean infantile cirrhosis (ETIC) (107), and idiopathic copper toxicosis (ICT) (108) are all characterized by liver

cirrhosis with hepatic copper buildup. These diseases all manifest in early childhood, though symptoms are predicated on exposure to a copper-rich diet. While all three of these diseases appear to be inherited, and present in a similar fashion to early-onset Wilson's Disease, ATP7B has been excluded as the underlying disease gene (109). Attempts at identifying inherited mutations have been made in ATOX1 and COMMD1, among others, with no success (110). While neurological symptoms are not commonly associated with these diseases, abnormal brain MRI patterns have been seen in some patients (111).

As discussed earlier, a growing number of neurodegenerative disorders are associated with copper accumulation in the brain or motor neurons. Some cases of familial ALS are caused by mutations in SOD1, the copper-zinc containing superoxide dismutase (112). Both the ß-amyloid (Alzheimer's) and prion protein appear to use copper as a cofactor (113, 114), though it is not clear how the ion is utilized. While it is not clear that copper plays a role in disease progression, the buildup of high concentrations of copper in neurons could potentially contribute to oxidative stress and damage. Studies focusing on the normal function of proteins such as ß-amyloid may provide a clearer understanding of how copper is used in the CNS.

IV. Architecture and regulation of ATP7A and ATP7B

IV-a. Domain Organization and the Transport Cycle

ATP7A and ATP7B are P-Type ATPases, specifically members of the P_{-1B} subfamily, a category that includes over 100 heavy-metal transporting ATPases (115). These transporters are characterized by cytosolic metal binding domains (either N or C terminal) as well as a conserved membrane topology featuring eight transmembrane segments (Fig 1.3A, 1.3B). The Cu-ATPases are asymmetric molecules with the majority of protein mass (and key functional domains) facing the cytosolic portion of the membrane. The cytosolic side includes three domains required for phosphorylation and dephosphorylation – the nucleotide-binding domain (N-Domain), phosphorylation domain (P-Domain) and actuator domain (A-Domain) (See Figs 1.3a, 1.3b).

Like all P-Type ATPases, ATP7A and ATP7B translocate cations (in this case, copper) from the cytosol to luminal compartments using the hydrolysis of ATP, which proceeds via formation of a transient acyl-phosphate intermediate (116). This facilitates transformation of the ATPase between the E1 and E2 states and provides the catalytic energy to move copper across the membrane. In the E1 state, the intramembrane copper-binding site (a conserved CPC motif discussed in detail below) is accessible from the cytosolic side. In the E2 state, the copper-binding site is exposed to the luminal side of the membrane, allowing copper to be released on this side of the membrane. ATP binds

to the N-Domain in the E1 state (See Fig 1.3.C). Proceeding with ATP hydrolysis requires copper being bound to the cytosolic side of the intra-membrane region. Phosphorylation occurs on the invariant Asp residue in the DKTG motif of the P-Domain. A conformational change from the E1P to the E2P state is then required to move copper from the cytosolic side of the membrane to the luminal side. Copper release is followed by dephosphorylation and return to the E1 state.

The N and P domains are independently folded subunits of the cytosolic loop between transmembrane segments TM6 and TM7. The subdomains are separated by a short (~5aa) linker, which allows them to be bridged together in the presence of ATP (117). The P domain is a highly conserved region found in all P-Type ATPases. Although the structure of this domain has not been solved for either human Cu-ATPase, they both share >70% similarity with the P-domain from the bacterial Cu-ATPase CopA and are predicted to have a similar fold. This structure, as well as the structure of the P-domain from the SERCA Ca++ pump (118), reveals a six-strand ß-sheet flanked on either side by three α-helices. The signature DKTG motif is positioned facing the N-Domain, allowing for the formation of the acyl-phosphate (See Fig 1.3).

A.

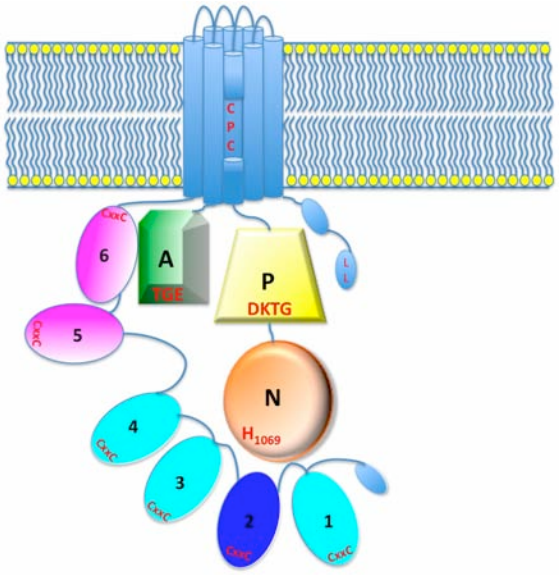

B.

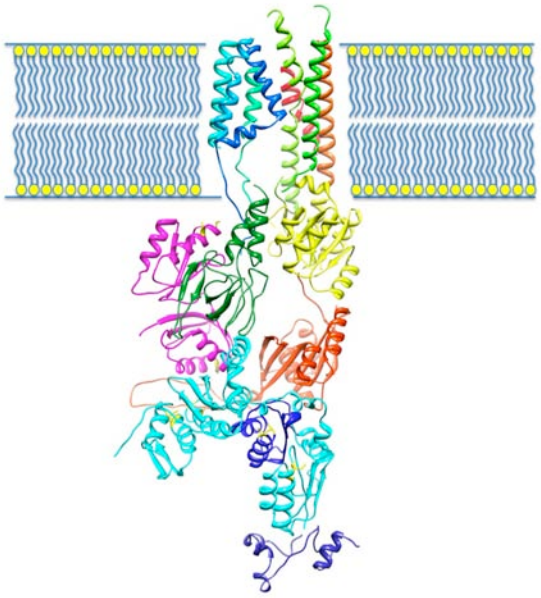

C.

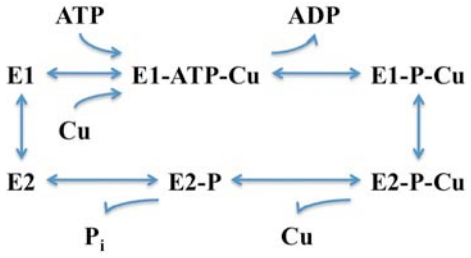

Figure 1.3. Structure and domain organization of ATP7B. A. Cartoon and **B.** Structural model of ATP7B based on the model of CopA by Wu et al 2008 (137) (Protein Data Bank (PDB) code : 2VOY). Nucleotide-binding ("N") Domain shown in orange, Phosphorylation ("P") domain shown in yellow, Actuator Domain ("A") shown in green. MBDs 5 and 6 shown in pink, MBDs 1-4 shown in cyan, with MBD2 highlighted in blue. The N and A domain structures were placed using replacement modeling based on published structures (119, 121); (PDB codes : 2arf and unpublished, respectively). MBDs 5 and 6 (124) (PDB code : 2ew9) were placed based on replacement modeling and Patchdock models of interaction with the A domain. MBDs 1-4 (Derived from a set of Rosetta models compiled by Dr. Ujwal Shinde) were placed based on Patchdock models of interaction with the N Domain. ATP7A shares domain organization with ATP7B. Key conserved residues shown in red. **C.** Phosphorylation cycle for the Cu-ATPases.

IV-b. Domain Structures and Functions

The N-Domain of ATP7A and ATP7B are representative of the P-$_{1B}$ family, which have unique characteristics within the P-Type ATPase family. The ATP binding site consists of a hydrophobic pocket with numerous residues conserved in Cu-ATPases. In ATP7B, this contains H1069, site of the most common Wilson's Disease mutation. Despite a lack of sequence similarity to other P-Type ATPases, the structures of the N-Domains of ATP7A and ATP7B retain the same conserved core structure, consisting of six ß-helices bracketed by two α-helices on either side (119, 120). Both ATP7A and ATP7B have a flexible loop situated between the ß3 and ß4 strands that can be removed without affecting ATP binding (119). The two loops have no sequence similarity, but are conserved in mammalian Cu-ATPases, suggesting an unknown regulatory function.

The actuator domain (A-Domain) is located between TM4 and TM5, and is essential for mediating the dephosphorylation of the P-Domain in the transition from the E2P state to the E2 state. The conserved TGE motif acts as the site of phosphatase activity. The structure consists of seven anti-parallel ß-strands folded into two adjacent ß-sheets (121). The A-Domains of ATP7A and ATP7B have nearly identical structures and placement of the TGE motif. When the TGE motif is mutated to AAA, the ATPase remains in the E2P state, and becomes hypersensitive to copper, trafficking out of the TGN into vesicles even at low copper concentrations (122). This suggests that the A-domain may mediate the conformational changes necessary for copper dependent regulation and trafficking, and/or that persistent phosphorylation may induce trafficking.

Functionally, ATP7A and ATP7B show differences with regard to catalytic activity. In vitro, ATP7A shows higher rates of catalytic turnover (both phosphorylation and dephosphorylation rates). However, ATP7B has a faster response to copper (27). It is unknown how many copper molecules are transported per ATP hydrolyzed, but most evidence points to ATP7A as being the faster transporter. It has been suggested that in cells where both Cu-ATPases are expressed, that APT7A is responsible for most of the maintenance of cellular copper levels, while ATP7B is posited with supplying copper to specific enzymes (70). This would seem to be supported by ATP7A being able to transport copper into vesicles for secretion at a high rate.

Copper is translocated through the membrane by way of the CPC motif in TM6 of the Cu-ATPases (123), which facilitates intra-membrane coordination. This motif is conserved (as CPX) in all P-$_{1B}$ heavy-metal ATPases. Other conserved residues in TM7 and TM8 are presumed to be involved in Cu transport as well. The final six transmembrane segments (TM3-8) are fairly homologous to transmembrane segments found in all P-Type ATPases, with short luminal loops connecting TM3-4, 5-6 and 7-8. In contrast, TM1 and 2 are unique to the P-$_{1B}$ family. Each TM has a single Cys residue, and they are bridged by a His-Met rich hairpin sequence that has been proposed to facilitate copper release into the lumen (116). This hairpin is considerably longer in ATP7A, which may contribute to the differences in turnover rates between the two Cu-ATPases.

The activity and trafficking of ATP7A and ATP7B are both responsive to changes in cytosolic copper concentration. The N-Terminal domains of the ATPases are vital for detecting cellular copper levels. Through a series of structural changes, inter-domain, and inter-protein interactions, this information is relayed from the N-Terminus to the rest of the ATPase in a regulatory fashion. However, the mechanism by which copper binding to the N-Terminus results in these significant changes has not been well defined. The bulk of this dissertation focuses on discerning this mechanism.

V. N-Terminal Domains of ATP7A and ATP7B

V-a. N-Terminal Domain Architecture

The N-Terminal domains of ATP7A and ATP7B consist of six individually folded metal binding domains (MBDs) connected by loops of varied lengths. The MBDs are characterized by a conserved GMxCxxC motif, each of which is capable of binding a single copper ion between the two Cys residues (124-131). Each MBD folds into a ferredoxin-like domain consisting of four ß-sheets and two α-helices in a compact ßαßßαß structure (Fig 1.4). The copper-binding motif is solvent exposed between the ß1 sheet and α1 helix at the surface of the fold. The copper is bound in a linear coordinate fashion [S-Cu(I)-S] with bond lengths of ~2.2 Å (132).

A.

```
ATP7B - MBD1   VATSTVRILG MTCQSCVKSI EDRISNLKGI ISMKVSLEQD SATVKYVPSV VCLQQVCHQI GDMGFEASIA EG
ATP7B - MBD2   EAVVKLRVEG MTCQSCVSSI EGKVRKLQGV VRVKVSLSNQ EAVITYQPYL IQPEDLRDHV NDMGFEAAIK SK
ATP7B - MBD3   VVTLQLRIDG MHCKSCVLNI EENIGQLLGV QSIQVSLENK TAQVKYDPSC TSPVALQRAI EALPPGNFKV SL
ATP7B - MBD4   CSTTLIAIAG MTCASCVHSI EGMISQLEGV QQISVSLAEG TATVLYNPSV ISPEELRAAI EDMGFEASVV SE
ATP7B - MBD5   PQKCFLQIKG MTCASCVSNI ERNLQKEAGV LSVLVALMAG KAEIKYDPEV IQPLEIAQFI QDLGFEAAVM ED
ATP7B - MBD6   DGNIELTITG MTCASCVHNI ESKLTRTNGI TYASVALATS KALVKFDPEI IGPRDIIKII EEIGFHASLA QR

ATP7A - MBD1   VNSVTISVEG MTCNSCVWTI EQQIGKVNGV HHIKVSLEEK NATIIYDPKL QTPKTLQEAI DDMGFDAVIH NP
ATP7A - MBD2   EVVLKMKVEG MTCHSCTSTI EGKIGKLQGV QRIKVSLDNQ EATIVYQPHL ISVEEMKKQI EAMGFPAFVK KQ
ATP7A - MBD3   DSTATFIIDG MHCKSCVSNI ESTLSALQYV SSIVVSLENR SAIVKYNASS VTPESLRKAI EAVSPGLYRV SI
ATP7A - MBD4   TQETVINIDG MTCNSCVQSI EGVISKKPGV KSIRVSLANS NGTVEYDPLL TSPETLRGAI EDMGFDATLS DT
ATP7A - MBD5   SSKCYIQVTG MTCASCVANI ERNLRREEGI YSILVALMAG KAEVRYNPAV IQPPMIAEFI RELGFGATVI EN
ATP7A - MBD6   DGVLELVVRG MTCASCVHKI ESSLTKHRGI LYCSVALATN KAHIKYDPEI IGPRDIIHTI ESLGFEASLV KK

ATOX1          -MPKHEFSVD MTCGGCAEAV SRVLNKLGGV KYDIDLPNKK VCIESEHSMD TLLATLKKTG KTVSYLGLE- --
```

B. **C.**

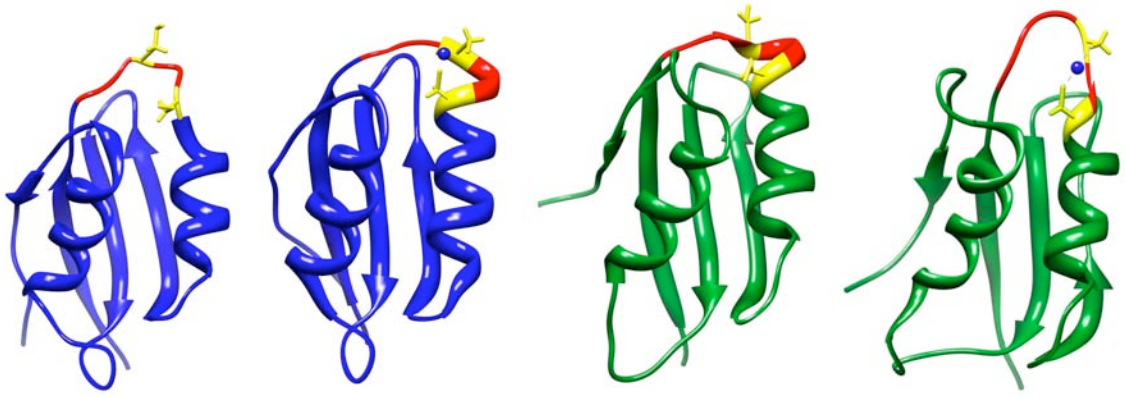

Figure 1.4. Sequences and structures of metal binding domains. A. Sequence alignments of N-Terminal MBDs from ATP7A and ATP7B along with metallochaperone ATOX1. Conserved residues, including the GMxCxxC copper binding loop shown in red. **B.** Structures of MBD2 from ATP7A in the Apo (left) and +Cu (right) states. GMxCxxC shown in red, metal binding Cys residues shown in yellow. Adapted from Banci et al, 2004 (129); PDB codes 1s6o and 1s6u, respectively. **C.** Structures of MBD3 from ATP7A in the Apo (left) and +Cu (right) states. GMxCxxC shown in red, metal binding Cys residues shown in yellow. Adapted from Banci et al, 2006 (126); PDB codes 2g9o and 2ga7, respectively. Although similar in overall structure, subtle differences between MBD2 and MBD3, such as the structure of the copper-binding loop may belie different properties.

All P-$_{1B}$ ATPases have similar domains at their N or C terminus, with the exact nature of the metal binding loops determining metal binding specificity. However, domains containing six MBDs are unique to mammals. Cu-ATPases from some lower organisms (bacteria, yeast) have a single N-Terminal metal binding site (65). ATP7A and ATP7B are capable of complementing yeast devoid of their copper transporter CCC2 even if their N-Terminal domains are truncated to having only a single functional MBD (133, 134). This is apparently the minimum required for copper translocation. While rat and mouse homologs of ATP7A and ATP7B feature six MBDs, the ATP7B variants have a non-functional MBD4.

V-b. Differential Roles for N-Terminal MBDs

The presence of six functional metal binding sites in ATP7A and ATP7B provide for additional layers of copper dependent regulation. Defining the unique roles of each MBD has been a subject of much query. A consensus is emerging that the MBDs located closest to the membrane (MBDs 5 and 6) are essential for the transport function of the ATPases, while the N-Terminal domains (MBDs 1-4) play a regulatory role, as their deletion increases the rate of formation of phosphorylated intermediate (135).

MBDs 5 and 6 are the most evolutionarily conserved domains (65). For ATP7B, they have been demonstrated to be sufficient for copper transport (135) and trafficking (136). Mutating the metal binding Cys residues also alters the affinity of the intramembrane copper-binding site (135). Based on the CopA structure (137) (see Fig 1.3), these

domains are in close proximity to the P and A domains, and influence copper transport by interacting with these domains. Truncating the N-Terminal domain by removing MBDs 4-6 inhibited trafficking (136), suggesting that these MBDs have specific sequence characteristics necessary for mediating domain-domain interactions. Studies of ATP7A show similar reliance on MBDs 5 and 6 for effective trafficking (138).

Although MBDs 1-4 may not be essential for function of ATP7B, they do appear to play an important role. Indeed, these domains have been shown to interact with the nucleotide-binding domain in the apo form, dissociating in the presence of copper (139). It is likely that this segment of the N-Terminal domain inhibits progression through the catalytic cycle in the absence of copper; copper binding causes the dissociation of the domains and allows for catalytic phosphorylation. MBDs 1-4 may also regulate copper binding to MBDs 5-6. Mutation of the metal binding Cys residues of MBD2 blocks transfer of copper from ATOX1, as well as subsequent catalytic phosphorylation (140) (discussed further below).

V-c. Structures and Dynamics of N-Terminal MBDs

Solution and crystal structures for all of the MBDs from ATP7A, and well as MBDs 3-6 of ATP7B have now been solved, allowing for more specific analysis of the similarities and differences amongst the domains (124-126, 128-131, 141). The corresponding MBDs from ATP7A and ATP7B are most closely related in sequence (Fig 1.4.A) and structure. Each MBD shows a similar positioning of the GMxCxxC loop between the ß1

sheet and the α1 helix, with the N-Terminal Cys exposed to solution and the C-Terminal Cys at the beginning of the helix (Figs 1.4.B, 1.4.C). Copper binding has a modest effect on the structure of the individual domain. The loop takes on a more compact, rigid structure, allowing for the two Cys residues to face each other and bind copper in a linear fashion. The rest of the MBD remains unchanged.

Aside from the copper coordinating Cys residues, the entire metal binding pocket shows a high degree of conservation amongst MBDs. The residue prior to the N-terminal Cys residue is either a Thr or His in each of the 12 MBDs; the residue prior to the C-terminal Cys residue is a conserved Ser. Substituting Ala residues for the Asn-Ser pair between the Cys residues in MBD1 of ATP7A alters the dynamics of the loop (130). The MBDs have a conserved hydrophobic core, which is likely to stabilize the structure of the domain, allowing for the loop to be more flexible.

The third MBD of each ATPase is the most unique based on sequence and structure, and as an individual domain in solution has the lowest rate of copper retention (126). Both MBD3 structures place the two metal binding Cys residues in the α1 helix, requiring a much greater conformational change to bind copper in a linear motif (125) (Fig 1.4.C). For both ATP7A and ATP7B, MBD3 is still capable of receiving copper from ATOX1, both in the context of the full N-Terminal domain, and also as an individual domain in solution. This raises the possibility that either the chaperone or other MBDs influence the structure of MBD3, though this is as of yet undetectable for an individual domain in solution.

Copper binding measurements suggest that the different MBDs have similar affinities for copper in solution (142). However, their affinities for accepting copper from the Cu-ATOX1 complex (discussed further below) are not equivalent. One explanation comes from differences in the flexibility of the loop. NMR structures show MBD3 as having a much more rigid loop, due to the extended α1 helix. Molecular dynamics (MD) simulations showed a similar tendency for MBD3 of ATP7B (143). Out of the other ATP7B MBDs, MBD4 and 5 showed the greatest loop flexibility in the Apo form, while MBDs 1, 2, and 6 displayed a more defined loop structure.

MD simulations on the copper bound forms of the ATP7B MBDs further supported the idea of the copper-binding loop gaining structure and increased rigidity upon binding copper. MBD4 was the only domain tested to retain some flexibility in these simulations (143). Interestingly, while the flexibility in the copper binding loop decreases, the flexibility of the opposite side of the domain is unchanged, or even enhanced in some cases (144), particularly in the loop connecting the ß3 and α2 helix. This is important when considering that the MBDs are all linked together as a domain.

V-d. Roles of the Inter-MBD Loops

Compared to the collection of structures of individual MBDs, very little is known about their relative organization within the entire N-Terminal domain. However, there is emerging evidence that there is a specific tertiary structure that is modulated by copper binding. Circular dichroism studies show an increased α-helical content in the copper-

bound form of ATP7B (145). Seeing as copper binding does not strongly impact the structure of individual MBDs, these large-scale rearrangements are likely to come from changes in the structure of the loops in between the MBDs, although it is not known how copper binding to the exposed metal-binding loops would impact the structure of the loop regions. Limited prototeolysis also reveals differences between the apo and copper-bound states of N-ATP7B, with the copper bound state more resistant to digestion, but exposing residues in the loops adjacent to MBD4 (140, 146). There is currently no data to suggest whether N-ATP7A has a similar response to copper binding. In Chapter 2, we further dissect the mechanism of N-ATP7B rearrangement upon copper binding. Then, in Chapter 3 we evaluate how N-ATP7A responds to copper transfer from ATOX1.

The loops interconnecting the MBDs vary in length, but common motifs are seen between ATP7A and ATP7B (Fig 1.5). Both have a very short (4 aa) linker between MBD 5 and 6, compared with a significantly longer loop between MBD 4 and 5. This supports the notion of MBD 1-4 performing a separate role from MBD 5-6, but also serves to reinforce that they cannot act completely independent from one another. The loop between MBD 3 and 4 contains a stretch of Ser residues that are subject to kinase-mediated phosphorylation in both ATP7A and ATP7B (Fig 1.5). In ATP7B, this stretch is exposed in the copper-bound conformation (146). Both ATPases have additional Cys residues besides those in the CxxC motifs. In particular, ATP7B has Cys residues flanking the 3-4 loop and the 4-5 loop (Fig 1.5). While there do not appear to be disulfide bonds formed in the copper bound state (145), some of these residues are conserved in Rat and Mouse Atp7a, suggesting they may play some function.

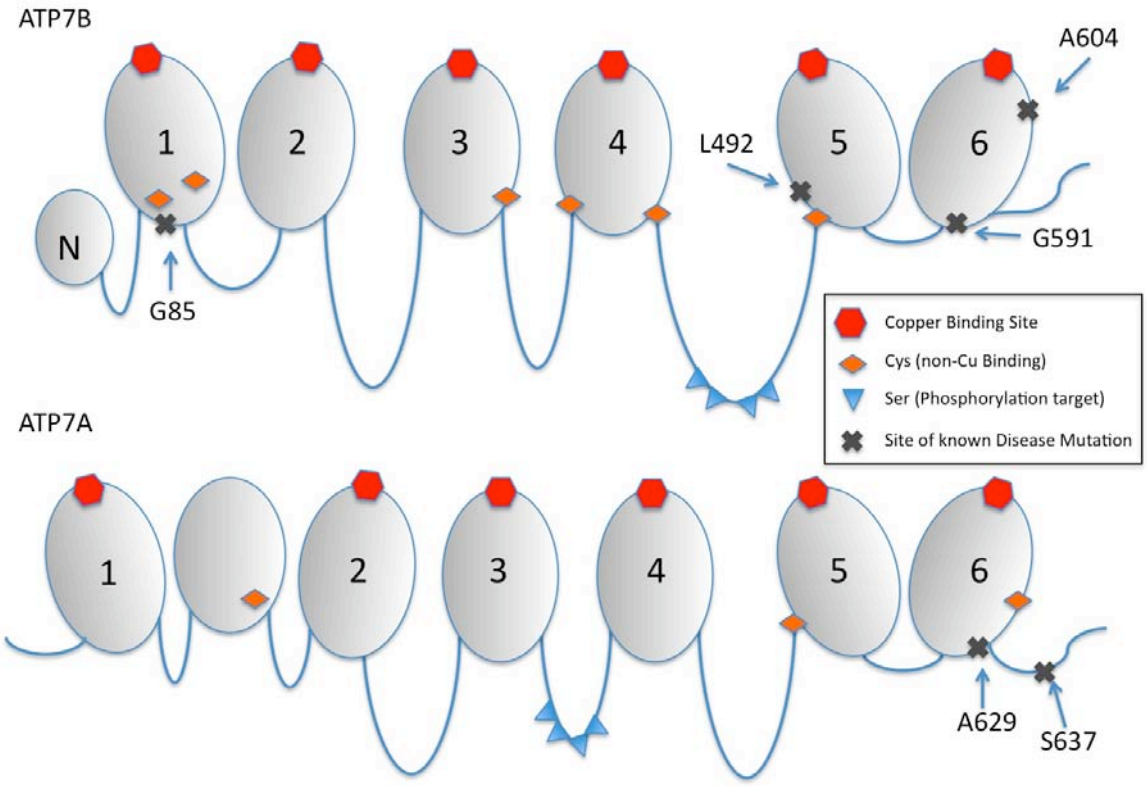

Figure 1.5. Organization of N-ATP7A and N-ATP7B. Schematic of N-Terminal domains of APT7B (top) and ATP7A (bottom) showing the relative length of the inter-MBD loop regions; copper binding sites, non-metal binding cysteine residues, serine residues subject to phosphorylation, and locations of common disease residues are shown as indicated.

Whether these additional Cys residues can be used in maintaining the reduction status of the metal binding Cys residues is unknown, but the loops between MBD2-3 and 3-4 are long enough to allow for this to occur. While purified and fully copper loaded N-ATP7B shows consistent two-ligand coordination, DTT and TCEP have been shown to be able to provide a third ligand for bound copper atoms, raising the question of whether any the non-coordinating cysteines could act as a temporary third ligand in mediating N-Terminal conformational changes. EXAFS analysis also reveals a Cu-Cu distance of 2.6 Å in N-ATP7B, suggesting that in the Cu-bound state, some MBDs are in very close proximity.

The solution structure of MBD5-6, the first solved for a multi-MBD construct, showed the two MBDs separated by a short linker, essentially tumbling as one rigid molecule. The relative conformation of the two MBDs did not change with the addition of copper (and placed the two copper atoms > 6Å apart). The structures of MBDs 3 and 4 of ATP7B were also solved concurrently, but the interceding loop was too long and flexible to obtain useful data on loop structure or interactions between the two MBDs (125). As such, the structure and organization of the full N-Terminal domains remains largely a mystery. In Chapter 2, we further discern the organization of N-ATP7B in the Apo state, and show how this begets a mechanism for responding to changes in copper binding.

Key differences between N-ATP7B and N-ATP7A lie at their N-termini. ATP7B features a 56-aa N-terminal sequence prior to MBD1, with MBD1 and MBD2 separated by a short (12 aa) linker. ATP7A has a very short N-terminus, with MBD1 and MBD2 separated by a 91 aa loop. Homology and Rosetta models suggest that this loop may fold

into an MBD-like structure, albeit one that cannot bind copper (116). The N-Terminus of ATP7B has been shown to be essential for proper trafficking and membrane targeting of ATP7B (64). Truncation mutants that retain this sequence are still able to traffic normally. A conserved 9-aa sequence appears to be critical for targeting of ATP7B to the apical membrane and proper return the TGN (147).

V-e. Interactions Between the N-Terminal Domain and ATOX1

The copper chaperone ATOX1 shares the same architecture as the N-Terminal MBDs, binding a single copper atom within its CxxC motif (148). This motif is able to accept a third sulfur ligand, and is presumed to be the basis of copper transfer whereby ATOX1 forms a heterodimer with an MBD and passes copper through a three-coordinate intermediate from one CxxC to another (46) (See Fig 1.6). ATOX1 is capable of filling all six MBDs of N-ATP7B when presented in excess, and can stimulate catalytic activity of ATP7B in a similar concentration dependent manner (51). In vitro ATOX1 is capable of this on its own, but other scaffold proteins found in the cell may enhance this interaction (149).

For ATP7B, all six MBDs can receive copper from ATOX1 in the context of N-ATP7B (150). Apo-ATOX1 is also capable of retrieving copper from copper loaded N-ATP7B (51). However, the individual relationships between the chaperone and the six MBDs do not appear to be equivalent. MBDs 1, 2 and 4 form a detectable copper-mediated adduct with ATOX1, but MBDs 3, 5 and 6 do not (151). When presented as individual domains

in solution, ATOX1 shows a preference for MBD4, perhaps due to the high flexibility of the metal binding loop of this domain (124). However, when presented to the entire N-ATP7B, ATOX1 first transfers copper to MBD2 (140). Mutating the copper binding Cys residues of MBD2 is enough to abrogate Cu-ATOX1 stimulated catalytic phosphorylation in ATP7B. This suggests that MBD2 is either preferentially exposed or otherwise biased towards interacting with ATOX1 when N-ATP7B is in the Apo state. The unique properties and significance of MBD2 are explored in Chapter 2.

For ATP7A, MBDs 1 and 4 are capable of forming adducts with Cu-ATOX1 (152). When presented with a construct containing MBDs 4-6, ATOX1 preferentially donated copper to MBD4, though it is capable of donating to MBDs 5 and 6 (153). MBD3 is particularly poorly metallated by ATOX1 in solution, possibly owing to the structural differences described above (126). It is not known if transfer occurs in a specific sequence as for ATP7B. There has been no direct comparison of concentration dependence of copper transfer from ATOX1 to the two N-Termini, nor is it known how ATOX1 distinguishes between the two ATPases when both are present at the same time. This is a central focus of Chapter 3 of this dissertation.

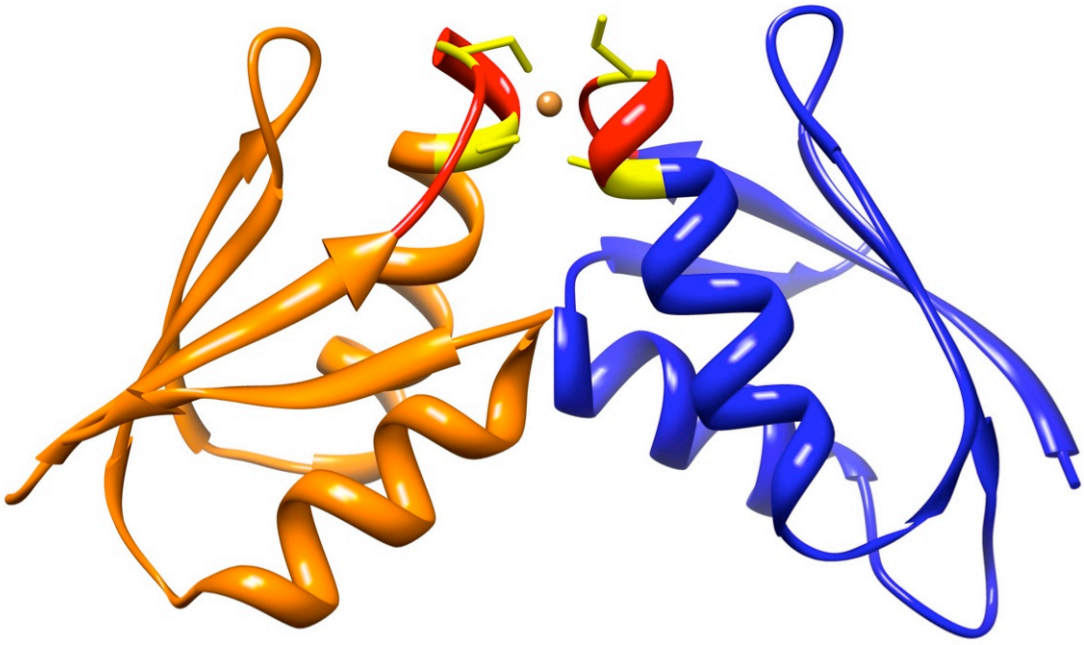

Figure 1.6. Transfer of copper from ATOX1 to a metal binding domain. Model of ATOX1 and MBD2 from ATP7B, based on the crystal structure of ATOX1 (46) (PDB code : 1fe4) and a model of MBD2 (140). Cu-ATOX1 forms a heterodimer with a target MBD, using a three-coordinate intermediate to transfer copper from the chaperone to the target.

V-f. Other Interacting Partners for the N-Terminal Domains

Copper dependent trafficking of ATP7A and ATP7B is at least in part regulated by the interactions of the N-Terminal domain with other cytosolic proteins. As mentioned above, kinase-mediated phosphorylation takes place in the loop between MBD3 and 4 of both ATPases (146, 154). Phosphorylation of this loop directly correlates with trafficking. Mutating all of the copper binding Cys residues in ATP7A disrupts both this phosphorylation as well as trafficking. The identity of the kinase is not known, nor is it known when phosphorylation occurs (prior to or following departure from the TGN).

The canine copper toxicosis gene COMMD1 interacts with the N-Terminal domain of ATP7B, but not ATP7A (155). This relationship is enhanced in the presence of copper. Current data suggests that COMMD1 may be involved in proper vesicular targeting of ATP7B (103) (and other proteins as well (156)). As ATP7A seems to target different membranes and intracellular compartments than ATP7B, it may require unique adaptors for correct trafficking. Similarly, the p62 unit of dynactin interacts with the N-Terminal of ATP7B, but not ATP7A (55). These interactions may be specific to ATP7B expressed in hepatocytes (157). Interacting partners for ATP7A or ATP7B expressed in other cell types remain to be identified.

Another recently identified N-Terminal interacting partner is Glutaredoxin, and both N-ATP7A and N-ATP7B were shown to be capable of being modified with glutathione. Both N-Terminal domains are highly susceptible to oxidation, even in cellular environs

(158), and this represents a possible mechanism for maintaining the reduced status of MBDs when they are not copper-bound.

V-g. Disease Causing Mutations

As discussed above, only a handful of disease causing mutations have been identified in the N-Terminal domain of ATP7A. A patient with a mild form of Menkes Disease was determined to have a splicing mutation that truncated ATP7A to only contain MBDs 5 and 6. This protein complements yeast, and effectively transports copper, but traffics with extremely high sensitivity to copper (159). Another mutation, A629P is located in the final ß-sheet of MBD6. The structure of the mutant MBD6 was analyzed by NMR, and revealed modest structural changes and a slightly decreased affinity for copper (127). The domain was also more structurally dynamic, suggesting it could alter interactions with the other domains of the protein. The S637L mutation is located in the linker between MBD6 and TM1 (Fig 1.5). This variant of ATP7A is also capable of complementing yeast, but may be more rapidly degraded (160).

More mutations of N-ATP7B leading to Wilson's Disease have been identified, but only a few have been characterized to date. The G85V mutation is located in a conserved Gly residue in MBD1, while the G591D mutant is located in the same Gly position in MBD6. L492S is in the first ß-sheet of MBD5, and A604P is located between MBD6 and TM1 (Fig 1.5). All four of these mutations have been shown to have an increased association with COMMD1 (56). Overexpressed G85V and G591D mutants have been shown to

mislocalize to the ER in some cases (56), but not others (161). Also suggestive of misfolding, the G85V mutant shows increased expression in the presence of pharmacological chaperones (162). There is some evidence for altered association with ATOX1 in these mutants (161). Perhaps most interestingly, the G591D mutation ablates kinase-mediated phosphorylation of ATP7B (58). There is currently no data on how these mutations affect the structure and function of N-ATP7B, whether they influence copper binding or transfer from Cu-ATOX1. We explore the functional consequences of the G85V and G591D mutations in Chapter 4 of this dissertation.

VI. Questions Addressed in this Thesis

The research presented here is focused on the central question of how the N-Terminal domains of ATP7A and ATP7B interpret information about cytosolic copper concentrations so that it can be conveyed to the rest of the ATPase. Within that context, this work addresses the roles of individual metal binding domains, their organization and function as a domain, their interaction with ATOX1, and characteristics of mutations, both artificial and disease-associated.

Chapter Two focuses on N-ATP7B, addressing the role of MBD2 as an essential regulator of copper delivery to the entire domain. The effects of numerous mutations are explored with regard to their effect on domain conformation, copper binding and transfer, and susceptibility to oxidation. The effects of altered hydrogen bonding on inter-MBD interactions are addressed, as well as questions regarding the organization of N-ATP7B

domains and their interceding loop regions in the apo form of the protein, and how copper transfer may alter this organization.

In **Chapter Three**, the relationship between N-ATP7A and ATOX1 is characterized, looking at the specificity and concentration dependence of copper transfer, and how N-ATP7A alters conformation in response to copper binding. These properties are compared to those for N-ATP7B. In addition, a novel mechanism belying concentration dependence of ATOX1 transfer is explored.

Chapter Four focuses on two disease causing mutations in N-ATP7B, G85V and G591D, and attempts to address how these mutations effect the organization and function of N-ATP7B with regard to copper binding, tertiary structure of the domain, oxidation, and relationship with ATOX1.

Additionally, the **Appendix** explores the role of the N-Terminal domains of ATP7A and ATP7B in the binding and detoxification of the platinum based chemotherapeutic drug Cisplatin.

Chapter 2

Interactions between copper-binding sites determine the redox status and conformation of the regulatory N-Terminal domain of ATP7B

This chapter is adapted from LeShane et al, 2010 (163) published in the Journal of Biological Chemistry. Contributions of co-authors are indicated alongside the relevant figures. Critical reading and helpful comments from all co-authors, as well as members of the Lutsenko and Hubbard laboratories at the Johns Hopkins Medical Institute were essential in the preparation of the final manuscript.

Abstract

Copper-transporting ATPase ATP7B is essential for human copper homeostasis and normal liver function. ATP7B has six N-terminal metal-binding domains (MBDs) that sense cytosolic copper levels and regulate ATP7B. The mechanism of copper sensing and signal integration from multiple MBDs is poorly understood. We show that MBDs communicate and that this communication determines the oxidation state and conformation of the entire N-terminal domain of ATP7B (N-ATP7B). Mutations of copper-coordinating Cys to Ala in any MBD (2, 3, 4, or 6) change the N-ATP7B conformation and have distinct functional consequences. Mutating MBD2 or MBD3 causes Cys oxidation in other MBDs and loss of copper binding. In contrast, mutation of MBD4 and MBD6 does not alter the redox status and function of other sites. Our results suggest that MBD2 and MBD3 work together to regulate access to other metal-binding sites, whereas MBD4 and MBD6 receive copper independently, downstream of MBD2 and MBD3. Unlike Ala substitutions, the Cys-to-Ser mutation in MBD2 preserves the conformation and reduced state of N-ATP7B, suggesting that hydrogen bonds contribute to interdomain communications. Tight coupling between MBDs suggests a mechanism by which small changes in individual sites (induced by copper binding or mutation) result in stabilization of distinct conformations of the entire N-ATP7B and altered exposure of sites for interactions with regulatory proteins.

Introduction

Copper is an essential trace element used as a cofactor by numerous enzymes, which take advantage of its low redox potential to catalyze electron transfer reactions. Perhaps because of this high reactivity, copper is kept under strict homeostatic control. The copper-transporting P-type ATPases (Cu-ATPases), ATP7A and ATP7B, are essential for maintaining cellular copper levels. These transporters deliver copper into the secretory pathway for the biosynthesis of cuproenzymes and facilitate export of excess copper from the cells. In humans, mutations in either ATP7A or ATP7B disrupt copper homeostasis and lead to the severe disorders Menkes disease and Wilson's disease, respectively (164). Copper is not only transported by Cu-ATPases; it also acts as a regulator of their activity, post-translational modification, and intracellular localization (116). The mechanism of copper-dependent regulation of Cu-ATPases is poorly understood.

ATP7A and ATP7B are highly homologous proteins and share many aspects of function and regulation. In this study, we focus on ATP7B. Cu-ATPase ATP7B is a 165-kDa protein with eight transmembrane segments and most of the soluble parts exposed to the cytosol. The large cytosolic N-terminal domain of ATP7B (N-ATP7B) binds copper and plays a key role in regulation of ATP7B. The intracellular copper donor metallochaperone ATOX1 docks to N-ATP7B, transfers copper, and stimulates the activity of ATP7B. N-ATP7B is also phosphorylated by a kinase in response to copper binding (146), houses the sequence determinants for the copper-dependent apical targeting of ATP7B (64), and recognizes dynactin, a component of the trafficking machinery, in a copper-dependent manner (55). It remains unknown whether all of these

copper-induced events are directly coupled. It is also unclear how many copper-binding sites in N-ATP7B participate in each regulatory event or how signals from multiple copper-binding events are integrated, if at all.

N-ATP7B contains six metal-binding subdomains (MBDs), each coordinating one copper between 2 Cys residues in an invariant CxxC motif (57, 158). The six MBDs are connected by flexible loops of varying lengths (Fig 2.1.A). The three-dimensional structure of N-ATP7B is unknown; however, the structures of individual subdomains and two pairs (MBD3/4 and MBD5/6) have been solved (124-131). These studies revealed that all MBDs have a ferridoxin-like βαββαβ-fold, with the copper-coordinating site situated in a solvent-exposed loop between the β1-strand and α1-helix (Fig 2.1.B). In individual recombinant MBDs, copper binding to this loop does not induce significant changes in the structure of MBDs: the loop takes on a more fixed, rigid state (125), whereas the rest of the protein shows very minor changes. However, when copper binds to N-ATP7B, significant changes in secondary structure are detected by circular dichroism and proteolysis (57, 146). Thus, very small structural alterations in individual MBDs upon copper binding are sufficient to trigger a rearrangement of the entire N-terminal domain.

The mechanism by which copper regulates the N-ATP7B conformation is not obvious because, in N-ATP7B, the copper-binding sites of MBDs appear fairly exposed. Specifically, all MBDs in N-ATP7B can be labeled with a Cys-directed fluorescent probe, although with different efficiency (140, 150), indicating accessibility of sites to solvent. Similarly, all six sites in N-ATP7B can be loaded with copper in the presence of

Cu-ATOX1 (51). Although copper exchange between individual MBDs can occur in solution (57, 146), such interdomain exchange is not essential for ATOX1-mediated metallation of N-ATP7B (150).

The above structural data showing relative exposure of metal-binding sites (MBSs) and the lack of significant structural changes upon copper binding appear at odds with the studies showing functional coupling between MBDs. In N-ATP7B, MBD2 is the preferential site for copper transfer from ATOX1, and only after MBD2 is filled can other sites be loaded with copper (140). In the context of the full-length ATP7B, the CxxC-to-AxxA substitution within MBD2 completely disrupts the activation of ATP7B by Cu-ATOX1 without altering the protein's ability to be activated by free copper (140). This observation suggests that MBD2 may act as a gateway for ATOX1-mediated copper transfer to the rest of the protein and modulate access to other N-terminal MBDs.

To better understand the relationship between MBDs in the context of a fully folded N-ATP7B, we characterized the effect of mutating individual sites on copper binding by N-ATP7B. Our studies revealed the key roles of MBD2 and MBD3 in maintaining the structural and functional integrity of N-ATP7B. We observed a tight packing of MBDs within N-ATP7B that depends on the ability of the CxxC-containing loops to form hydrogen bonds and that has important functional consequences. The interdomain contacts maintain the reduced state of MBSs as well as distinct conformations of loops connecting MBDs. Our results suggest a mechanism that allows for small perturbations in structure (because of mutation or copper binding) to alter the tertiary structure of the entire N-ATP7B.

A. **B.**

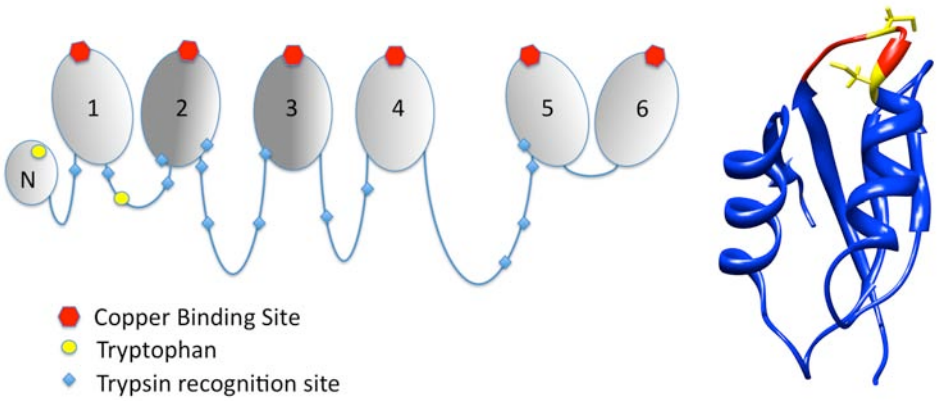

Figure 2.1. Organization of N-ATP7B. A. Schematic illustrating the relative length of the loops connecting the N-terminal MBDs; copper-binding sites, tryptophan residues, and trypsin recognition sites are as indicated. **B.** Structure of a representative MBD (MBD5; adapted from Achila et al 2006 (124)) **(**PDB code : 2ew9) The GMxCxxC metal-binding loop is shown in red; Cys residues are indicated in yellow.

Materials and Methods

Constructs/Mutants. Mutations in N-ATP7B were generated using the pMal-N-ATP7B plasmid as a template and the Stratagene QuikChange XLII kit with the following mutagenic primers (or combinations thereof in the case of m2/3A): M2A, GCATGACCGCCCAGTCCGCTGTCAGCTCCATTGAAGG (forward) and CTGACAGCGGACTGGGCGGTCATGCCCTCCACCC (reverse); M2S, AGGGCATGACCAGCCAGTCCAGTGTCAGCTCC (forward) and GGAGCTGACACTGGACTGGCTGGTCATGCCCT (reverse); M3A, GGAATGCATGCTAAGTCTGCCGTCTTGAATATTG (forward) and CAAGACGGCAGACTTAGCATGCATTCCATCTATTC (reverse); M4A, CCATTGCCGGCATGACCGCTGCATCCGCTGTCCATTCCATTGAAG (forward) and CTTCAATGGAATGGACAGCGGATGCAGCGGTCATGCCGGCAATGG (reverse); and M6A, GGATGACCGCCGCGTCCGCTGTCCACAACATAGAGTC (forward) and GGACAGCGGACGCGGCGGTCATCCCTGTGATTGTCAG (reverse). The correctness of the coding sequences in all constructs was verified by automated DNA sequencing. Further details on these constructs may be found in the Appendix.

Expression and Purification of Recombinant Proteins. N-ATP7B (and mutants thereof) derived from human ATP7B was expressed and purified as a fusion with maltose-binding protein (MBP) as described previously (158). Further details can be found in the Appendix. In brief, the fusion protein was coexpressed with thioredoxin in *E. coli* to maintain solubility and reducing state, purified by affinity chromatography over amylose

resin (New England Biolabs, Ipswich, MA), and eluted into buffer containing 10 mM maltose, 25 mM NaH_2PO_4, and 150 mM NaCl (pH 7.5). The levels of protein expression for mutants and wild-type N-ATP7B were comparable. For copper binding in vivo, 250 μM $CuCl_2$ was added to the growth medium prior to inducing protein expression for 3 h at 25 °C. Human ATOX1 was expressed in *E. coli* as a fusion with the chitin-binding protein in the pTYB12-intein vector as described previously (51) and purified by affinity chromatography over chitin resin (New England Biolabs). Further details can be found in the Appendix. Intein-mediated cleavage of chitin-binding protein and elution of ATOX1 were accomplished by incubating resin-bound fusion protein with buffer containing 50 mM dithiothreitol, 25 mM NaH_2PO_4, and 150 mM NaCl (pH 7.5) for 36 h at room temperature. ATOX1 was concentrated using Amicon ultrafiltration devices (Millipore, Billerica, MA) and then dialyzed against buffer containing 25 mM NaH_2PO_4 and 150 mM NaCl (pH 7.5) overnight at 4 °C to remove dithiothreitol.

ATOX1-mediated Copper Transfer. Prior to copper transfer experiments, 1 mg of purified N-ATP7B (at 9 mM) or 1 mg of ATOX1 (at 130 μM) was reduced with 1 mM tris (carboxyethyl)phosphine (TCEP) and then dialyzed into 1 liter of buffer A (25 mM NaH_2PO_4 and 150 mM NaCl (pH 7.5)) for 1 h. A 10:1 GSH/$CuCl_2$ solution made in buffer A was added to the reduced ATOX1 at a 1:1 molar ratio for 15 min at room temperature, followed by overnight dialysis to remove excess glutathione. For transfer reactions, increasing amounts of Cu-ATOX1 were added to 100 ng of apo-N-ATP7B for 15 min at room temperature. ATOX1 was then removed from the mixture by centrifugation through a Microcon YM-50 filter (Millipore); the concentrate containing

N-ATP7B was diluted with buffer A, and centrifugations were repeated three times to completely remove ATOX1. N-ATP7B was eluted with 100 µl of 25 mM NaH_2PO_4 (pH 7.5) containing 25 mM NaCl.

Copper-binding Stoichiometry. The concentration of purified proteins was determined with the Lowry assay (165). Copper concentration in samples was measured using atomic absorption spectroscopy (AA-6650G, Shimadzu, Columbia, MO), and a copper/protein molar ratio was averaged for each mutant in four independent experiments. Further details can be found in the Appendix.

X-ray Absorption Spectroscopy. N-ATP7B mutants were loaded with copper in cells as described above, purified, and concentrated to concentrations yielding >100 µM bound copper. CuK edge (8.9 keV) extended x-ray absorption fine structures (EXAFS) were collected at the Stanford Synchrotron Radiation Laboratory operating at 3 GeV with currents between 100 and 50 mA. All samples were measured and analyzed as described previously (166). For edge comparisons, all edges were normalized to have an intensity of 0 at 8970 eV and an intensity of 1 at 9000 eV.

Fluorescent Labeling of Cys Residues. 10 µg (91 pmol) of purified apo-N-ATP7B (wild-type and mutant) in elution buffer was taken for labeling of cysteines. 7-Diethylamino-3-(4′-maleimidylphenyl)-4-methylcoumarin (CPM; Invitrogen; Carlsbad, CA) was added in the dark for 5 min at a concentration of 10 µM and then quenched with 100 µM glutathione. Samples were run on a 12% Laemmli gel and rinsed 2×15 min in double-

distilled H_2O, and fluorescent images were taken using a FluorChem 5500 (Alpha Innotech Corp., San Leandro, CA). Gels were then fixed in 50% ethanol and 8% phosphoric acid for a minimum of 3 h, stained with colloidal Coomassie Blue G-250, and imaged again to normalize fluorescence intensity per protein present in the corresponding band. The fluorescence of fully copper-loaded N-ATP7B was defined as the background and was subtracted. Where indicated, samples were incubated in solutions containing either 100 μM TCEP for 10 min (to reduce disulfide bonds) or 6 M urea for 30 min (to expose buried Cys residues) prior to labeling with 10 μM CPM as described above.

Quantitation of Reduced Cys Residues. Quantitation of available cysteine residues was carried out using Ellman's reagent (5,5′-dithiobis(2-nitrobenzoic acid)) as described (167). Briefly, 10 μg (91 pmol) of purified apo-N-ATP7B (wild-type ± copper and m2A) in elution buffer was used for Ellman's reaction after adjusting the protein concentration for A_{280} measurements. Where indicated, samples were incubated in solutions containing either 100 μM TCEP for 10 min (to reduce oxidized cysteines) or 6 M urea for 30 min (to expose buried Cys residues), with all samples suspended in final volumes of 50 μl. Samples were added to 750 μl of 1 M Tris-HCl (pH 8.0), followed by the addition of 50 μl of 2 mM 5,5′-dithiobis(2-nitrobenzoic acid (in 50 mM sodium acetate) for 15 min and reading the absorbance at 412 nm. A calibration curve of acetylcysteine ranging from 31.25 μM to 1 mM was assayed in duplicate along with each set of test samples. The assay was repeated three times using the calibration curve to estimate total cysteines available per protein in the N-ATP7B samples.

Limited Proteolysis. 15 µg of eluted apo-N-ATP7B (wild-type and mutant) at 10 µM was digested with tosylphenylalanyl chloromethyl ketone-treated bovine pancreatic trypsin (Sigma) for 3 h at room temperature at a 1:3000 (w/w) protease/protein ratio in 83 mM ammonium bicarbonate (pH 8.0) containing 10 mM $CaCl_2$. The reaction was stopped by the addition of 1 mM 4-(2-aminoethyl)benzenesulfonyl fluoride hydrochloride. The protein fragments were separated on a 15% Laemmli gel and then fixed and stained with colloidal Coomassie Blue G-250. In some instances, CPM labeling and quenching were performed as described above prior to proteolysis.

Native Gel Electrophoresis. 20 µg of wild-type N-ATP7B was subject to limited proteolysis (see above) and then separated on a 10% Tris/glycine gel that did not contain urea, SDS, or reducing agents. The gel was fixed in 50% ethanol and 8% phosphoric acid for a minimum of 3 h and stained overnight with colloidal Coomassie Blue G-250. The lane containing the protein fragments was destained in 7% acetic acid, equilibrated in Laemmli running buffer containing 2 M urea for 1 h to redissolve proteins, layered onto a 12.5% Laemmli gel, and separated in the presence of 2 M urea and 0.1% SDS. This gel was then fixed and silver-stained as described (168).

In-gel Digests/Extractions. For protein identification by tandem mass spectrometry, Coomassie Blue-stained gels were washed in double-distilled H_2O, and relevant spots were excised. Spots were incubated twice in 500 µl of 50 mM NH_4HCO_3 in 50% acetonitrile for 30 min and then dried by removing the wash buffer and incubating in 100% acetonitrile for 2 min. If the samples had not been previously reduced and

alkylated, 100 µl of buffer containing 10 mM dithiothreitol and 100 mM NH_4HCO_3 was added for 45 min at 56 °C and removed, and 100 µl of buffer containing 55 mM iodoacetamide and 100 mM NH_4HCO_3 was added for 30 min at room temperature. This solution was removed, and 500 µl of buffer containing 50 mM NH_4HCO_3 and 50% acetonitrile was added for 15 min at room temperature. This solution was replaced with 200 µl of 100% acetonitrile for 2 min at room temperature. 20 µl of digestion solution (0.01 µg of trypsin, 44 mM NH_4HCO_3, and 4.4 mM $CaCl_2$) was added for 15 min at 4 °C. (For large spots, this was repeated until liquid was no longer absorbed.) Excess solution was removed, and 60 µl of digestion solution (without trypsin) was added at 37 °C for 16 h. To extract peptides, 3 µl of 88% formic acid was added for 15 min at 37 °C, and all of the supernatant was then collected for tandem mass spectrometry analysis.

Fluorescence Spectroscopy. Purified N-ATP7B-MBP was dialyzed into buffer containing 25 mM NaH_2PO_4 and 150 mM NaCl (pH 7.5) for 1 h and diluted to 0.3 mg/ml in the same buffer using A_{280} to evaluate and equate final concentrations. MBP was prepared in the same manner as N-ATP7B-MBP, dialyzed, and diluted to a final concentration of 0.12 mg/ml. 400-µl samples were taken for fluorescence emission scans using a SpectraMax M2 fluorescence cuvette reader (Molecular Devices, Sunnyvale, CA). Excitation wavelengths were set at either 280 or 295 nm, and emission readings were taken between 250 and 450 nm at 1-nm intervals using 10 scans per emission wavelength. Following scans, A_{280} measurements were taken to normalize the data for protein concentration. The experiment was performed three times, with a representative scan presented herein.

Modeling and Molecular Dynamics Simulations. Structures for MBD1 and MBD2 were generated through homology modeling (Modeler version 9v6) using human ATP7B (NCBI Protein Database accession number P35670) and then used to generate distance constraints for *Ab initio* modeling. *Ab initio* structure prediction was carried out using locally installed Rosetta *Ab initio* software (version 2.0, licensed through the University of Washington). The fragment libraries were generated using the Web version of the Rosetta fragment server (Robetta). Briefly, fragments for residues 56–214 of ATP7B were generated using the Robetta fragment server, and 10,000 independent structures were predicted using the above-generated distance constraints for MBD1 and MBD2. The connecting loop along with 5-residue anchors from MBD1 and MBD2 (residues 121–148) were extracted using the MMTSB tool set and subjected to a clustering analysis. Loop extraction was performed to avoid biasing the clustering algorithm through constrained MBDs (which are significantly longer than the connecting loop). The centers of the three largest clusters were chosen as the best models. The MBDs were then "ligated" back to the models for the connecting loops using the 5-residue anchors. The final models were minimized using CHARMM27 force fields and validated as described previously (169).

A 10.0-ns molecular dynamics simulation of MBD2 from ATP7A in explicit solvent was conducted using the NAMD version 2.6 molecular dynamics simulation package and the CHARMM27 force field. Because the structure of MBD2 from ATP7B was not available and because one can argue that the *Ab initio* models generated from Rosetta may not be accurate enough for molecular dynamics simulations, we used the structure of MBD2

from ATP7A (Protein Data Bank code 1s6o) (129). This structure of MBD2 (code 1s6o) was introduced in a box of TIP3P explicit water molecules that extended at least 10 Å away from the protein surface, and counterions were introduced to obtain a neutral system. The protonation status of the titratable residues corresponds to pH 7.0. The system was minimized in two steps: water minimization and entire system minimization. First, the system was subjected to 1000 steps of conjugate gradient energy minimization with the coordinates of the protein frozen to allow the solvent molecules to relax. A second 1000 steps of conjugate gradient energy minimization were then performed after unfreezing the protein to remove steric clashes found in the protein structure. The root mean square deviation (r.m.s.d.) as a function of time for the simulated structures was stable for 200 ps. The final equilibrated system that uses periodic boundary conditions has dimensions of 59.18, 64.22, and 64.92 Å. The resulting system was used in a 10.0-ns simulation that was performed in the NVT ensemble using a 2-fs time step and a Langevin thermostat with a 5 ps^{-1} damping parameter. The system temperature was coupled using the Berendsen algorithm at 300 K. Electrostatic interactions were calculated using the particle mesh Ewald with a real space cutoff of 0.9 nm. Cutoff for van der Waals interactions was set at 0.9 nm. A SHAKE algorithm was applied using a tolerance of 10^{-8}Å to maintain all bonds containing hydrogen at their equilibrium length. The time step for integration was 2 fs, and coordinates and velocities were saved every 2 ps. Simulations were analyzed using NAMD routines, and the data were plotted using GraphPad version 4.0.

Results

MBD2 Influences the Copper-binding Capability of Other N-terminal MBDs. To understand the relationships between different MBDs, we first generated and characterized the m2A mutant of N-ATP7B, in which the copper-binding CxxC motif of MBD2 was replaced with AxxA (Fig 2.2.A). Earlier experiments suggested that MBD2 may regulate access to other MBSs (see above). We hypothesized that MBD2 performs this gating role by interacting with other MBDs and changing the protein conformation of N-ATP7B (thus allowing access to other sites) in response to copper binding. Mutating MBD2 would disrupt this communication and cause insufficient exposure of other MBDs to ATOX1 and inadequate copper transfer. To test this hypothesis, we compared the copper loading of wild-type N-ATP7B and the m2A mutant by Cu-ATOX1. For wild-type N-ATP7B, as shown previously (51), all six MBDs could be loaded with copper (Fig 2.2.B). However, for the m2A mutant, instead of the expected stoichiometry of 5 copper atoms/protein, <3 copper atoms were transferred (maximum of 2.8 ± 0.5) (Fig 2.2.B) even using up to 60-fold excess of Cu-ATOX1 over N-ATP7B.

To test whether the decreased copper-binding stoichiometry of the m2A mutant was due to structural changes, we performed limited proteolysis on wild-type and m2A N-ATP7B and compared proteolytic patterns by separating fragments on an SDS-polyacrylamide gel (Fig 2.3). At the concentration used for limited proteolysis, trypsin cuts N-ATP7B at a limited number of specific sites in the loops connecting the MBDs, whereas individual 7–8-kDa MBDs and the 16-kDa MBD5/6 pair remain intact (see Fig 2.1.A) (140, 146).

FIG 2.2

A.

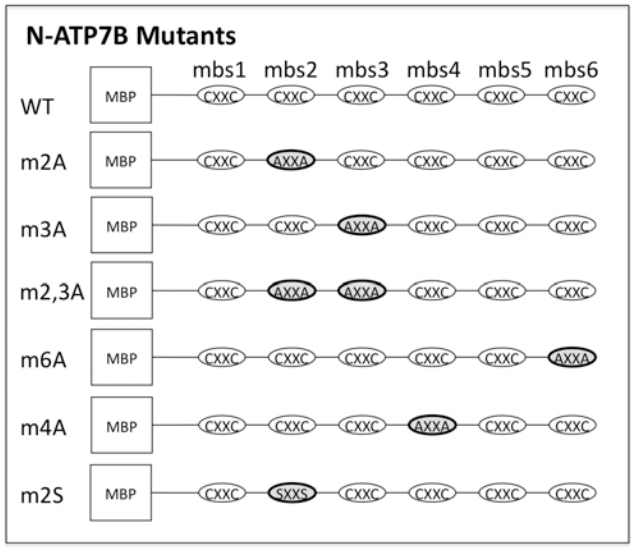

B.

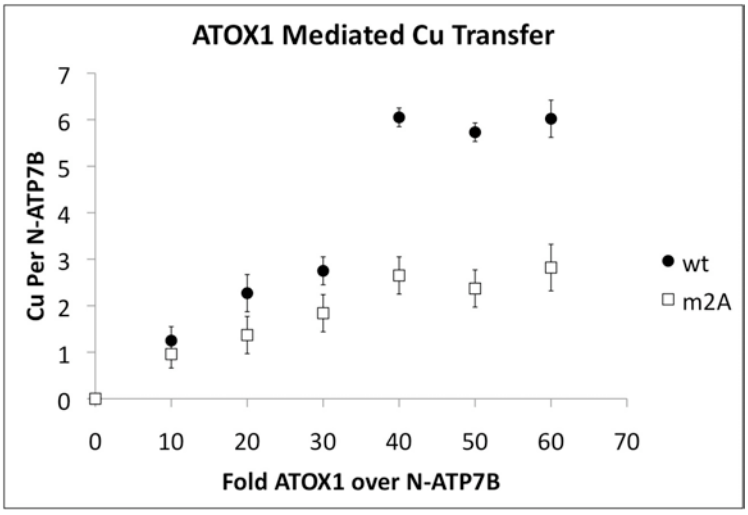

Figure 2.2. ATOX1-mediated copper transfer is impaired in the MBD2 mutant. **A.** Diagram of the N-ATP7B mutants used in this work. **B.** Copper transfer from Atox1 to N-ATP7B. Points represent the amount of copper that remains bound to N-ATP7B after incubation with the indicated amounts of Cu-ATOX1 and removal of Cu-ATOX1 from the mixture. Error bars indicate S.D. across three independent experiments. wt, wild-type N-ATP7B.

The fragmentation patterns of wild-type and mutant N-ATP7B were markedly different (Fig 2.3), demonstrating that the m2A mutation caused a conformational change in N-ATP7B. The mobility of several bands was increased (i.e. the fragments became shorter), suggesting that additional trypsin recognition sites in the loops were exposed. We investigated the kinetics of the proteolysis and found that the difference in pattern remained stable for several hours before patterns converged (Fig 2.S.1). Thus, the change in the MBS led to a new configuration of the loops connecting MBDs (see more in Discussion).

If the structural changes in the m2A mutant preclude appropriate exposure of the remaining MBDs to ATOX1, then incubating m2A with free copper (rather than with a relatively bulky ATOX1) is likely to yield higher copper-binding stoichiometry. To test this prediction, wild-type N-ATP7B and the m2A mutant were loaded with copper in cells by growing *E. coli* in medium supplemented with $CuCl_2$. Although *E. coli* lacks ATOX1 orthologs, wild-type N-ATP7B can be loaded with ~5.5 copper atoms/protein by metal taken up by cells (158). Contrary to our expectations, the m2A mutant still showed significantly reduced copper binding (2.6 ± 0.3 copper atoms/protein compared with the control at 5.3 ± 0.1 copper atoms/protein) (Fig 2.4). This result suggested that the m2A mutation impeded more than one MBD from binding (or retaining) copper and that the copper-binding status of the N-terminal MBDs depends on a functional MBD2.

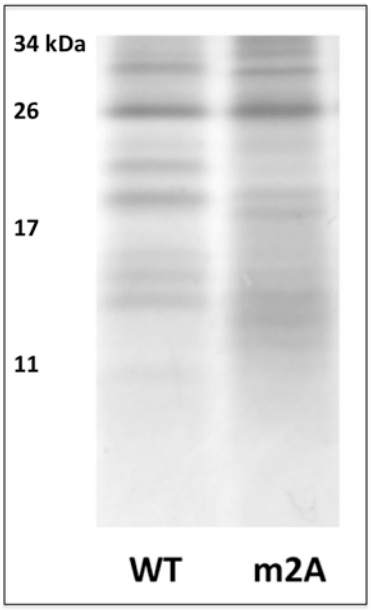

Figure 2.3. Mutation m2A induces structural changes in N-ATP7B. The Coomassie Blue-stained gel compares limited proteolytic patterns of wild-type (WT) and m2A N-ATP7B.

Mutations of Different MBDs Have Distinct Effects on Copper Binding by N-ATP7B. To determine whether the CxxC-to-AxxA mutations in other MBDs would have a similar effect on copper binding by N-ATP7B, we generated a series of mutants (Fig 2.2.A). The mutant proteins were expressed in *E. coli*, loaded with copper in cells, and purified, and their copper-binding stoichiometry was measured (Fig 2.4). Mutating MBD3 (m3A) decreased copper binding (2.2 ± 0.4 copper atoms/molecule) to a level similar to the m2A mutation. In contrast, mutants of MBD4 (m4A) and MBD6 (m6A) bound copper with stoichiometry close to what was expected for domains containing five intact MBSs (4.6 ± 0.2 and 4.9 ± 0.1, respectively). Interestingly, when both MBD2 and MBD3 were mutated (in the m2/3A variant), the remaining sites bound copper with a stoichiometry close to the expected 4 copper atoms (3.6 ± 0.3) as if a negative effect of each individual mutation was counteracted. Altogether, these data suggest that MBD2 and MBD3 may work together to regulate access to other MBSs, whereas MBD4 and MBD6 receive copper independently, following transfer of copper to MBD2 and MBD3.

Decrease in Copper-binding Stoichiometry Is Due to Cys Oxidation. To better understand how mutation in MBD2 decreases the number of available copper-binding sites, we first examined whether the mutation altered the arrangement of the remaining intact sites, possibly causing more than one MBD to coordinate the same copper molecule. In wild-type N-ATP7B, each copper is coordinated by two sulfur groups of the CxxC motif in a linear fashion with bond lengths of 2.2 Å (132). EXAFS characterization of copper bound to m2A showed no significant deviation from this wild-type coordination (Fig 2.S.2). Similar copper coordination was also observed for the

m2/3A mutant. These results suggested that the decrease in copper-binding stoichiometry was unlikely due to changes in the copper-coordinating environment but rather was caused by the loss of copper-binding sites.

To estimate the number of available sites, Cys residues in both wild-type and mutant apo-N-ATP7B were labeled with the Cys-directed fluorescent maleimide CPM (Fig 2.5.A). The m2A mutant showed a marked decrease in CPM labeling (~33% compared with wild-type N-ATP7B). To further test for specificity of the m2A mutation with respect to Cys reactivity, we performed CPM labeling of other mutants described in Fig 2.2.A. The only mutant besides m2A to have a significant reduction in CPM labeling was m3A (Fig 2.5.B), which was also the only mutant to have a sharp decrease in copper binding. To ensure that this observation was not the artifact of the purification procedure, we labeled crude *E. coli* lysates with CPM prior to protein purification (Fig 2.S.3.A). Lower fluorescence of m2A was again detected, demonstrating that the loss of available cysteines happened during the expression of the protein, consistent with the loss of in-cell copper binding by these mutants (Fig 2.4).

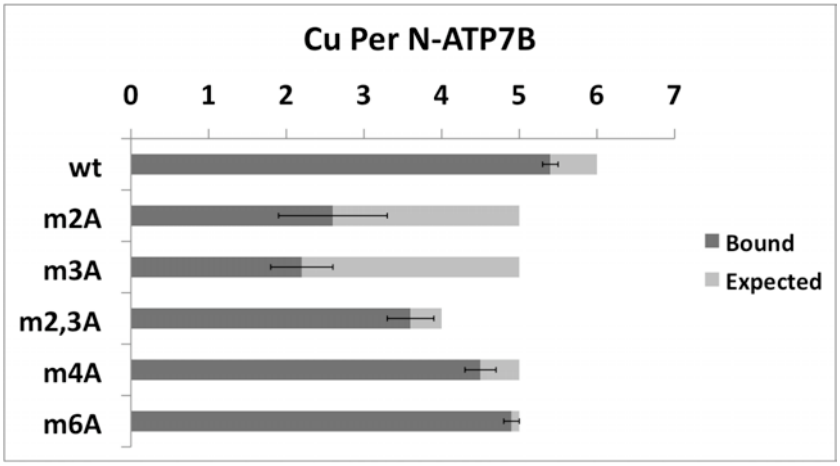

Figure 2.4. Mutations in MBDs have distinct effects on the copper-binding stoichiometry of N-ATP7B mutants. Wild-type (wt) and mutant N-ATP7B were loaded with copper in *E. coli* prior to purification. Light gray bars indicate the number of CxxC motifs left intact. Dark gray bars represent experimental values as determined by atomic absorption (copper) and Lowry assay (protein). Error bars indicate S.D. across three experimental repeats.

A.

	WT	WT	m2A	m2A	WT +Cu
TCEP	+	-	+	-	-
% of wt	110±5	100	66±5	33±7	N/A

B.

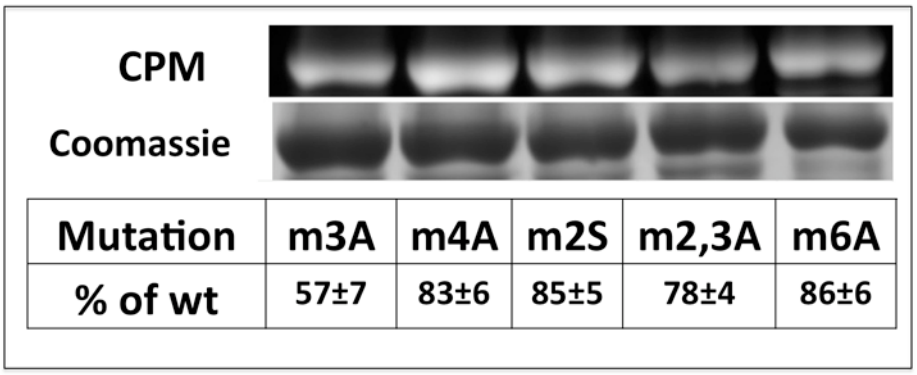

Mutation	m3A	m4A	m2S	m2,3A	m6A
% of wt	57±7	83±6	85±5	78±4	86±6

Figure 2.5. Comparison of Cys-directed fluorescent labeling for wild-type and mutant N-ATP7B. A. fluorescent (upper) and Coomassie Blue-stained gel (lower) images of wild-type (WT) and m2A N-ATP7B labeled with CPM. The tables indicate intensity of fluorescent labeling per protein compared with wild-type apo-N-ATP7B. The indicated samples were treated with TCEP prior to labeling. The lane on the right shows CPM labeling of copper-loaded wild-type N-ATP7B used as a background control. N/A, not applicable. **B.** Fluorescent (upper) and Coomassie Blue-stained gel (lower) images of additional mutants shown in Fig. 2A, with label/protein ratios indicated in the table. Average percentages and S.D. are indicated for three experimental repeats.

To examine whether the decrease in CPM labeling was due to blocked access to the sites or oxidation of Cys residues, we repeated labeling experiments after treatment of N-ATP7B with the disulfide-reducing agent TCEP (Fig 2.5.A). With TCEP treatment, the m2A mutant regained about half of the lost fluorescence (to 67% of the wild-type protein). (The wild-type protein also gained ~10% CPM labeling after TCEP treatment, which we ascribe to the recovery from normal oxidation during protein purification.) The lower free thiol reactivity of the m2A mutant was further confirmed using Ellman's reaction (Fig 2.S.3.B). Altogether, these data suggest that the m2A and m3A mutations render N-ATP7B susceptible to oxidation.

Tight Packing of MBDs Allows for Cross-communication. The marked effect of the m2A and m3A mutations on other MBDs suggested that the MBDs closely interact with each other despite being connected by long loops. To examine how tightly the MBDs interact, we subjected wild-type apo-N-ATP7B to limited proteolysis and separated the resulting fragments on a native Tris/glycine gel. Fig 2.6.A illustrates that, under nondenaturing conditions, most of the fragments remained associated and migrated together. The 8–12-kDa bands that did dissociate were further trypsinized in-gel, extracted, and analyzed by mass spectroscopy. They were identified as containing peptides from MBD1 and MBD2 (Fig 2.S.4). The band containing associated fragments was excised and separated on a regular Laemmli gel. The reducing and denaturing conditions restored the banding pattern (Fig 2.6.B). The 8–12-kDa bands were also detected in the second dimension, indicating that these fragments interact with the rest of the bundle, but perhaps less tightly.

The interdependence of MBDs in N-ATP7B was further confirmed by performing limited proteolysis of other mutants described in Fig 2.2.A. Distinct proteolytic patterns for these mutants (Fig 2.S.5) indicated that MBD packing controls the exposure/orientation of connecting loops in a very precise manner.

Flexibility of the Copper-binding Loop Allows for Changing Exposure of Sulfhydryl Groups. Having established interaction between MBDs, we investigated the mechanism of inter-domain communication. The copper-binding CxxC site is situated at the surface of MBD2 and must be sufficiently exposed for ATOX1 to dock and transfer copper (Fig 2.1.B). Therefore, it was not apparent how mutating Cys residues to Ala in the exposed loop would affect the conformation of the entire N-ATP7B. We considered that the sulfhydryl group of Cys, unlike the side chain of Ala, is capable of forming a hydrogen bond. Others have demonstrated differential dynamics and flexibility of the metal-binding loops of various MBDs using molecular dynamics simulations (143). We hypothesized that, in the apo form, the metal-binding loop of MBD2 may be flexible enough to reach and interact with other MBDs and that the ability of sulfhydryl groups to hydrogen bond would be important for the inter-domain contacts.

A. **B.**

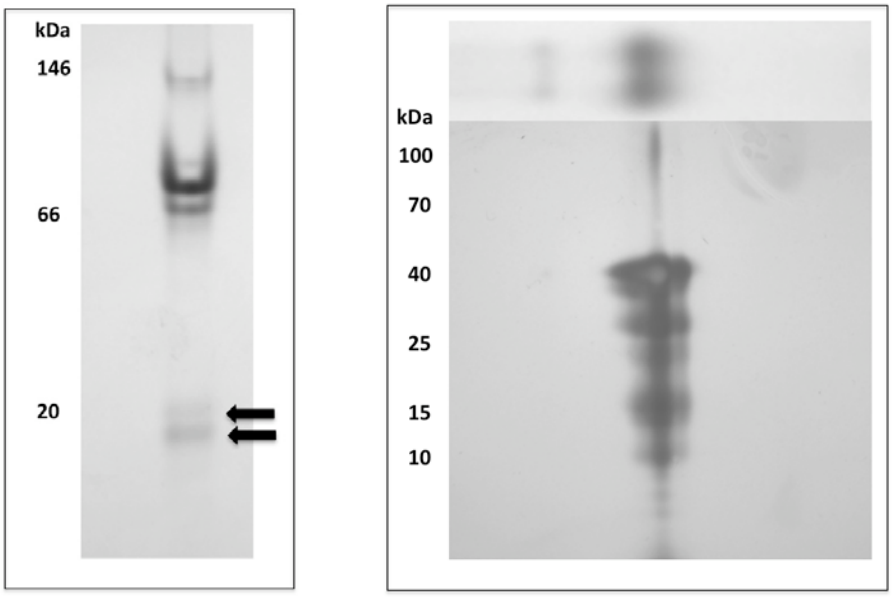

Figure 2.6. MBDs in N-ATP7B are tightly packed. A. Wild-type N-ATP7B was subjected to limited proteolysis as described in the legend to Fig. 3 and separated on a native Tris/glycine gel. Under these conditions, most of the fragments stayed together. The gel was stained with Coomassie Blue. Arrows indicate bands that were ID'd with MS/MS as containing MBD1 and MBD2 (See Supplimentary Fig 2.S.4) **B.** The gel lane containing fragments run on a native gel was then cut and placed on top of a Laemmli gel and separated in the second dimension under reducing and denaturing conditions. The fragments no longer migrated together (silver staining).

To test this hypothesis, we first examined the flexibility of MBD2 using molecular dynamics simulations. The structure of MBD2 of ATP7B is not available; rather than using a model, we characterized the dynamics of MBD2 of ATP7A, for which structures have been solved (129) and which has 60% identity and 77% similarity to MBS2 of ATP7B. Figure 2.S.6 compares the structure of MBD2 (Protein Data Bank code 1s6o) with the TIP3P explicit solvent-equilibrated structure used for the molecular dynamics simulation. The results show that the initial structure and the equilibrated structure used for this simulation display a r.m.s.d. of <1.0 Å. Following a 10,000-ps simulation of dynamic movement in solution, we calculated r.m.s.d. values for the backbone carbons, as well as distances between the α-carbons and sulfurs of the metal-binding Cys residues (Fig 2.7.A). Overall, the structure was quite stable, with a maximum backbone r.m.s.d. of 2.12 Å. The distance between the α-carbons of the Cys residues showed higher flexibility (between 5.0 and 8.4 Å) but overall remained fairly constant. The R-groups of the Cys residues have larger rotational freedom (particularly the N-terminal Cys), as evidenced by S–S distances that ranged from 3.2 to 12.5 Å. This flexibility allowed the CxxC-containing loop to adopt conformations in which the metal-coordinating sulfurs faced either toward or away from each other (Fig 2.7.B). In the former conformation, the cysteines are well positioned to bind copper. In the latter conformation, the N-terminal Cys is angled away from the rest of the MBD and could potentially be involved in inter-MBD interactions.

A. **B.**

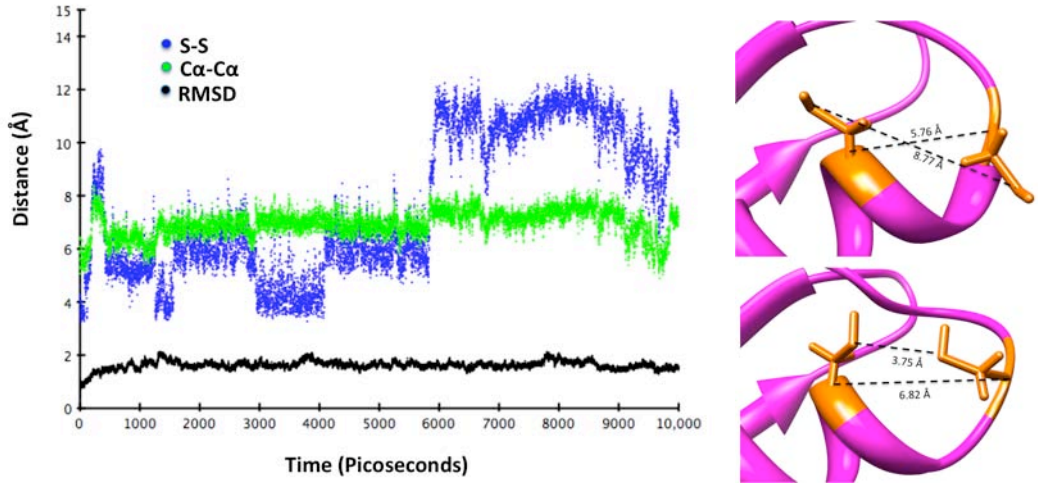

Figure 2.7. Molecular dynamics simulation of MBD2 of ATP7A illustrates the mobility and exposure of cysteines. A. Relevant distances calculated for each frame of a 10,000-ps simulation. Black dots (RMSD) indicate overall backbone r.m.s.d. for the protein. Green dots (Cα–Cα) indicate the distance between α-carbons of metal-binding cysteines. Blue dots (S–S) indicate the distance between sulfur atoms of metal-binding cysteines. **B.** Different orientation of the metal-binding loop from molecular dynamics simulation. Upper, loop with metal-binding cysteines facing away from each other; lower, loop with metal-binding cysteines facing toward each other. The molecular dynamics simulations were performed by Dr. Ujwal Shinde.

Hydrogen Bonding May Play a Role in the N-ATP7B Folding and Redox State. To examine the role of hydrogen bonding, we generated an N-ATP7B mutant with the CxxC motif of MBD2 mutated to SxxS (m2S). We hypothesized that this mutant would lose copper binding at MBD2 but would retain the hydrogen-bonding characteristics of the wild-type protein; thus, the reduced state of other MBDs and their ability to bind copper would be preserved. Indeed, in contrast to the m2A mutant, the m2S mutant bound close to the expected 5 copper atoms (4.7 ± 0.3) (Fig 2.8.A). Similarly to m4A and m6A, which bound close to the expected amount of copper, the m2S mutant did not show any significant decrease in CPM labeling (Fig 2.5.B). In addition, when subjected to limited proteolysis, the m2S mutant displayed a fragmentation pattern that was more similar to the wild-type than to the m2A pattern (Fig 2.8.B).

These results strongly suggest that the hydrogen-bonding ability of the Cys residues is critical for the overall folding of N-ATP7B. To further test this conclusion, we compared intrinsic Trp fluorescence in wild-type N-ATP7B and the m2 mutants (Fig 2.8.C). N-ATP7B contains 2 Trp residues: at the very N terminus before MBD1 (residue 29) and in the loop between MBD1 and MBD2 (Fig 2.1.A). Compared with apo-N-ATP7B, the m2A mutant had a higher fluorescence (110 ± 4% of the wild-type protein), suggesting a greater exposure of Trp to solution. Unlike m2A, the m2S mutant did not show an increase in fluorescence (96 ± 2% compared with the wild-type protein), a result consistent with its behavior in other tests. Similar results were obtained when fluorescence was measured using an excitation wavelength of 295 nm (data not shown).

Finally, if the metal-binding Cys residues in MBD2 play a role in interdomain communication, then the transfer of copper from ATOX1 to N-ATP7B is expected to have an effect on N-ATP7B conformation. Figure 2.8.D illustrates that the proteolytic pattern of ATP7B indeed changed significantly with each copper transferred. The changes were not identical to those observed in m2A (perhaps reflecting different functional consequences of copper binding and mutation), although the downward shift of bands resembling the m2A pattern was detected after 2 copper atoms were bound (Fig 2.8.D).

Ab Initio Modeling of MBD1 and MBD2 Suggests Potential Orientations for These Domains. To visualize how MBD2 might interact with neighboring MBDs, we performed *Ab initio* folding simulations on the Val^{57}–Lys^{213} sequence, corresponding to MBD1-loop-MBD2. As a control of accuracy of our predictions, we subjected sequence Gly^{169}–Gln^{241} of ATP7A (corresponding to MBD2) to the same folding prediction protocol and compared the obtained model with the available structure. Supplemental figure 2.S.8 illustrates that the most common solution cluster for MBD2 is similar to the published structure (r.m.s.d. of 1.928). For MBD1-loop-MBD2, the minimized centers of the three largest solution clusters are shown in Figure 9. In each cluster, MBDs are folded into the expected ferridoxin-like structures. The inter-MBD loop shows a tendency to form an α-helix, giving the two-domain construct a clamshell-like structure. In this structure, the MBDs and their respective MBSs can be brought together when the loop takes on a more structured conformation, which in turns alters the exposure of proteolytic sites located within the loop.

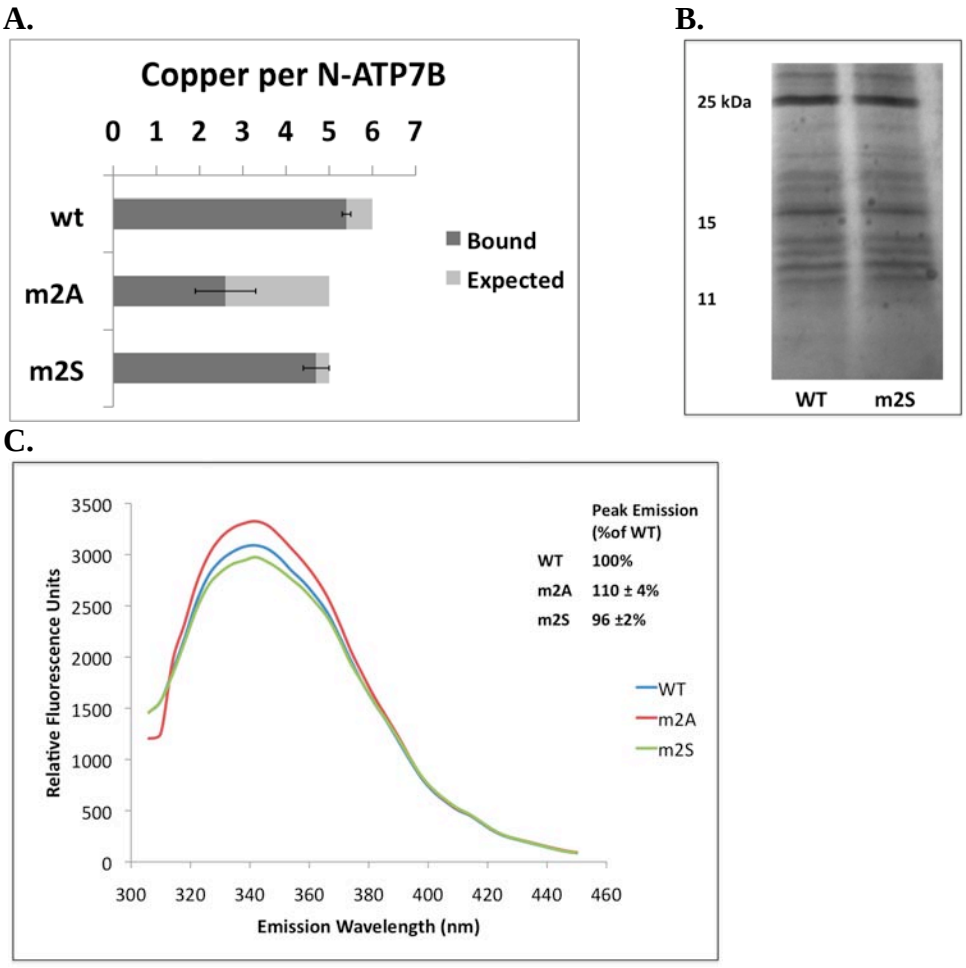

Figure 2.8. Mutations m2A and m2S have different effects on the conformation and oxidation state of N-ATP7B. **A**. Copper-binding stoichiometries of wild-type N-ATP7B (wt) and the m2A and m2S mutants. **B.** Coomassie Blue-stained gel comparing limited proteolysis of wild-type and m2S N-ATP7B. **C.** Fluorescence emission spectra of apo-N-ATP7B when excited with 280 nm UV light. Representative curves are shown for wild-type (blue), m2A (red), and m2S (green) N-ATP7B, with average peak emissions (342 nm) for three experiments shown in the inset. **D.** Proteolytic patterns of wild-type apo-N-ATP7B and N-ATP7B with one or two Cu^{+} atoms transferred from ATOX1.

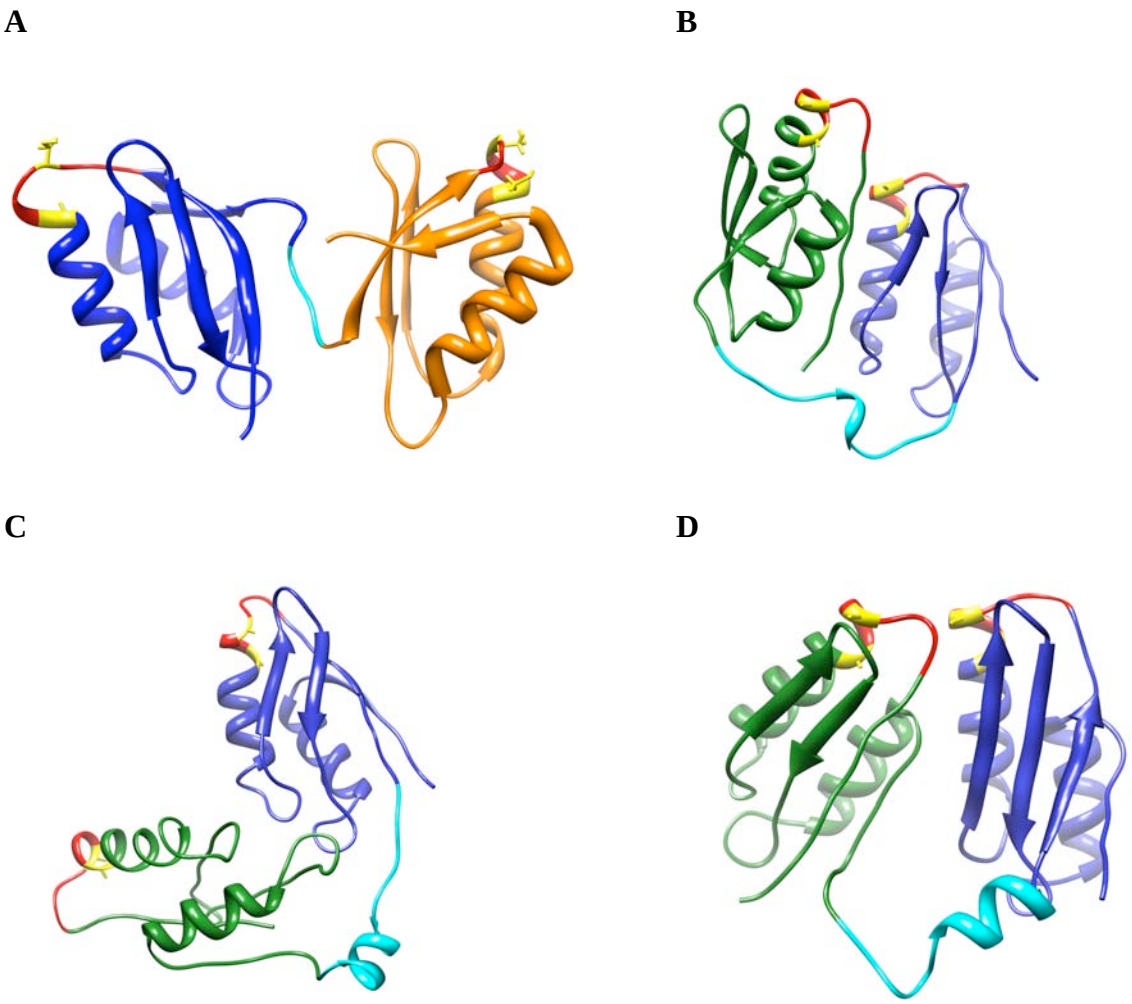

Figure 2.9. Structures of pairs of neighboring MBDs. A. Structure of MBD5 and MBD6 of ATP7B **(**adapted from Achila et al 2006 (124)) **(**PDB code : 2ew9). **B-D**. Ab initio structures for MBD1 and MBD2. MBD1 is shown in green, the inter-MBD loop in cyan, and MBD2 in blue. The GMxCxxC loop is shown in red, and copper-binding Cys residues are shown in yellow. Ab initio structures were compiled in Rosetta by Dr. Ujwal Shinde.

Discussion

We have demonstrated that the regulatory N-terminal domain of ATP7B is arranged with the MBDs in close contact and communication with each other. The tight packing of MBDs fixes the connecting loops in distinct conformations and allows for small structural changes in individual MBDs to be transmitted to other MBDs and modify the exposure of the connecting loops. The inter-domain communication appears to require hydrogen bonding, which also contributes to the maintenance of the redox status of metal-binding Cys residues. MBD2, the site of primary copper transfer from ATOX1 (when the fully folded N-ATP7B is used), along with MBD3 plays a central role in maintaining the conformation and reduced state of the entire N-terminal domain.

NMR and crystal structures of individual MBDs show only minor differences between the copper-bound and apo forms (124-131). However, the conformation and secondary structure of apo-N-ATP7B and copper-loaded N-ATP7B differ significantly (57, 146). Our data show that, even in the apo form, MBDs are packed tightly, albeit not rigidly, together. Copper binding to the CxxC site, which causes the inward movement of the loop, making it rigid and less exposed (129), appears to alter the contacts between MBDs (as do the Cys-to-Ala mutations) and induces changes in the structure of loops connecting MBDs. The change in loop structures/orientations is likely to be an important event in regulating ATP7B because it may expose sites for kinase-mediated phosphorylation located within the loops (146, 170).

Conformational changes in the loops may also provide docking sites for trafficking machinery (55) while burying residues that interact with the ATP-binding domain and disrupting inte-rdomain interactions (139). It is interesting that the conformational effects of mutating different MBDs (or sequential copper binding) are not identical as evidenced by distinct and stable proteolytic patterns. This diversity of consequences may be necessary for a fined-tuned response to various concentrations of copper and may explain the poorly understood need for multiple copper-binding sites in N-ATP7B.

The effect of m2A and m3A mutations on the oxidation state and copper-binding ability of other MBDs was unexpected. The drastic difference between m2A and m2S was particularly striking. These results suggest that hydrogen bonding may be required for both the precise packing and maintenance of the reduced state of N-ATP7B. The flexibility of the metal-binding loop in MBD2 could be critical for allowing communications between MBDs (and between MBD and ATOX1) (143). It is interesting to consider that the stabilization of a Cys residue in a more extended conformation through hydrogen bonding is likely to decrease the probability of forming disulfide bonds and thus preserve the reduced state of the MBDs. This view is supported by our observation that, in wild-type N-ATP7B, MBD2 is reduced and available for Cys labeling, whereas following proteolysis (when precise contacts are disrupted), MBD2 rapidly oxidizes and cannot be labeled with CPM (Fig 2.S.7). Our data also suggest that some Cys residues could be oxidized irreversibly (Fig 2.S.3.B) possibly to sulfinic or sulfonic acid, as has been observed for other Cys-containing metalloproteins (171). Although this may be a by-product of our expression system, these in vitro data raise an interesting question as to how the reduced state of N-ATP7B is maintained in a cell. A

previous report on a copper-dependent interaction between N-ATP7B and glutaredoxin suggests one possible reduction mechanism (172).

It is also intriguing that the m2A and m3A mutants have a similar increase in oxidation and loss of copper binding, whereas mutating both MBDs in tandem relieves this effect (Figs 2.4 and 2.5.B). This observation suggests that, although both MBDs play an important role in regulating the status of other MBDs, they each do not have individual downstream partners. The proteolytic pattern of the m2/3A mutant is distinct from that of either m2A or m3A (Fig 2.S.5.B). It is possible that this distinct conformation favors the "proper" orientation of the remaining MBDs, although we did not explore this further in this study. It is clear that not every change in conformation is associated with increased susceptibility to oxidation. The m6A mutant had a similar proteolysis pattern to the m2A mutant (Fig 2.S.5.A), even though it bound copper and labeled with CPM at predicted levels. This suggests that the conformational changes in loops and redox sensitivity of MBSs are related but not dependent on one another and further demonstrates the unique role MBD2 plays in regulating access to other MBSs in N-ATP7B.

We attribute the changes in the proteolytic pattern of the m2A mutant to be predominantly due to the dissociation of MBD3 and MBD1 from MBD2 and exposure of additional trypsin sites that are inaccessible when the domains are packed tightly together (Fig 2.1.A). This is supported by the increase in tryptophan fluorescence in the mutant, which we think is likely due to the exposure of the Trp residue in the loop connecting MBD1 and MBD2. We also observed some dissociation of MBD1 and MBD2 when the

digested domain was separated on a native gel (Fig 2.6.A). Our *Ab initio* structures (Fig 2.9) provide a clue to the potential interaction between MBD1 and MBD2. The loop connecting the two domains seems to have some inherent α-helical tendencies, which could bring the two MBDs close together, but can also unfold and increase the distance between the MBDs. Molecular dynamics simulations of apo- and Cu-ATOX1, which is a structural homolog of MBDs, suggest that copper binding may increase the flexibility of the portion of the MBD opposite from the metal-binding loop, thus influencing pairing of other MBDs (144). This change could be transmitted through the loop region, imparting more structure to the loop in the copper-bound state and bringing the MBDs closer together. Previous EXAFS analysis of copper-loaded N-ATP7B consistently showed a Cu–Cu distance of 2.6 Å (132), indicative of close proximity between pairs of MBSs.

In summary, we have presented a working model in which close packing of N-ATP7B allows cross-talk among MBSs. This interdomain communication is necessary for maintenance of reduced cysteines and proper copper acquisition. The MBD interactions may involve a hydrogen-bonding network that allows copper binding to be translated into larger structural rearrangements via the loops between the MBDs. These rearrangements are likely to play a major role in regulating ATPase activity as well as mediating interactions with cellular trafficking machinery. Maintaining the precise interdomain contacts could also be essential for success of high-resolution structural studies of N-ATP7B, which, so far, have represented a significant challenge.

Supplemental Figures

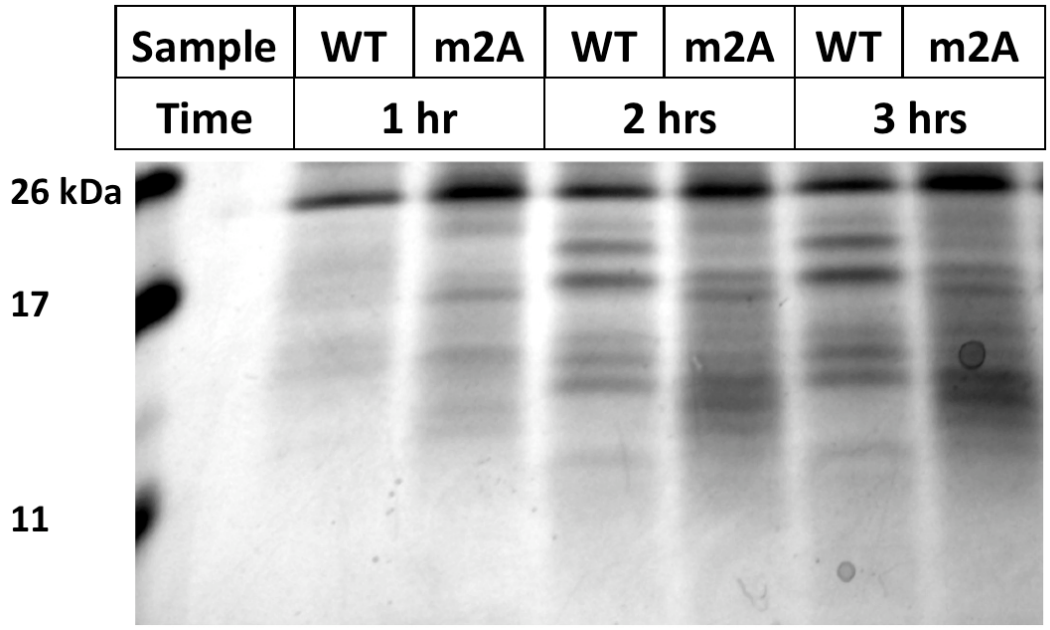

Figure 2.S.1. Time course of limited proteolysis of wt and m2A N-ATP7B. Coomassie stained gel showing limited proteolysis of wt and m2A N-ATP7B after different digestion periods.

Experimental Series				1st Shell			2nd Shell			-E_o (eV)	*F*
Sample	[Cu] μM	Cu/P	Reconstitution	Scatterer	Distance (Å)	Debye-Waller (Å²)	Scatterer	Distance (Å)	Debye-Waller (Å²)		
WND-2	250	2.8	In vivo	2.0 Cu-S	2.21	0.010	0.5 Cu	2.66	0.014	3.36	0.410
WND-2,3	310	3.4	In vivo	2.0 Cu-S	2.20	0.010	0.4 Cu	2.69	0.019	3.55	0.500

Figure 2.S.2. EXAFS analysis of copper loaded m2A and m2,3A. Refined data models for mutant N-ATP7B loaded with Cu in *E. Coli*. EXAFS data was collected and evaluated by Drs. Amanda Barry and Ninian Blackburn.

2.S.3

A.

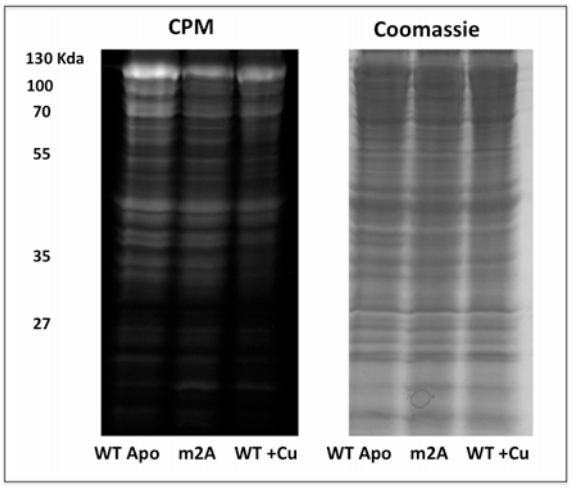

B.

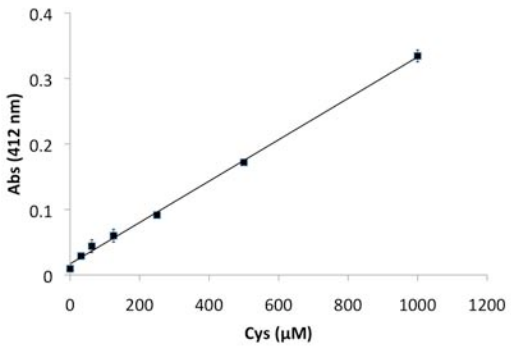

C.

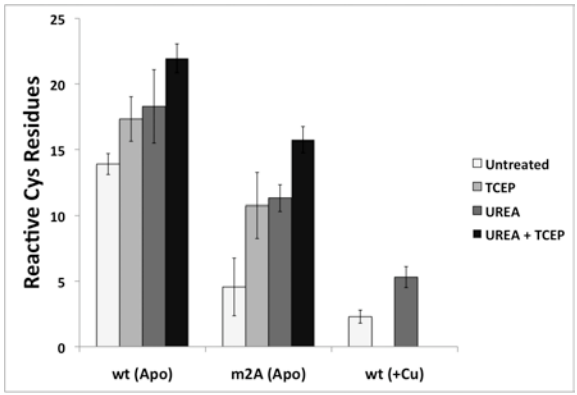

Figure 2.S.3. MBD2 mutation leads to rapid oxidation of N-ATP7B. A. CPM labeling of unrefined *E Coli* lysate from cells expressing N-ATP7B and Thioredoxin. N-ATP7B is the major band with a mw of 108 kDa. **B.** Ellman's reaction to determine quantitation of reduced cysteine. **Top**– Calibration curve of acyl-cysteine. **Bottom** – calculated values for wt and m2A ATP7B under untreated, reducing and denaturing conditions. Under untreated and reducing conditions the data closely resembles the densitometry data in Figure 5. The m2A mutant recovered some additional cys reactivity under denaturing conditions (when compared to wt recovery), suggesting some of the loss of labeling was due to accessibility of Cys residues.

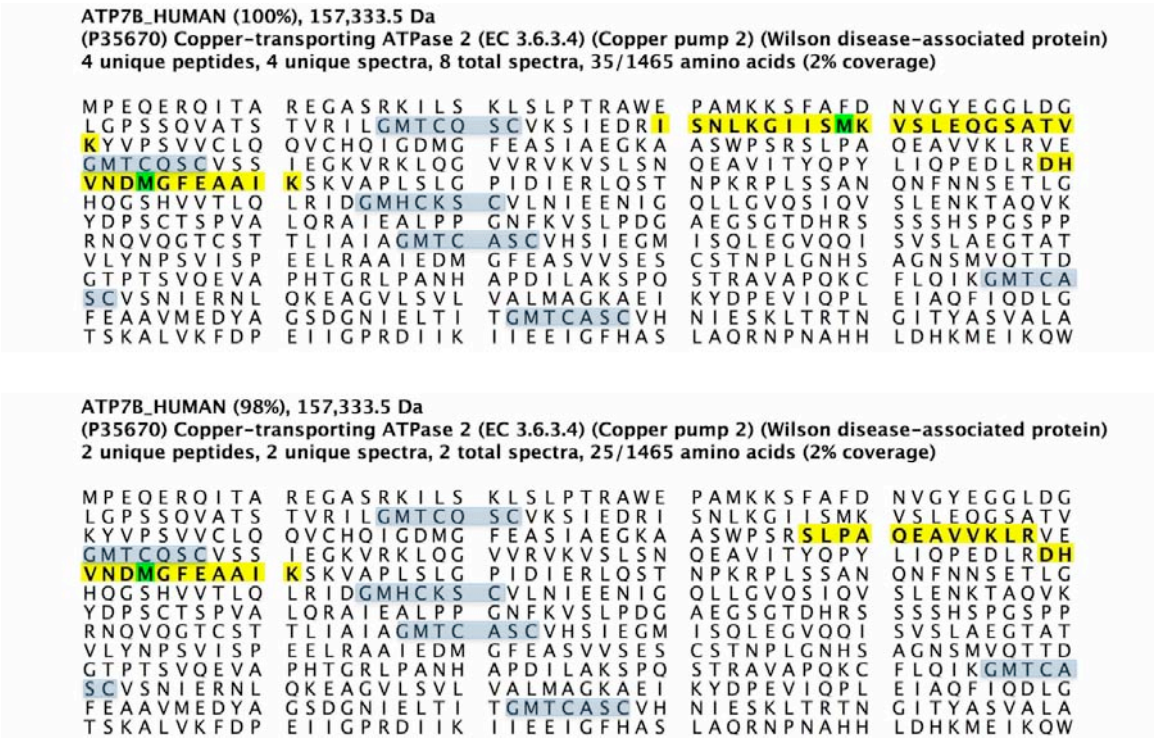

Figure 2.S.4. MS peptide IDs from native gel electrophoresis. Peptides recovered from excised bands in figure 2.6 (top). **Top -** upper dissociated band**. Bottom** – lower dissociated band. Yellow highlighted regions were identified by MS/MS. Metal binding sites are indicated in blue. MS/MS experiments were performed and analyzed by Dr. Martina Ralle.

A. **B.**

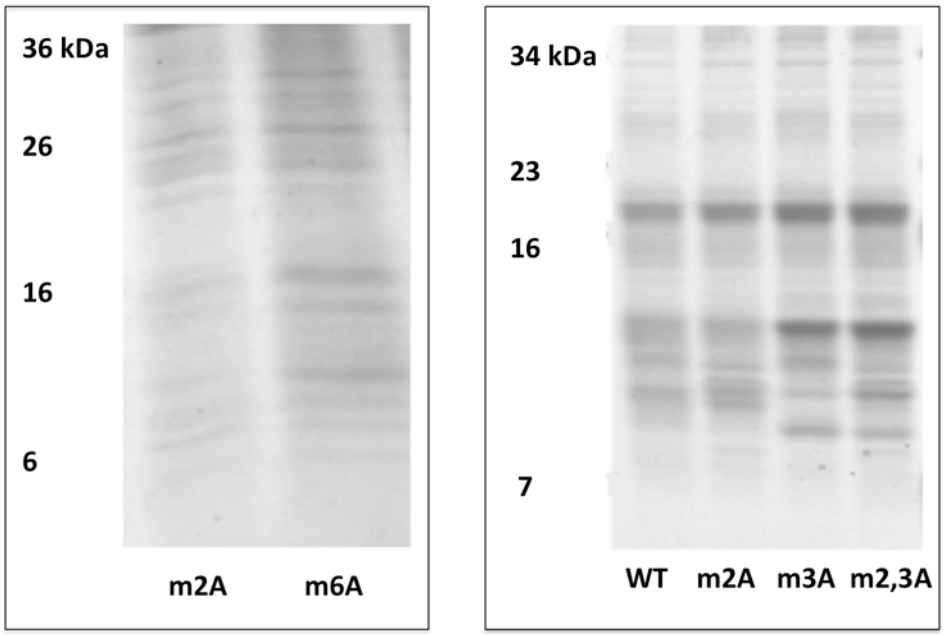

Figure 2.S.5. Limited proteolysis of mutant N-ATP7B. **A.** Coomassie stained gel showing limited proteolysis of m2A and m6A mutant. **B.** Coomassie stained gel showing limited proteolysis of wt, m2A, m3A and m2.3A mutants. Proteolysis experiments in panel B were performed by Dr. Joel Walker.

Figure 2.S.6. Molecular dynamics of MBD2 of ATP7A. Orange : Structure of Apo-MBD2 of ATP7A (from Banci et al., 2004 (129) PDB code: 1s6o) used as 0 ps time point in MD simulation. Pink : Structure of Apo-MBD2 of ATP7A at 200 ps time point of MD simulation. The RMSD of these two structures was less than 1 Å, demonstrating the stability of the structure throughout the simulation. MD simulation performed by Dr. Ujwal Shinde.

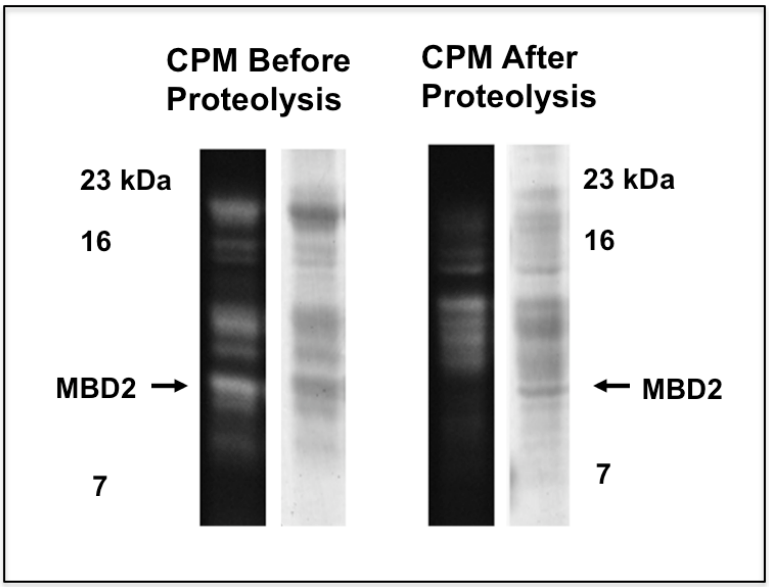

Figure 2.S.7. Oxidation of MBS2 following proteolysis. **Left** : Fluorescence and Coomassie stained images of WT N-ATP7B that was labeled with CPM, then subject to limited proteolysis, and separated on a Laemmli gel. **Right** : Fluoresence and Coomassie stained images of WT N-ATP7B that was subject to limited proteolysis, then labeled with CPM, then subject to limited proteolysis. Indicated band corresponding to MBD2 identified by MS/MS. Labeling and proteolysis experiments were performed by Dr. Joel Walker. MS/MS data was collected by Dr. Martina Ralle.

A. **B.**

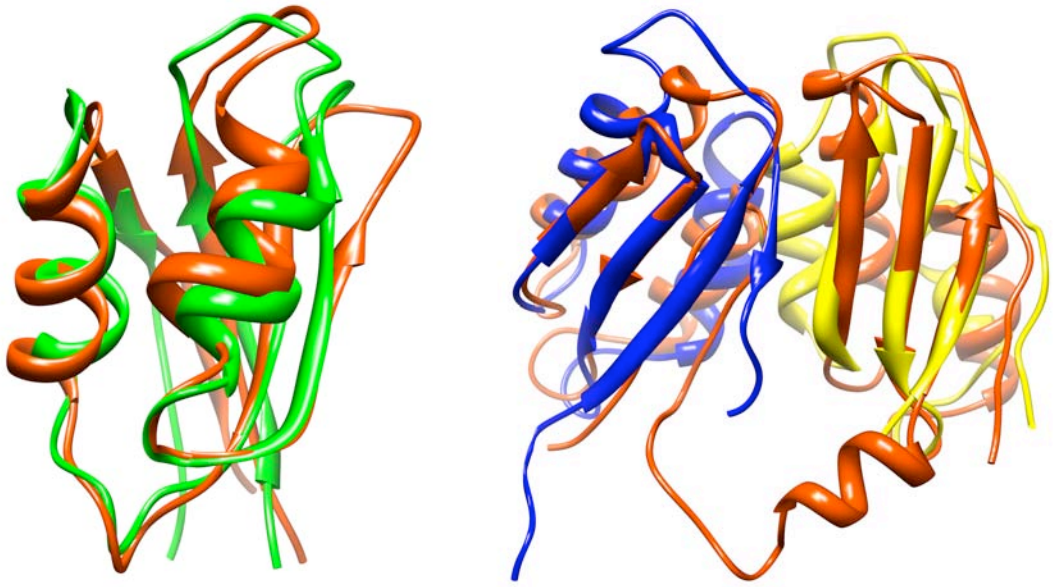

Figure 2.S.8. Superposition of solution structures and *Ab initio* simulations. (A) Alignment of ATP7A MBD2 solution structure and *Ab initio* model. Orange : Minimized *Ab initio* structure of Apo-MBD2 of ATP7A. Green : Solution structure of Apo-MBD2 of ATP7A (adapted from Banci et al., 2004 (129) PDB code : 1s6o). **(B)** Alignment of ATP7B MBD1-2 *Ab intio* structure with solution structures of MBD1 and 2 from ATP7A. Orange : *Ab initio* structure of Apo-MBD1-2 of ATP7B. Blue : Solution structure of Apo-MBD1 of ATP7A (adapted from De Silva et al., 2005 (130) PDB code : 1kvi). Yellow : Solution structure of Apo-MBD2 of ATP7A (adapted from Banci et al., 2004 (126) PDB code : 1s6o). In this alignment, MBD1 had an RMSD of 3.54 Å, whereas MDB2 had an RMSD of 4.58 Å. *Ab initio* structures were compiled in Rosetta by Dr. Ujwal Shinde.

Chapter 3

Characterization of copper transfer from ATOX1 to the N-Terminal domain of ATP7A uncovers functional differences between ATP7A and ATP7B

Abstract

ATP7A and ATP7B are two related Cu-ATPases essential for human copper homeostasis with similar, but complementary functions. Both ATPases are characterized by cytosolic N-Termini that contain six metal binding domains (MBDs) each capable of binding copper. Through interactions with the copper chaperone ATOX1, the N-Terminal domains sense cytosolic copper levels, and use this information to regulate ATPase activity and localization. We demonstrate here that ATOX1 transfers up to six copper atoms to either N-ATP7A or N-ATP7B, but that N-ATP7B acquires all six copper with a lower concentration of ATOX1. ATOX1 can also fully metallate N-ATP7B at less than a maximum concentration if presented repeatedly. For both N-Terminal domains, copper acquisition from ATOX1 is an ordered event with a preferential target site for the primary copper transferred. Unlike N-ATP7B, N-ATP7A does not show an altered proteolysis pattern upon copper binding, although a change in the electrophoretic mobility of the domain is seen in the Cu-bound state. These data suggest that N-ATP7A has a different response to copper binding than does N-ATP7B. When simultaneously presented with the N-Terminal domains of both Cu-ATPases, ATOX1 does not prefer one domain to the other. However, N-ATP7B shows stronger cooperativity compared to N-ATP7A; in the cell, this property may allow ATP7B to acquire copper at lower chaperone concentrations.

Introduction

Copper is an essential cofactor used by numerous enzymes that utilize the metal's redox potential to catalyze electron transfer reactions. Copper is kept under strict homeostatic control on both the cellular and organismal levels to ensure proper distribution and removal of this necessary, but highly reactive molecule. Disruptions in copper homeostasis are seen in the severe genetic disorders Menkes disease and Wilson's disease, which map to the copper transporting ATPases ATP7A and ATP7B, respectively (173, 174). These ATPases perform a dual role, transporting copper into the biosynthetic pathway at the Trans-Golgi Network (TGN), as well as trafficking to vesicular compartments to sequester excess copper for removal from the cell (50).

Numerous differences between the Cu-ATPases have been demonstrated that help explain how both may be needed in a single cell. ATP7A and ATP7B appear to supply different proteins with copper in the TGN, and in polarized cells may also traffic to different membranes at high copper concentrations. ATP7A is thought to go through the catalytic cycle faster than ATP7B, though ATP7B appears to undergo catalytic phosphorylation with a greater sensitivity to copper concentrations (27). However, the relative rates of copper acquisition by the two ATPases has not been well studied.

Copper binding to the N-Terminus constitutes the basis for both regulation of ATPase activity and intracellular trafficking; this regulation is mediated by altering inter-domain and inter-protein interactions (116). Both ATP7A and ATP7B rely on ATOX1 to deliver

copper to their N-terminal metal-binding domains (MBDs) (150, 175). ATOX1 has been shown to be capable of both delivering and removing copper from N-ATP7B, as well as stimulating ATP7B's catalytic activity (51). In the absence of ATOX1, the ATPases are still functional, but do not transport copper or traffic with the same efficiency (161, 176). For ATP7B, all 6 MBDs can be filled with copper by Cu-ATOX1 *in vitro*, however this requires a 40-fold ratio of Cu-ATOX1 to N-ATP7B. (51). The relative concentrations of these proteins in cells are not known; quantitative PCR suggests only a 4-fold difference in mRNA levels (Lutsenko Lab unpublished data). This raises a question as to whether the N-terminal domain of Cu-ATPases can be fully metallated if presented repeatedly with low amounts of Cu-ATOX1 or additional cellular factors are needed for copper transfer in these conditions. Also, in cells where both Cu-ATPases are expressed, it is not clear how ATOX1 distinguishes between the two, or if any preference exists for copper transfer. These questions will be addressed in this chapter.

The N-Terminal domains of ATP7A and ATP7B contain a series of six MBDs connected by a series of loops of differing lengths. The individual MBDs share a structural homology with ATOX1, folding into a compact ßaßßaß and binding copper through a GMxCxxC motif (116). Copper is presumably transferred from the chaperone to an MBD through the formation of a hetero-dimer (46). Based on sequence alignments and currently known structures, the MBDs from ATP7A share closest homology with their corresponding MBD from ATP7B (see Fig 1a for alignments of MBD3 and MBD4 from ATP7A and ATP7B). In contrast, there are numerous differences in the inter-MBD loops that may beget different interactions and tertiary structure between the two N-Terminal

Domains (Fig 1b). The loops between MBD2-3, 3-4, and 4-5 are all shorter in ATP7A. However, ATP7A has a large "loop" between MBD1 and 2 that shares sequence homology with other MBDs, and may fold into a compact domain, albeit one that can not bind copper. ATP7B does not have a corresponding segment, but possesses a unique N-Terminal region that is essential for proper trafficking to the apical membrane in polarized cells (64).

Much less is known about N-ATP7A compared to N-ATP7B in regard to copper acquisition. ATOX1 delivers copper preferentially to MBD2 of ATP7B (140), but it is not known whether this mechanism is conserved in ATP7A. N-ATP7B undergoes a significant conformational change upon copper binding, becoming more compact and rigid (57, 146); whether N-ATP7A undergoes a similar change is unknown. Understanding these functional differences between the N-Terminal domains of the Cu-ATPases should shed light on how copper distribution is prioritized in cells where both Cu-ATPases are present.

In this chapter, we demonstrate that N-ATP7B requires a lower concentration of ATOX1 to be fully metallated than does N-ATP7A. This holds when both N-Terminal domains are present simultaneously. We show that relatively small amounts of ATOX1 may be sufficient to fully metallate N-ATP7B if they are recycled. We also show that N-ATP7A undergoes a conformational change upon copper binding, and that ATOX1 has a preference for certain MBDs when transferring copper to N-ATP7A.

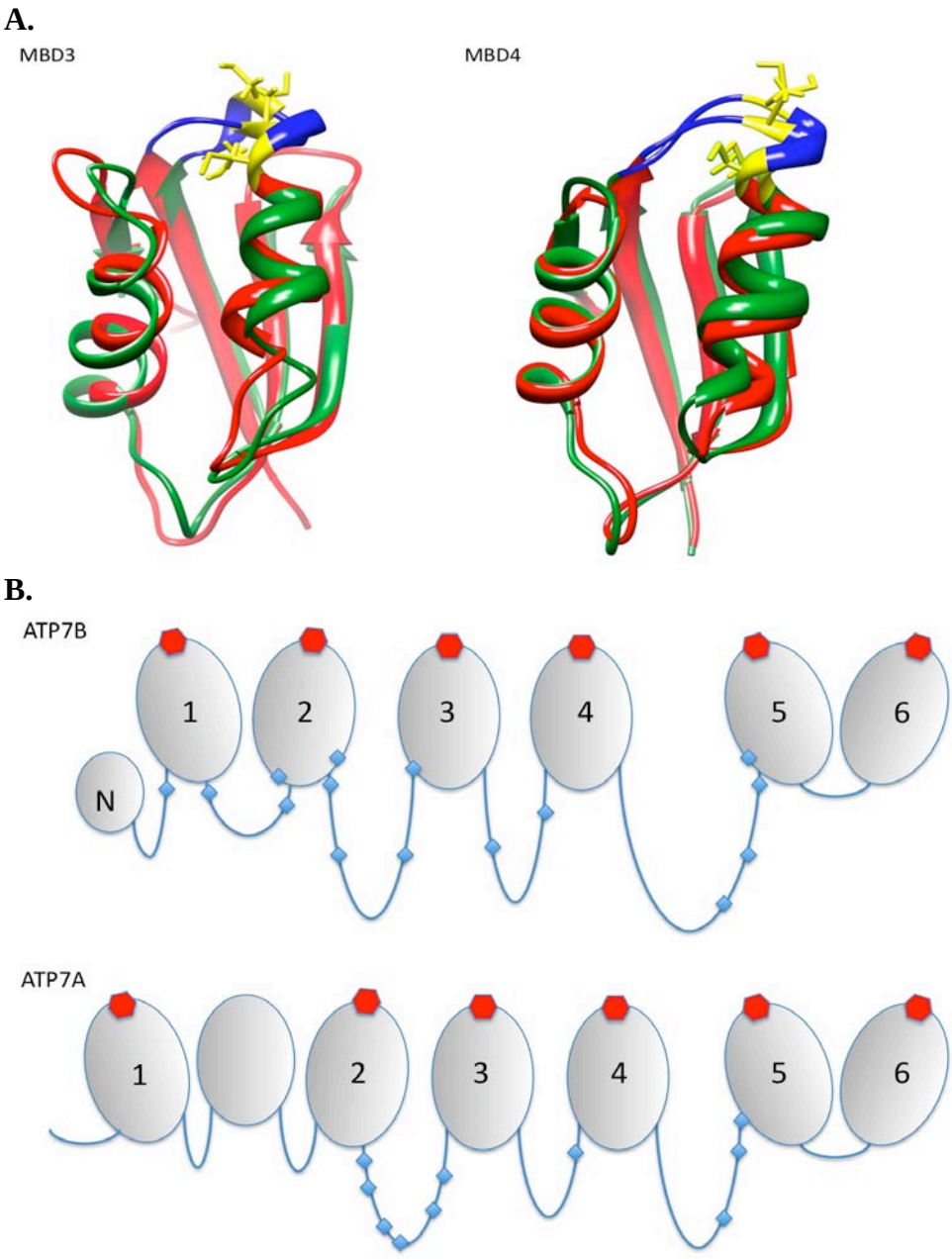

Figure 3.1. Structure and organization of the metal binding domains of N-ATP7A and N-ATP7B. A. Left - Alignment of MBD3 of ATP7A (red) with MBD3 of ATP7B (green). Right – Alignment of MBD4 of ATP7A (red) with MBD4 of ATP7B (green). GMxCxxC motif shown in blue, metal binding Cys residues shown in yellow. Adapted from Banci et al, 2006 (126) (PDB code : 2g9o); Gitschier et al, 1998 (131) (PDB code : 1aw0); and Banci et al, 2008 (125) (PDB code : 2rop). **B.** Cartoon illustrating the relative length of the loops connecting the N-terminal MBDs; copper binding sites shown in red, trypsin recognition sites indicated in blue. Top: N-ATP7B. Bottom: N-ATP7A.

Materials & Methods

Expression and Purification of Recombinant Proteins. N-ATP7A and N-ATP7B derived from Human ATP7A and ATP7B, respectively, were expressed and purified as a fusion with Maltose-Binding Protein (MBP) as previously described (158). Human ATOX1 was expressed in *E. coli* as a fusion with the chitin binding protein (CBP) in the PTYB12 Intein vector, as previously described (51), and purified using affinity chromatography over chitin resin (New England Biolabs; Ipswich, MA). Detailed procedures are described in the Appendix.

ATOX1 Mediated Copper Transfer in solution. Cu-ATOX1 was prepared as previously described (51). Transfer reactions and subsequent removal of ATOX1 was performed as detailed in chapter 2.

On column copper transfer. 1 ml of N-ATP7A or N-ATP7B lysate was diluted in 14 ml of buffer A and bound to maltose resin, then washed with 100 ml of buffer A. The bound protein was reduced with 1 mL of 1 mM TCEP in buffer A for 15 min, then washed again. At this stage, protein was eluted from one column in four sequential fractions. The protein in these fractions was quantified with the Lowry assay (165), and summed to determine total protein bound to the column. Using this measurement, Cu-ATOX1 was added to the remaining columns in varying molar ratios. After 15 minute incubation, ATOX1 was washed off the column with buffer A, and N-ATP7A/B was eluted as described above.

Copper Binding Stochiometry. Concentration of purified proteins was determined with the Lowry assay. Copper concentration in samples was measured using atomic absorption spectroscopy (AA-6650G, Shimadzu; Columbia MO), and a molar ratio of copper/protein was averaged for each transfer ratio in three independent experiments. Further details can be found in the Appendix.

Limited Proteolysis. Apo N-ATP7A, or N-ATP7A that had been subject to copper transfer from ATOX1 was subject to limited proteolysis using trypsin and separated on an SDS-PAGE gel as described in chapter 1. Where indicated, samples were labeled with CPM (as described below) prior to digestion.

Fluorescent labeling of Cys residues. 7-Diethylamino-3-(4'-maleimidyl-phenyl)-4-methylcoumarin (CPM) (Invitrogen; Carlsbad, CA) was used as a probe to label available Cys residues as detailed in chapter 1. Labeled samples were separated on an SDS-PAGE gel and quantitated as described.

Results

Concentration dependence of ATOX1 mediated copper transfer. While ATP7A and ATP7B have been shown to have different sensitivities to copper in stimulating catalytic activity (27), the relationship between the copper-delivering chaperone ATOX1 and N-ATP7A and N-ATP7B remains poorly characterized. We hypothesized that the corresponding MBDs of the two ATPases have similar affinities for and rates of copper transfer from ATOX1, but that the distinct inter-domain loops of N-ATP7A and N-ATP7B confer unique inter-domain organizations, leading to differences in how the domains interact with ATOX1 and respond to copper binding. To test this hypothesis, we compared copper transfer from ATOX1 to N-ATP7A and N-ATP7B at a range of molar ratios from 1 to 72 fold Cu-ATOX1 over Apo-N-Terminal domain (Fig 3.2). In accordance with our previous findings (51, 163), we were able to transfer the maximum 6 copper to N-ATP7B with a 40-fold ratio of Cu-ATOX1. For N-ATP7A, a higher ratio (56-fold) was necessary to reach saturation. At lower ratios (<20-fold), the two proteins have similar amounts of copper acquired. Between 20 and 48 fold, N-ATP7B acquired and retained more copper, suggesting a degree of cooperativity not seen with N-ATP7A. To demonstrate that the copper bound to N-ATP7A is coordinated by the metal binding Cys residues of each MBD, we took aliquots of the samples post-transfer, and labeled them with the Cys-directed maleimide CPM. As expected, the amount of labeling decreased with exposure to increased concentrations of ATOX1 (Fig 3.2b). The protection against CPM labeling was incomplete, likely due to the presence of 3 Cys residues in the domain in addition to the metal-binding cysteines (see Fig 1.5).

A.

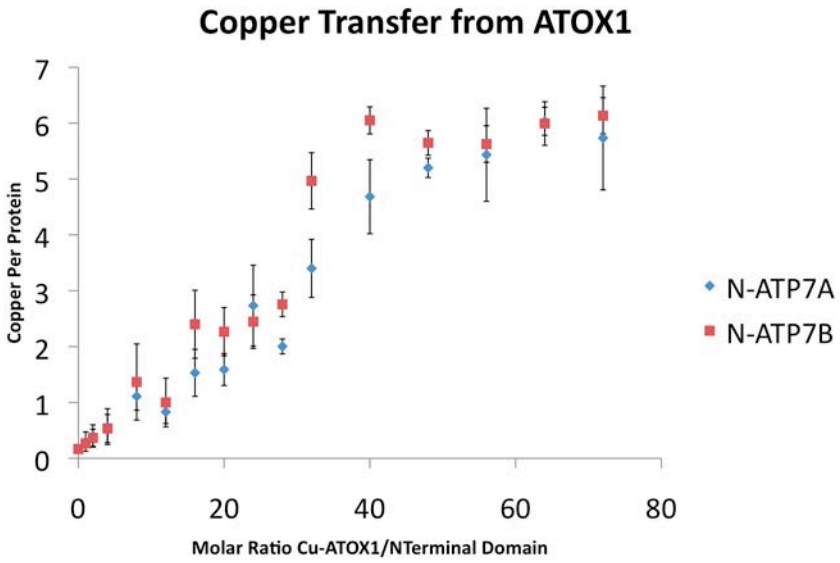

B.

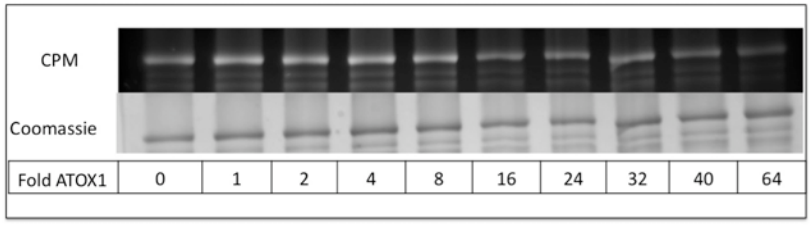

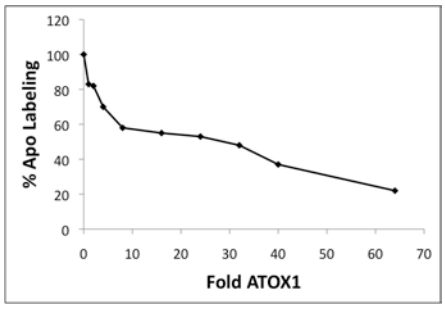

Figure 3.2. ATOX1 mediated copper transfer to N-ATP7A. A. Copper transfer from ATOX1 to N-ATP7A (Blue) and N-ATP7B (Red). Points represent the amount of copper that remains bound to the N-Terminal domain after incubation with the indicated ratios of Cu-ATOX1 and subsequent removal of Cu-ATOX1 from the mixture. Error bars indicate standard deviations across three independent experiments. **B.** Above: Fluorescent (top) and coomassie stained gel images of N-ATP7A that has been labeled with CPM following copper transfer from ATOX1 in the indicated ratios. Below: Chart representing changes in fluorescence per protein.

Copper is transferred rapidly from ATOX1 to N-ATP7B. In order to remove ATOX1 from the solution transfer reactions, we repeatedly pass the reaction mixture through a 50 kD cutoff column. We were concerned that this process extended the length of the incubation period, which might cause differences in copper transfer to become less apparent. To test this, we bound N-ATP7B to maltose resin and incubated with either 16-fold or 32-fold Cu-ATOX1 for varying lengths of time from 2 to 16 minutes (Fig 3.3). No significant differences were seen in the amount of copper transferred over time, suggesting that the exchange happens rapidly (on the scale of seconds).

Sequential transfers of copper from ATOX1 to N-ATP7B have an additive effect. The intracellular concentration of ATOX1 is unknown, so it is not clear whether the 40-60 fold excesses of Cu-ATOX1 needed to saturate N-ATP7B and N-ATP7A exists in the cell. We hypothesized that repeated exposure to low concentrations of Cu-ATOX1 might have an additive effect on the amount of copper transferred and be sufficient to fully metallate the N-terminus. We performed solution transfers using either a single exposure to Cu-ATOX1 (from 10-50 fold), or repeated exposures to 10 fold Cu-ATOX1, using 50 kD cutoff columns to remove ATOX1 after each transfer. We found that the amount of copper transferred was similar for total amount of Cu-ATOX1 that N-ATP7B was exposed to, whether all at once (bulk) or in sequential transfer reactions (Fig 3.4). This suggests a mechanism whereby lower amounts of ATOX1 could still regulate ATP7A/B in a copper dependent fashion.

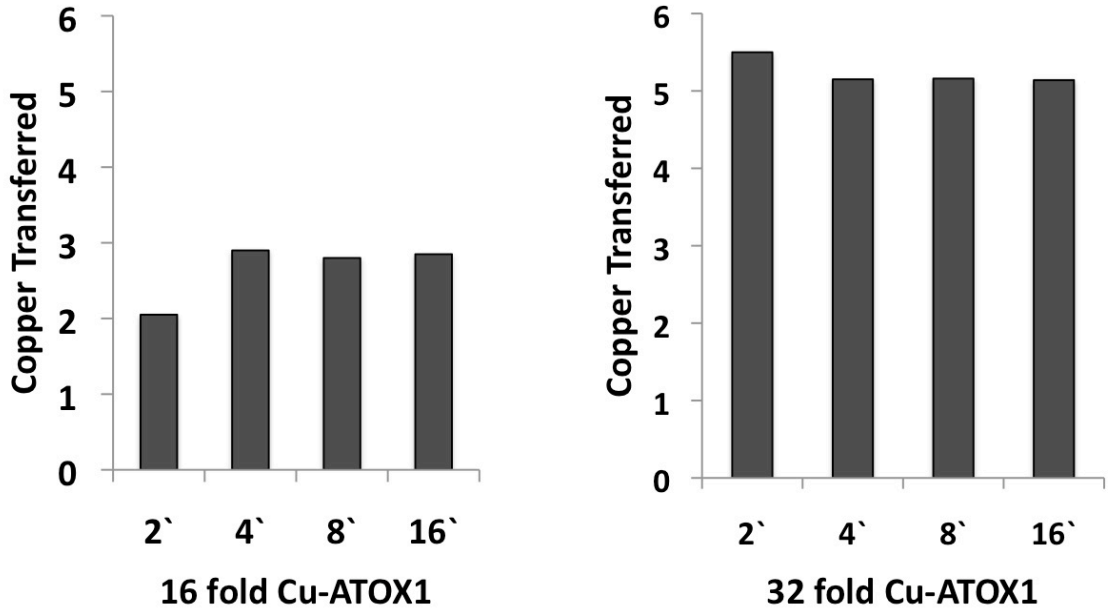

Figure 3.3. Copper is exchanged rapidly between ATOX1 and N-ATP7B. Copper transferred from ATOX1 to maltose resin-bound N-ATP7B at various time points. Left: transfers using a 16:1 molar ratio of Cu-ATOX1 to Apo-N-ATP7B. Right: transfers using a 32:1 molar ratio of Cu-ATOX1 to Apo-N-ATP7B.

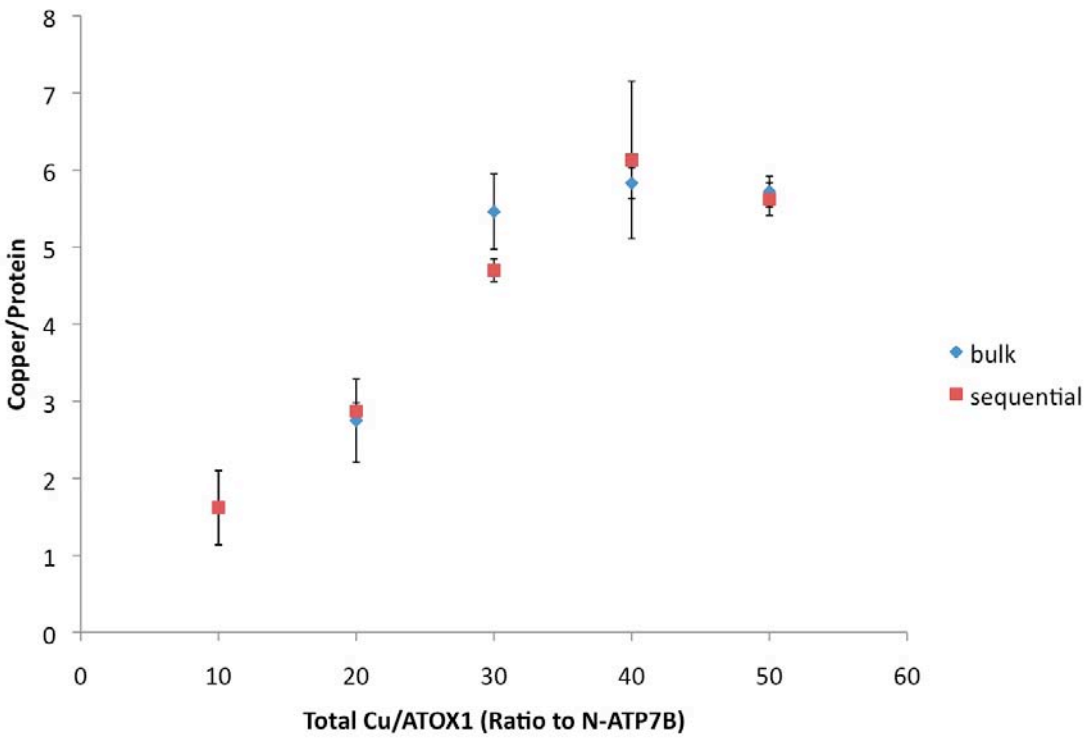

Figure 3.4. Sequential exposure to Cu-ATOX1 results in cumulative transfer. In-solution transfers of copper from ATOX1 to N-ATP7B. Blue : copper transfer using one exposure to ATOX1 (Bulk) at a 10, 20, 30, 40 or 50 fold molar ratio. Red : copper transfer using repeat exposures to ATOX1 (Sequential) at a 10 fold molar ratio, with ATOX1 removed from the reaction prior to subsequent transfer. Error bars represent standard deviation across three separate experiments.

N-ATP7A has altered conformation in the copper-bound state. N-ATP7B undergoes a conformational change upon copper binding that has been observed through circular dichroism (57) and limited proteolysis (146) and described in Chapter 2. It is not known whether N-ATP7A responds to copper binding in a similar fashion. In our initial transfer experiments with N-ATP7A, it appeared that the protein had decreased mobility on the gel as more copper was bound, suggesting a conformational change occurs upon copper binding (Fig 3.2b). To further test this, we performed copper transfer from Cu-ATOX1 to N-ATP7A bound to maltose resin. The eluted protein was run on an SDS-PAGE gel, where we again observed the mobility of the protein to decrease as additional copper was bound (Fig 3.5a). In the experiments where ATOX1 was removed prior to labeling, there was also a notable decrease in the amounts of protein in solution where more copper was bound (confirmed with Lowry assays, data not shown). We attribute this loss to a decrease in solubility or aggregation conferred by the conformation change brought by copper binding. However, this was not observed when the protein was not subject to concentration prior to electrophoresis (such as in Fig 3.2b).

To test this hypothesis, we subjected the protein to limited proteolysis using trypsin, and compared the proteolytic fragments after separation on an SDS-PAGE gel (Fig 3.5b). In contrast to previous observations for N-ATP7B (where copper binding markedly altered the exposure of loops connecting MBDs to trypsin), N-ATP7A showed similar proteolysis patterns regardless of the amount of copper bound. As shown in figure 1, there are fewer trypsin sites in the ATP7A loops than in ATP7B, and most are

concentrated between MBDs 2-3 and 4-5. The lack of change in trypsin digest patterns suggests that these two loops are equally exposed in the Apo and copper bound states. Therefore, the observed change in properties of N-ATP7A is likely due to mutual rearrangements of MBDs and perhaps altered exposure of MBD surfaces (see discussion).

The initial copper transferred from ATOX1 to N-ATP7A has a preferential target MBD. When Cu-ATOX1 is presented to Apo-N-ATP7B, copper is first transferred to MBD2, whereas subsequent copper transfer appears to proceed without preference for MBDs (140). As the individual MBDs of N-ATP7A are most similar to the corresponding MBD of N-ATP7B, we hypothesized that a similar pattern of copper transfer may hold for N-ATP7A. N-ATP7A that had been subject to on-column copper transfer (see above) was labeled with CPM, then subjected to limited proteolysis and separated on an SDS-PAGE gel (Fig 3.6a). As the stoichiometry became greater than 1 Cu bound per protein, a decrease in labeling (correlating with cysteines protected by copper binding) is seen, with two specific bands (indicated with boxes) displaying a more significant loss than others. Similar results were seen when copper transfers was performed in solution (Fig 3.6b). Attempts to identify the 27 and 16 kDa bands in question with MS/MS were unsuccessful, likely due to low concentrations of protein eluted from the gel slices.

A.

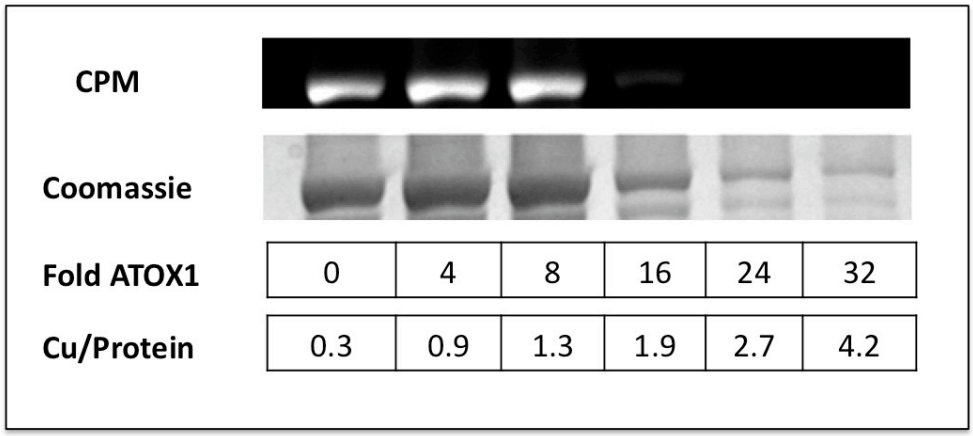

B.

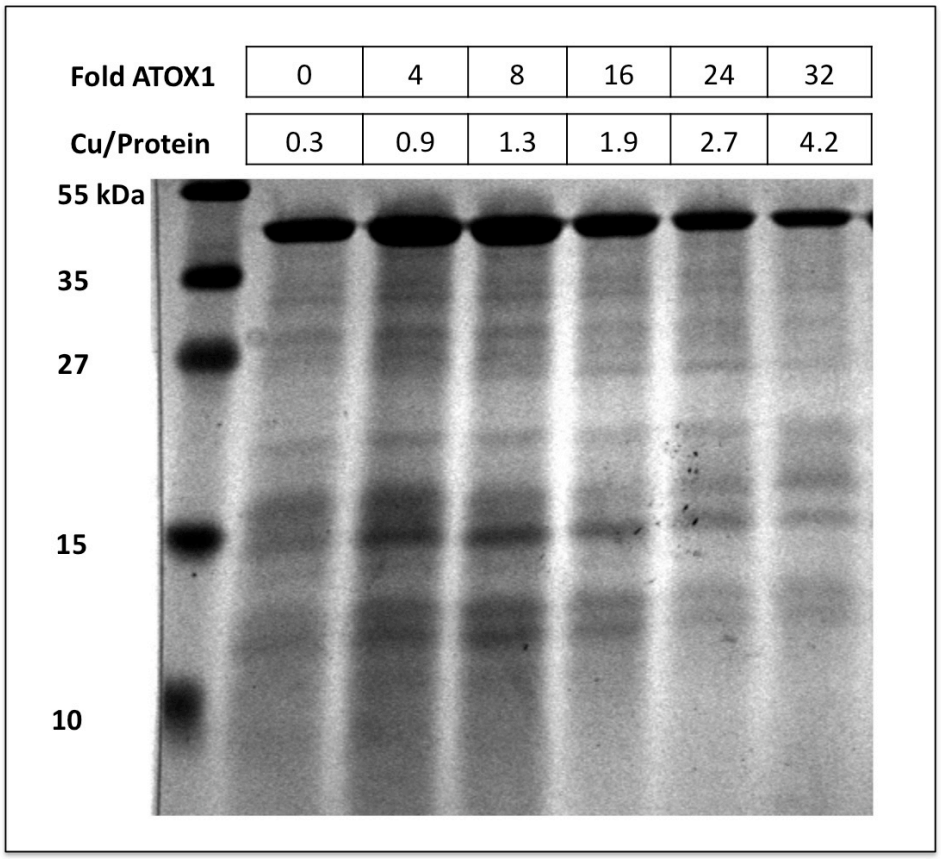

Figure 3.5. Copper transfer to N-ATP7A is accompanied by a mobility shift but with minimal changes in proteolysis pattern. A. CPM labeled (top) and Coomassie stained (bottom) images of N-ATP7A after incubation with Cu-ATOX1. Amounts of initial Cu-ATOX1:Apo-N-ATP7A ratio indicated below gels as "Fold ATOX1". Amount of Cu per protein retained by N-ATP7A indicated in bottom row. **B.** Coomassie stained gel of samples from (A) that had been subject to limited proteolysis and separated on an SDS-PAGE gel.

A.

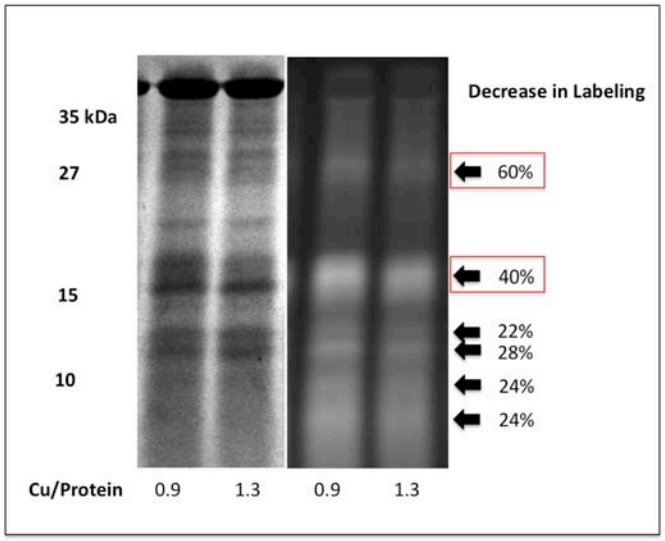

B.

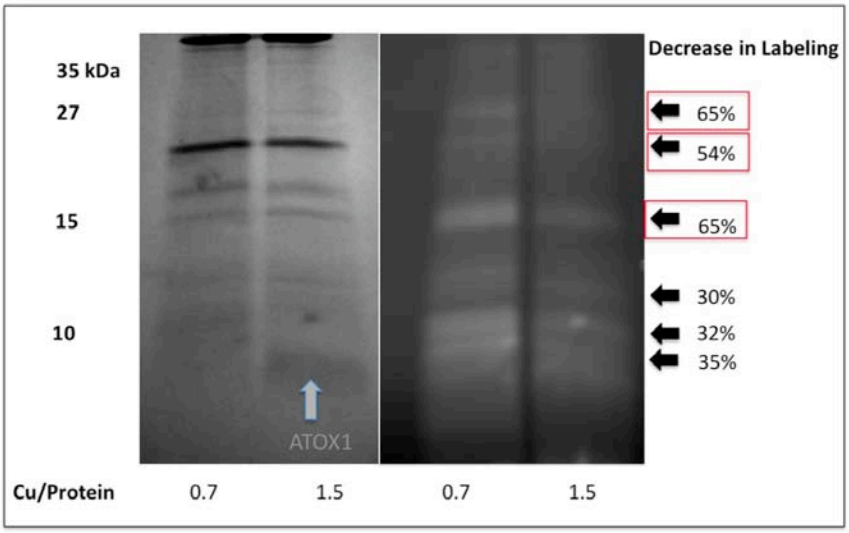

Figure 3.6. The initial copper transferred from ATOX1 to N-ATP7A has a specific target MBD. A. Coomassie stained (left) and CPM labeled (right) images of N-ATP7A subjected to on-column copper transfer from ATOX1 followed by CPM labeling and limited proteolysis. Copper bound per protein indicated below each lane. Percentages denote decrease in label per protein for corresponding bands. Boxes indicate bands with most significant loss of labeling. **B.** Coomassie stained (left) and CPM labeled (right) images of N-ATP7A subjected to in-solution copper transfer from ATOX1 followed by CPM labeling limited proteolysis. Copper bound per protein indicated below each lane. Percentages denote decrease in label per protein for corresponding bands. Boxes indicate bands with most significant loss of labeling. Residual ATOX1 from the transfer indicated with grey arrow.

ATOX1-mediated copper transfer when both N-Terminal domains are present. The results in Figure 3.2 show that N-ATP7B saturates with copper in the presence of a lower concentration of ATOX1 than N-ATP7A. We next wanted to know whether this would hold true in situations where both ATPases were present simultaneously. Equal amounts of purified, reduced N-ATP7A and N-ATP7B were incubated with various molar ratios of Cu-ATOX1. ATOX1 was removed, and the remaining protein was labeled with CPM and separated on an SDS-PAGE gel, with N-ATP7A being slightly larger than N-ATP7B (110 kDa to 108 kDa) (Fig 3.7A). For N-ATP7B, little to no CPM labeling was detected in the presence of 32-fold or higher Cu-ATOX1. Similar to the individual transfer curves in Figure 3.2a, there was a significant difference at 32-fold and 40-fold concentrations of ATOX1 (Fig 3.7). N-ATP7A does retain some fluorescent labeling, even when Atomic Absorption measurements suggest it is fully copper loaded, possibly due to labeling of non-metal binding cysteines (see Fig 1.3.D).

A.

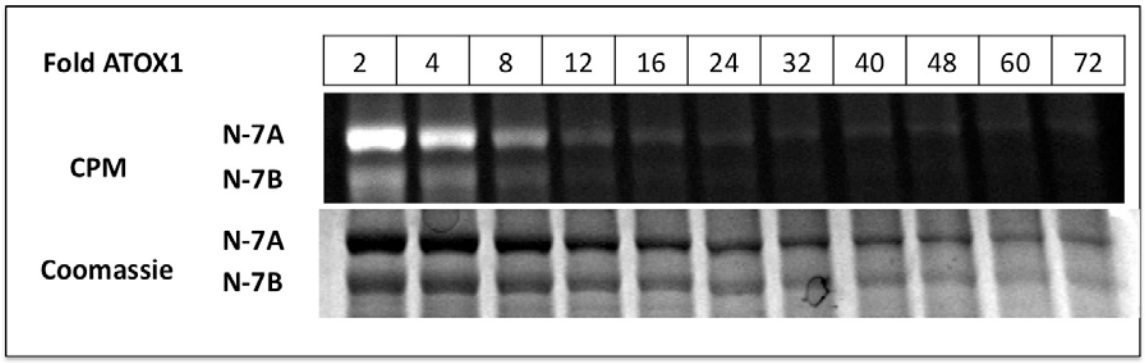

B.

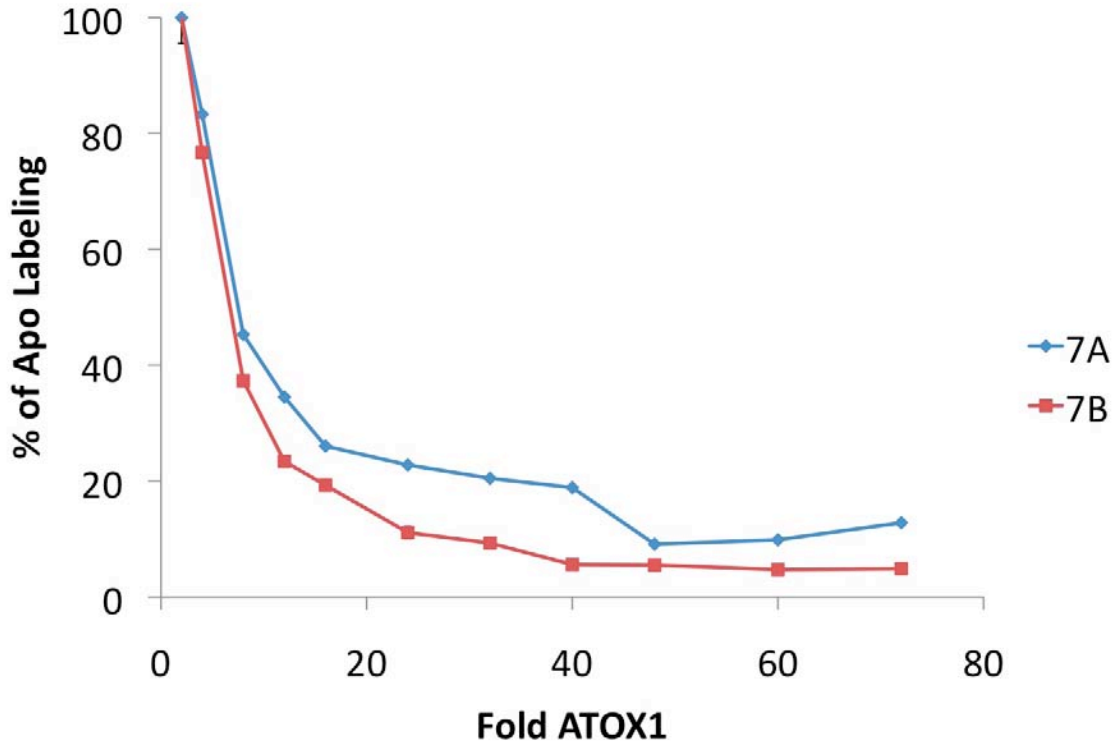

Figure 3.7. Copper transfer from ATOX1 in the presence of both N-ATP7A and N-ATP7B. **A.** CPM labeled (top) and Coomassie stained (bottom) images of N-ATP7A and N-ATP7B subjected to in-solution copper transfer from ATOX1 followed by CPM labeling and separated on an SDS-PAGE gel. Ratio of Cu-ATOX1 to Apo-N-ATP7A + Apo-N-ATP7B indicated above each lane. **B.** Graphic representation of fluorescence per protein for Fig 7A. ATP7A represented in blue, ATP7B in red. Data points represent the average of two experimental repeats.

Discussion

We demonstrate here that the ATOX1 interacts with and transfers copper to the N-Terminal domain of ATP7A in a similar fashion as has been shown for N-ATP7B, but with unique characteristics that may underlie some of the key differences between the two Cu-ATPases. N-ATP7A can be fully loaded with copper by ATOX1; this process requires Cu-ATOX1 concentrations higher than those necessary to metallate N-ATP7B. Copper transfer to N-ATP7A is accompanied by a change in conformation as evidenced by altered electrophoretic mobility and solubility of protein. In contrast to N-ATP7B, conformational changes do not modify the exposure of loops to proteolysis. ATOX1 mediated copper transfer occurs rapidly and, and while concentration dependent, may also occur in sequential transfer steps at low concentrations.

It appears that in solution, a high concentration of ATOX1 is necessary to fully saturate either N-ATP7A or N-ATP7B with copper. Although it is feasible that local concentrations of Cu-ATOX1 could reach these levels, there is currently no evidence that the cell maintains consistent ATOX1 concentrations of this magnitude. Our data suggesting that low concentrations of ATOX1 can fully metallate N-ATP7B when supplied sequentially provides an alternative mechanism. ATOX1 could donate copper to the N-Terminal domain, then cycle back upon re-acquiring copper. However, this seems somewhat at odds with a model where copper transfers occur rapidly, as it does not explain why such high concentrations of Cu-ATOX1 would be needed when presented altogether.

The following consideration may help to explain this discrepancy. It is of note that ATOX1 can be co-immunoprecipitated with N-Terminal MBDs in a copper dependent manner (177). This suggests a relatively stable adduct can be formed, and ATOX1 would not immediately dissociate after transferring copper. In our sequential transfer experiment, all of the ATOX1 was vigorously removed from the solution prior to the next addition of Cu-ATOX1. We propose a mechanism where copper moves through a specific pathway through the N-Terminal domains, requiring ATOX1 to dissociate in order for the cycle to continue. High Cu-ATOX1 concentrations may be able to force this displacement, but at lower concentrations, ATOX1 may form a copper-bridged adduct (or a stable, albeit transient intermediate), blocking further transfer.

Alternatively, this adduct may be the result of an off-rate that is greater than the time scale used in these experiments. While the initial binding of Cu-ATOX1 to a receptor MBD may happen rapidly, Apo-ATOX1 may dissociate slowly, not allowing for additional transfer to occur over the course of seconds or minutes as in these experiments. A stable ATOX1/N-ATP7A intermediate would explain the observed mobility shift of N-ATP7A, though this is not observed for Atox1 and N-ATP7B. It also remains unknown whether the initial copper transferred is subsequently transferred to another MBD, or if ATOX1 donates copper directly to other MBDs after the primary transfer. In the first scenario, a slowly dissociating ATOX1 would prevent the initial copper transferred from being moved to another MBD, inhibiting progression through the transfer cycle.

For N-ATP7B, this cycle begins with ATOX1 docking to MBD2 (140). Our data suggests that N-ATP7A also has a preferred site for initial copper transfer, but further experiments are needed to identify the MBD in question. Unlike N-ATP7B, which undergoes a significant conformational change with the addition of copper (57), we detected only a modest decrease in mobility in N-ATP7A upon copper binding. The conformational changes in N-ATP7B are predicated on altered Cys interactions upon copper binding as well as loop rearrangements. While copper binding is likely to have the same effect on MBD flexibility and Cys-mediated interactions, the loops of N-ATP7A may not undergo dramatic structural changes.

The changes in loop exposure seem essential for N-ATP7B mediated ATPase regulation. If this change does not occur in N-ATP7A, this may mean that N-ATP7A and N-ATP7B use different mechanisms by which they regulate ATPase activity and localization. With regard to intracellular trafficking, ATP7B shows copper dependent interactions with both COMMD1 (56) and the p62 unit of dynactin (55). Presumably, the conformational change in ATP7B exposes residues necessary for this interaction (along with copper-dependent kinase mediated phosphorylation (146)). These proteins do not interact with ATP7A, which likely utilizes a separate set of trafficking machinery. It has not been determined whether N-ATP7A is involved in copper-dependent interactions with the nucleotide-binding domain of ATP7A similar to that for ATP7B. If it does, the binding of copper and ATP to their respective domains may be sufficient to dissociate the domains and expose residues in N-ATP7A essential for interaction with trafficking partners.

While ATP7A appears to go through the catalytic cycle faster than ATP7B, ATP7B can undergo catalytic phosphorylation when exposed to lower levels of free copper (27). While there currently no data comparing rates of ATOX1 dependent catalytic phosphorylation, it would follow that if N-ATP7B receives copper more efficiently from the chaperone as we show here, the difference in copper sensitivity may be greater than previously thought. Whether this leads to ATP7B having a higher rate of copper transport, or a greater sensitivity to trafficking is not known. Comparing actual rates of copper transport and trafficking between the two ATPases will be essential to determine how copper is prioritized in cells where both Cu-ATPases are present.

Our data comparing copper transfer from ATOX1 assume the chaperone is unbiased in selecting a donor ATPase. However, ATP7A and ATP7B may traffic to vesicles at different rates, or potentially occupy different regions of the TGN. The local environment of the N-termini could be different in these locations due to different interacting partners (or the influence of the local lipid environment on the overall Cu-ATPase conformation). It will be important to further understand how ATOX1 is distributed throughout the cell, and if its localization and targeting changes in response to elevated copper.

Chapter 4

Wilson's Disease causing mutations G85V and G591D alter cooperativity between N-Terminal metal binding domains of ATP7B

Abstract

Wilson's disease is an autosomal recessive disorder caused by mutations to the copper transporter ATP7B. ATP7B contains six N-terminal metal binding domains (MBDs) that sense cytosolic copper concentrations and regulate ATP7B activity accordingly. Two known Wilson's disease causing mutations, G85V and G591D alter conserved glycine residues in MBD1 and MBD6, respectively. We hypothesized that these mutations could alter the folding of the N-terminal domain of ATP7B and/or decrease copper binding. However, our data indicate that these two mutations have modest effects on N-ATP7B. The G591D mutation causes a 10% decrease in copper binding, while the G85V mutation shows no change from WT. Both mutations can be fully copper loaded by the copper chaperone ATOX1, but the concentration dependence of transfer is altered, possibly due to a loss of cooperativity. Neither mutation causes a significant change in domain solubility, global conformation or oxidation susceptibility, suggesting the mutations do not significantly alter the interactions between the MBDs in either the apo or copper bound states. It is likely that the disease causative effects of these mutations are due to alterations in the interaction between the N-Terminal domain and other cytosolic domains of ATP7B.

Introduction

Disruption in copper homeostasis is a hallmark of many severe human disorders (178). One such example is Wilson's disease, an autosomal recessive disorder in which copper metabolism is impaired. The disease is most notably characterized by copper accumulation in the liver, leading to chronic liver disease (13). Kidney dysfunction and a severe neurological phenotype often accompany the hepatic symptoms (13). The disease is caused by mutations in the copper transporting ATPase ATP7B.

ATP7B plays a dual role in the liver, both delivering copper to the biosynthetic pathway as well as facilitating the removal of copper into the bile (50). In the absence of a functional ATP7B, copper still enters the cell through CTR1, but cannot be exported, leading to hepatic copper accumulation (13). Copper export is dependent on the ability of ATP7B to traffic between the Trans-Golgi Network (TGN) and the bile canalicular membrane in response to increased copper concentrations. (50). The job of sensing cytosolic copper levels by ATP7B is performed by the N-Terminal domain, which contains six repetitive copper binding sites (158).

The six metal binding domains (MBDs) fold individually into conserved ßaßßaß motifs, and are separated by loops of varied lengths (116). Copper binding to this domain stimulates ATPase activity by causing dissociation from the nucleotide-binding domain (139). This is accompanied by a conformational change in N-ATP7B that allows for increased interactions with the cellular trafficking machinery (55, 146). The function of

N-ATP7B is dependent on close packing of the MBDs (163). Subtle mutations have been shown to alter the conformation of the domain, its inter-domain and inter-protein interactions, as well as its susceptibility to oxidation (163). However, ATP7B retains function in the presence of a truncated N-terminal domain containing as few as two MBDs (135). This suggests that the additional regulation provided by six MBDs is dependent on very specific interactions that could be disrupted by mutations.

Several disease-causing mutations have been identified in the N-Terminal domain, but the functional consequences of these mutations remain unclear; no genotype-phenotype correlation has been reported. Two disease causing mutations, G85V and G591D, are found in a conserved glycine residue located between the first α-helix and second ß-strand, opposite to the GMxCxxC copper binding loop in MBD1 and MBD6, respectively (fig 4.1). The full-length G591D mutant shows impaired kinase-mediated phosphorylation in response to copper (58). Both mutants increase association with the interacting partner COMMD1 (56). There is conflicting data as to whether the expressed mutant proteins localize normally to the TGN (161) or have a tendency to misfold and traffic to the endoplasmic reticulum (ER) (56).

Essentially nothing is known about how these mutations affect the folding and function of either their respective MBD or N-ATP7B as a whole. With mounting evidence for cooperativity amongst MBDs, it seems plausible that the misfolding of one MBD could have a larger effect on function of the entire N-terminal domain by altering inter-MBD

contacts. Additionally, the mutations could affect the inter-domain and inter-protein interactions necessary for trafficking and proper ATPase regulation.

In this paper, we demonstrate that the G85V and G591D mutations have only modest effects on N-ATP7B when expressed as an individual domain. The G591D mutation causes a decrease in copper binding stoichiometry, presumably to MBD6. Both mutants show a decrease in the amount of copper transferred by ATOX1 and a loss of the cooperativity seen in the copper loading of the WT protein by ATOX1. The mutations do not cause a significant alteration in domain conformation, solubility, or susceptibility to oxidation. From this, we infer that the disease causing properties of these mutations are most likely to result from altering interactions with other domains of ATP7B and/or other proteins that interact with the N-Terminal domain.

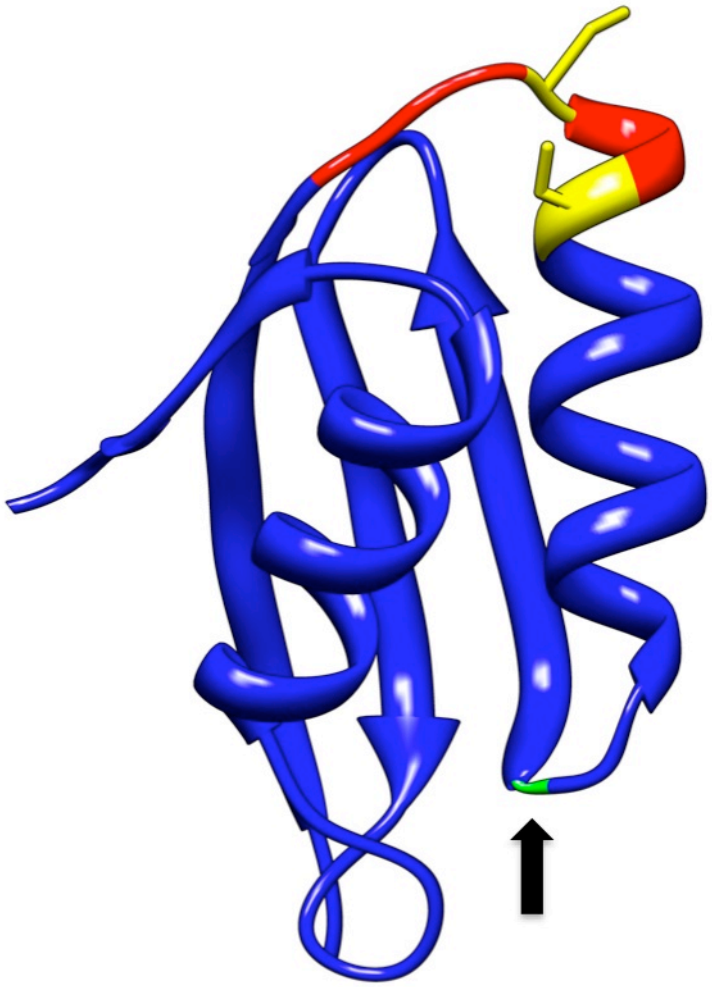

Figure 4.1. Structure of a representative MBD. Model of MBD1 from ATP7B (adapted from Walker et al, 2004 (140)). GMxCxxC motif shown in red, Cys residues in yellow. Conserved Gly (G85) residue shown in green and indicated by arrow. Val substitution at this residue is a Wilson's Disease causing mutation. Mutating the equivalent Gly to Asp in MBD6 (G591D) is also disease causative.

Materials and Methods

Constructs/Mutants. Mutations in N-ATP7B were generated using the N-ATP7B-pMal plasmid as a template and the Stratagene QuikChange XLII kit (Agilent; La Jolla, CA) with the following mutagenic primers G85V: F: GGACAGGATTTCCAATTTGAAAGTCATCAGCATGAAGGTT; R: AACCTTCATGCTGATGATGACTTTCAAATTGGAAATCCTGTCC. G591D: F: TCTGCAGAAAGAAGCTGTTGTTCTCTCCGTGTTGG; R: CCAACACGGAGAGAACAACAGCTTCTTTCTGCAGA. The veracity of the coding sequences in all constructs was verified by automated DNA sequencing.

Expression and Purification of Recombinant Proteins. N-ATP7B, derived from human ATP7B (and mutants thereof) was expressed and purified as a fusion with Maltose-Binding Protein (MBP) as previously described (158) and discussed further in the Appendix. Human ATOX1 was expressed in *E. coli* as a fusion with the chitin binding protein (CBP) in the pTYB12 Intein vector, as previously described (51), and purified using affinity chromatography over chitin resin (New England Biolabs; Ipswich, MA). Detailed procedures are described in the Appendix.

Copper Binding Stochiometry. Concentration of purified proteins was determined with the Lowry assay (165). Copper concentration in samples was measured using atomic absorption spectroscopy (AA-6650G, Shimadzu; Columbia MO), and a molar ratio of

copper/protein was averaged for each mutant in four independent experiments. Further details can be found in the Appendix.

ATOX1 Mediated Copper Transfer. Cu-ATOX1 was prepared as previously described (51). Transfer reactions and subsequent removal of ATOX1 was performed as detailed in chapter 1.

Native gel electrophoresis. 10 μg of wt N-ATP7B was separated on a 10% tris-glycine gel that did not contain Urea, SDS or reducing agents. The gel was fixed in 50% ethanol/8% phosphoric acid for a minimum of 3 hours, and then stained with colloidal Coomassie G250 overnight.

Limited Proteolysis. Apo and Cu-loaded N-ATP7B (and mutants) were subject to limited proteolysis using trypsin and separated on an SDS-PAGE gel as described in chapter 1.

Fluorescent labeling of Cys residues. 7-Diethylamino-3-(4'-maleimidyl-phenyl)-4-methylcoumarin (CPM) (Invitrogen; Carlsbad, CA) was used as a probe to label available Cys residues as detailed in chapter 1. Labeled samples were separated on an SDS-PAGE gel and quantitated as described.

Results

Expression of mutant N-ATP7Bs and Copper Binding in E. coli. Proper regulation of N-ATP7B has been shown to depend on a precise interaction amongst the individual MBDs (163). Altering this inter-domain network can lead to rapid oxidation, loss of copper binding and significant conformational changes, which can disrupt chaperone-mediated activation of full-length ATP7B (140). We hypothesized that the disease mutations G85V and G591D would disrupt the folding of MBD1 and MBD6, respectively, which would in turn alter the interactions amongst MBDs in N-ATP7B, leading to dysregulation.

The properties of wild-type N-ATP7B when expressed as a fusion protein with Maltose Binding Protein (MBP) have been extensively characterized (51, 132, 140, 146, 158, 163). The G85V and G591D mutants were made in this construct, then co-expressed in *E. coli* with thioredoxin and purified over amylose resin. Both mutants expressed and solubilized similarly to the WT protein (Fig 4.2a). WT N-ATP7B has been shown to bind and retain between 5 and 6 copper atoms per protein when copper is added to the growth media (158). If the G85V and G591D mutations alter the structure of their respective MBDs, we would expect the misfolded domains to have reduced affinity for copper. The G85V mutant bound copper similar to WT (5.4 ± 0.2 compared to 5.5 ± 0.1 for WT), whereas the G591D mutant bound slightly less (5.1 ± 0.2) (fig 4.2b), suggesting this mutation may effect the copper binding ability of MBD6, but does not influence copper binding by any of the other MBDs.

A.

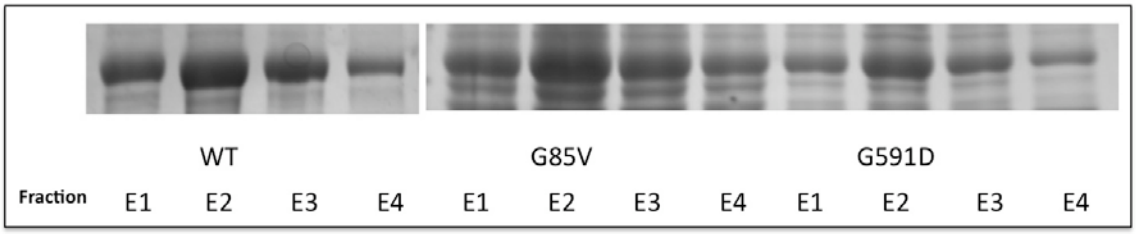

B.

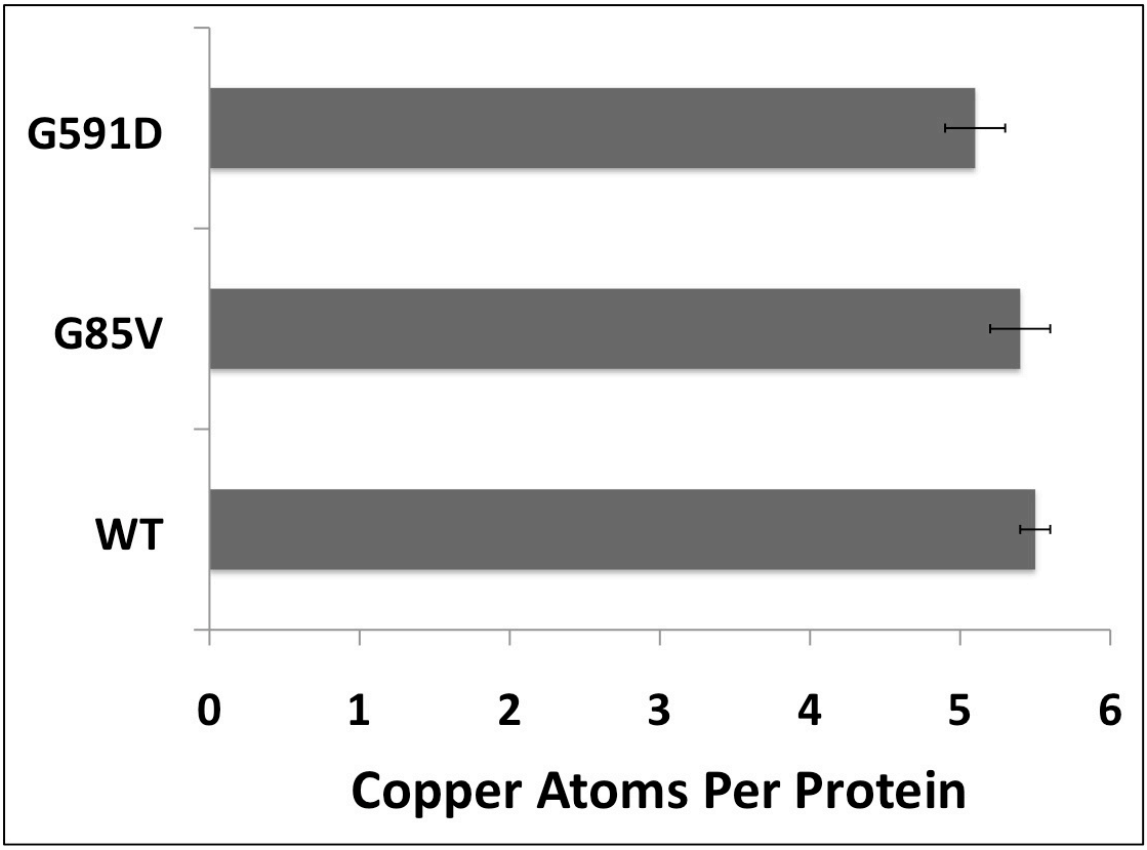

Figure 4.2. G85V and G591D variants of N-ATP7B are soluble and bind copper when expressed in *E Coli*. A. Subsequent elution fractions of N-ATP7B-MBP (Wt and mutants), eluted in the presence of 10 mM Maltose. **B.** WT and mutant N-ATP7B were loaded with copper in *E Coli* prior to purification. Bars represent experimental values as determined through atomic absorption (copper) and Lowry assay (protein). Error bars indicate standard deviations across three experimental repeats.

Decreased Copper Binding in the G85V mutant is not due to Cysteine oxidation. Previously, we characterized mutations to MBD2 and MBD3 where decreased copper binding correlated with a heightened sensitivity of metal binding Cys residues to oxidation (163). To test whether this phenomenon was responsible for the decreased copper binding of the G591D mutant, we took purified Apo-N-ATP7B (both wt and mutants) and labeled with the Cys-directed maleimide CPM. Both mutants labeled similarly to WT (fig 4.3), suggesting that any loss of copper binding in the G591D mutant was not due to oxidation.

The G85V and G591D mutations do not significantly alter the overall structure of N-ATP7B. We have shown that mutations that do not alter copper binding or oxidation sensitivity may still affect the conformation of N-ATP7B due to effects on the close packing of the MBDs (163). This change can be visualized by limited proteolysis (that takes advantage of trypsin sites situated in the loops connecting the MBDs) followed by SDS-PAGE of the resulting fragments. For the G85V and G591D mutants, the proteolysis pattern did not show any significant deviations from the WT protein in either the apo or copper-bound states (fig 4.4a). This implies that any changes due to the mutations are autonomous to the affected MBD. This was further confirmed by comparing mobility of the purified N-ATP7B on a native gel (fig 4.4b). In both the apo and copper-bound states, the disease mutants ran with similar mobility to that of the wt protein, further demonstrating that the mutations did not significantly disrupt inter-MBD contacts. The G591D mutant does show some change in the distribution of protein to the

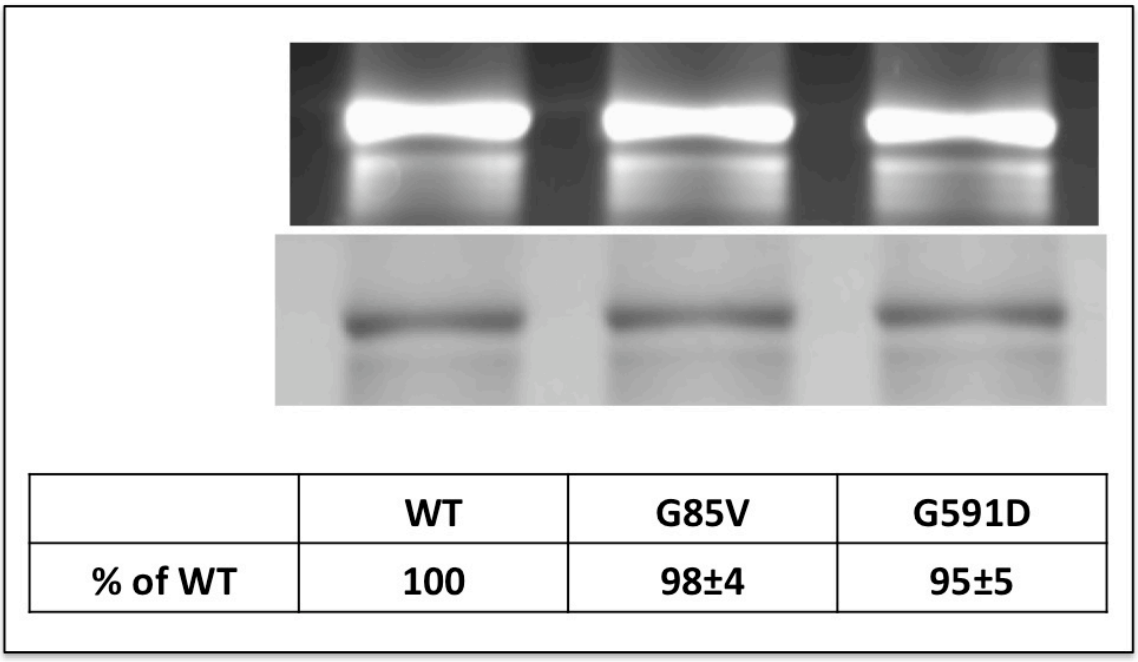

	WT	G85V	G591D
% of WT	100	98±4	95±5

Figure 4.3. Comparison of Cys-directed fluorescent labeling for the wild type and mutant N-ATP7Bs. Fluorescent (top) and coomassie stained (bottom) gel images of wt, G85V and G591D mutants of N-ATP7B that have been labeled with CPM. Table indicates ratio of label/protein to that of apo wt-N-ATP7B. Average percentages and standard deviations are indicated for three experimental repeats.

more mobile fragment of the doublet in the apo state. This may be due to biased degradation of MBD6 if this domain is slightly unfolded and not stabilized with copper.

The efficiency of copper transfer from ATOX1 to N-ATP7B is decreased in both disease mutants. If the G85V and G591D mutations do not significantly alter the properties of N-ATP7B itself, we hypothesized that the mutants may affect ATP7B regulation by altering the relationship of the copper-binding domain with other domains or proteins with which N-ATP7B is known to interact. To test this, we compared ATOX1 mediated copper transfer to WT and mutant N-ATP7Bs (fig 4.5). When Cu-ATOX1 was present in excess (60 fold over N-ATP7B), both mutants acquired nearly as much copper as they did when loaded in *E. coli* (G85V: 5.0 ± 0.2; G591D: 5.2 ± 0.3). However, WT N-ATP7B saturated with 6 (±0.2) copper atoms in the presence of 40 fold Cu-ATOX1, compared to 3.9 (±0.5) and 3.7 (±0.4) for G85V and G591D, respectively. Indeed, the transfer curves for the mutants were nearly linear, suggesting a loss of cooperativity characteristic of the WT protein.

A.

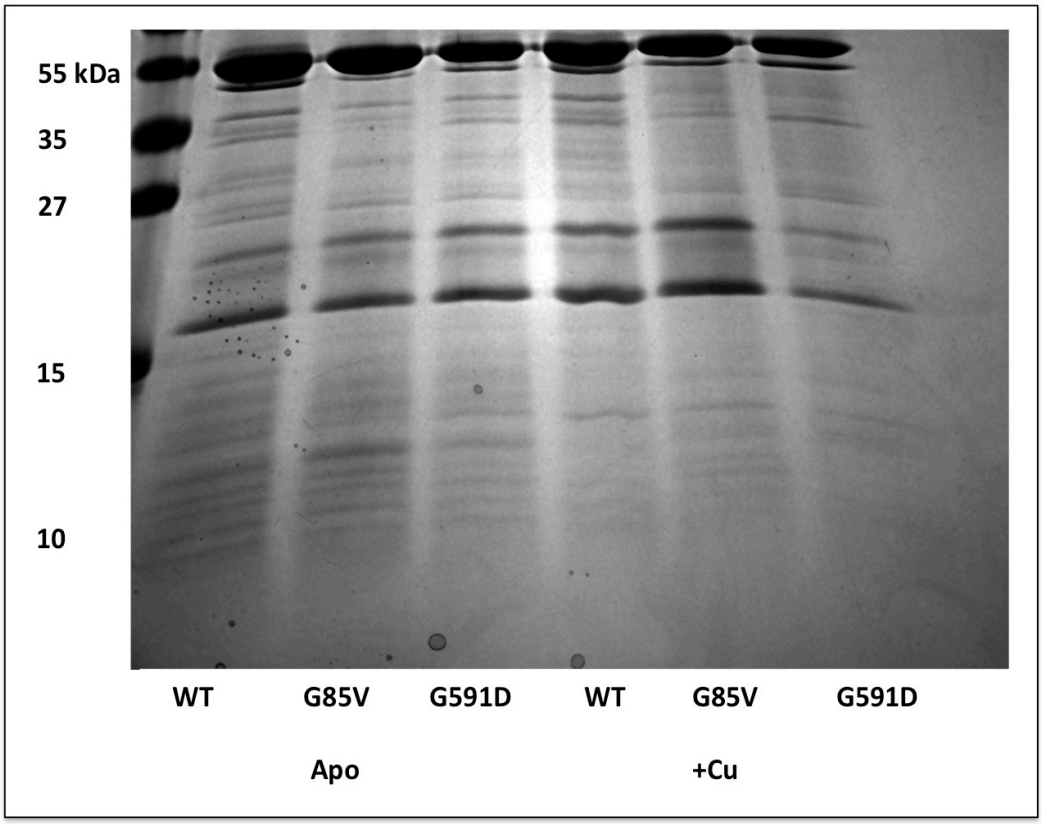

B.

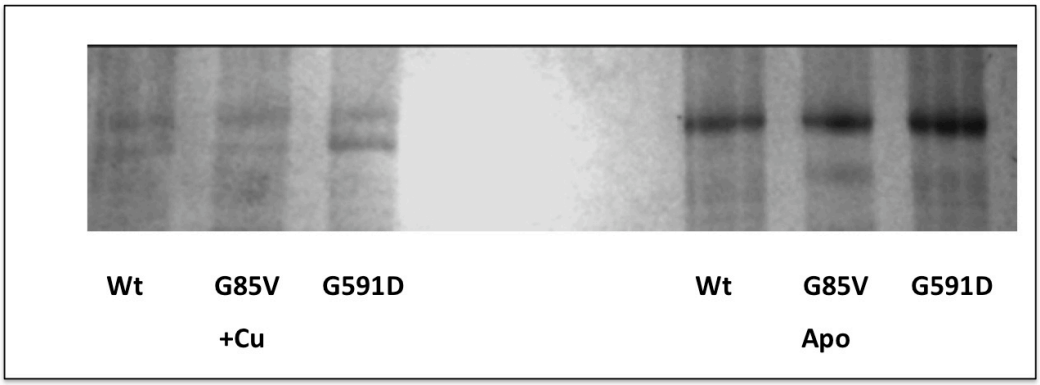

Figure 4.4. G85V and G591D mutants show no major structural changes from WT N-ATP7B. A. Coomassie stained gel comparing limited proteolytic patterns of WT, G85V and G591D mutants of N-ATP7B. Left – Apo proteins. Right – Copper loaded proteins. **B.** Coomassie stained native gel comparing mobility of WT, G85V and G591D mutant N-ATP7B. Left – Copper loaded proteins. Right – Apo proteins.

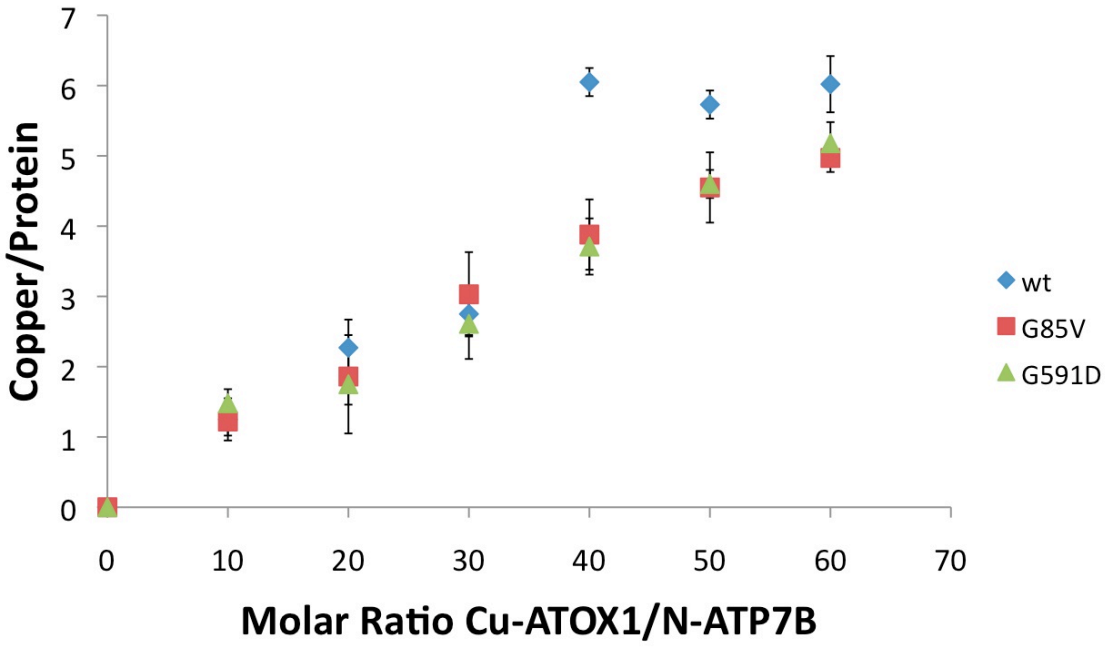

Figure 4.5. ATOX1-mediated copper transfer to N-ATP7B. Copper transfer from ATOX1 to N-ATP7B. Points represent the amount of copper that remains bound to N-ATP7B after incubation with the indicated amounts of Cu-ATOX1 and removal of Cu-ATOX1 from the mixture. Error bars indicate standard deviations across three independent experiments.

Discussion

We demonstrate that the Wilson's Disease mutations G85V and G591D have modest affects on the structure and function of N-ATP7B expressed as a soluble domain. The G591D mutation reduces copper binding to 5 of the 6 expected copper atoms per molecule when loaded in *E. coli*. Both mutations alter the cooperativity of copper transfer from ATOX1. The mutations do not seem to have a significant impact on the global folding of the domain, nor do they alter the susceptibility of metal binding Cys residues to oxidation.

Neither mutation altered Cys oxidation to other domains as seen for CxxC to AxxA mutations of MBD2 and MBD3 (163). It is also interesting that the G85V mutation did not affect copper binding at all when compared to WT. The WT construct also typically binds slightly less than the expected 6 copper atoms, though it is not known which MBD has reduced affinity in this construct (158).

It was somewhat surprising that both the G85V and G591D mutants had similar digestion patterns and native gel mobility when compared to WT in both the Apo and Cu-bound states, suggesting normal domain folding. This may be due in part to the stability conferred on the protein by the fusion with the maltose binding protein. However, both mutants required higher concentrations of ATOX1 to fully saturate with copper, and especially in transitioning from 3 copper bound to 4-5 copper bound. So while the global fold of the domain remains intact, the disease mutants may affect interactions necessary

for cooperativity. Further examination of the conformation of N-ATP7B with between 3 and 5 copper atoms bound will be critical for understanding this mechanism.

Both mutants generated in the context of full-length ATP7B tend to localize to the ER when overexpressed (56). This observation suggests they are misfolded, although the possibility that this is simply an artifact of overexpression cannot be excluded. Based on our data, the structural alterations to the N-Terminal domain are minimal, but may be more significant in the context of the entire ATPase, particularly if N-ATP7B acts as a chaperone to guide the folding of the other cytosolic domains. From the structure of CopA, MBDs 5 and 6 are most likely to interact with the A-domain (137). The G591D mutation could alter this interaction, affecting the folding or function of this domain (Fig 4.6a). These domains are likely to be located close to the lipid bilayer, which may also affect folding. MBDs 1-4 have been shown to interact with the N-domain in a copper dependent manner. The G85V mutation could affect the relationship between these domains.

The 56 amino acids at the very N-Terminus of N-ATP7B have been shown to be critical for properly directed trafficking. In particular, the 9aa sequence F_{37}-E_{45} is critical for proper apical targeting (147). A Rosetta model of the N-Terminus and MBD1 shows that G85 is situated in a position to interact with the key residues in this region (Fig 4.6b). Disrupting this interaction could alter trafficking even if copper binding remains unaffected.

Likewise, the demonstrated increased affinity for COMMD1 (56) may be a consequence of decreased interactions between the N-Terminal domain and the rest of ATP7B. COMMD1 interactions are copper dependent, and appear to be essential for proper trafficking. If the N-Terminal domain is dissociated from the N-Domain even in the apo state, this may expose residues that interact with COMMD1 that are normally buried, and only available when the N-Terminal domain binds copper.

To summarize, we have evaluated the properties of the Wilson's disease causing mutations G85V and G591D in the context of N-ATP7B. The mutations have modest effects on copper binding and copper transfer from ATOX1, but do not appear to significantly alter the structure of N-ATP7B or the interaction amongst metal binding domains. Further studies should investigate how these mutations alter the interactions between the N-Terminal domain and the N, P and A domains of ATP7B, in order to understand how these mutations lead to ATPase dysfunction.

A.

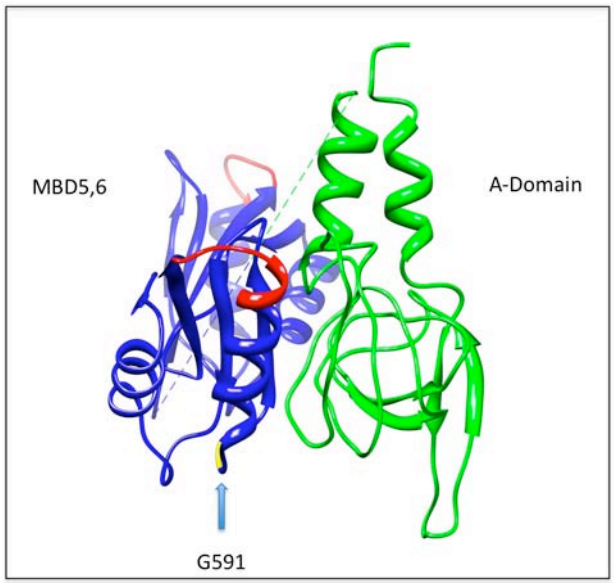

B.

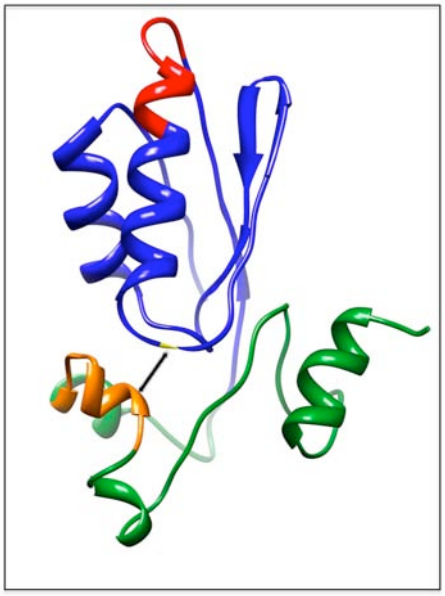

Figure 4.6. Disease-causing Mutations may be in close proximity to interacting domains. A. Model of MBD5-6 docked to A Domain of ATP7B. Metal binding sites are shown in blue, with GMxCxxC motifs in red. G591 is shown in yellow. (Adapted from Achila et al, 2006 (124) (PDB Code : 2ew9) and Banci et al, 2009 (121)) **B.** Model of MBD1 and the N-Terminal loop. MBD shown in blue with the GmxCxxC motif in red. G85 is shown in yellow. N-Terminus is shown in green, with the F_{37}-E_{45} segment in orange. Arrow indicates potential interaction between the conserved Gly residue and the essential trafficking loop. The model is derived from an *Ab initio* structure compiled in Rosetta by Dr. Ujwal Shinde.

Summary & Discussion

ATP7A and ATP7B are representative members of the heavy-metal transporting P-$_{1B}$ family of ATPases, functioning to transport copper across membranes for incorporation into the biosynthetic pathway or for sequestration and removal from the cell. These two functions also require the Cu-ATPases to have their activity and cellular location regulated by cytosolic copper concentrations. Each possesses an N-Terminal domain featuring six individual metal binding sites, which bind copper and function as a unit to regulate the ATPase in a concentration dependent fashion. The studies described in this dissertation yielded new information on the function of the N-terminal domain of ATP7B and the mechanism by which the N-terminal domain senses changing copper levels. The experiments uncovered unique properties of the individual MBDs, how they work together as a unit, and how mutations, both artificial and disease causing, affect the function and properties of the N-Terminal domains.

The Organization of N-Terminal Metal Binding Domains

The flexibility of the inter-MBD loops has made structural studies of multi-MBD constructs difficult. Current data suggests that the in the copper bound state, N-ATP7B is more compact and contains more ordered structural elements than in the apo state (57, 146). Our data demonstrates that the MBDs are organized in a close-packed conformation, even in the apo state (Fig 2.6). This packing, although compact, is not rigid and can respond to changing copper levels. The tight interactions between MBDs allow for minor perturbations in MBD structure due to mutation (Fig 2.3, 2.S.5) or copper

binding (Fig 2.8.D) to have a significant impact on the overall fold of the domain, which can be seen through the differential exposure of the inter-MBD loops.

Each of the MBDs of ATP7B has a unique, non-uniform distribution of surface charge (MBDs 2,4 and 5 are more electronegative, MBDs 1,3 and 6 are more electropositive) (140), which would allow for inter-MBD interactions through electrostatic interactions. Packing may also be dependent on hydrogen bonding that is mediated in part by the metal binding Cys residues of MBD2 (fig 2.7, 2.8). The ability of MBD2 to participate in H-bonding is suggested by our observation of markedly different consequences between Cys>Ala and Cys>Ser substitutions, which has shed light on how N-ATP7B may function. This bonding is critical for maintaining the ordered structure of the domain (Fig 2.3), and maintenance of reduced Cys residues (Fig 2.5, 2.S.7). It may also be necessary for keeping the MBD2 copper-binding loop in an open conformation, making it available for copper transfer (Fig 2.7). It is interesting that when analyzed individually, MBD2 is only the second best partner for ATOX1 (both with respect to protein-protein interactions and the rate of copper transfer). By itself, MBD4 in solution has a higher rate of copper transfer from the chaperone ATOX1 (124), perhaps due to having higher flexibility in the copper-binding loop (143). However, in the context of the entire N-Terminal domain, MBD2 is the primary recipient of copper from the chaperone (140). If the packing of N-ATP7B biases the copper-binding loop of MBD2 to a more open conformation due to hydrogen bonding, this could result in an increased likelihood for copper transfer and account for MBD2 being a preferential partner for ATOX1.

It is possible that the AxxA substitutions affect other properties of the MBDs. The metal binding loops of each MBD are likely to have different flexibilities and conformational dynamics (143). Substituting a large hydrophobic molecule like Alanine into this loop could limit or alter their flexibility and affect the local pKa. Ab initio structures of MBD2 did not reveal any significant structural differences between the CxxC and AxxA variants (data not shown) but molecular dynamics simulations could be more revealing. While the hydrogen bonds potentially formed by the CxxC of MBD2 may not have a high enough bond-energy to hold the entire domain in a fixed conformation, our data suggests that eliminating them does indeed alter MBD-MBD interactions. Monitoring the controlled unfolding of pairs of MBDs by circular dichroism could show whether the AxxA substitution does indeed cause the MBDs to dissociate from one another as implicated in Fig 2.9.

Interactions amongst MBDs protect N-ATP7B against oxidation in vitro and in cells

Our studies uncovered the importance of inter-MBD contacts for maintaining the reduced state of N-ATP7B. This property has not been previously appreciated, as buffers for the purification and functional analysis of N-ATP7B/ATOX1 typically contain large amounts of reducing reagents. Our results illustrate that aside from preventing its own oxidation, the putative hydrogen bonding mediated by MBD2 appears to maintain the reduced state of other MBDs (Fig 2.5). This is also the case for MBD3, but not MBD4 or 6. Interestingly, when the Cys residues of both MBD2 and MBD3 are mutated, the oxidative effect is countered. This suggests cooperativity between the domains, which is

also observed in experiments measuring dependence of copper transfer on concentration of Cu-ATOX1 (Figs 2.2.B, 3.2.A, 4.5).

The effects of CxxC >AxxA mutations in MBDs 2 and 3 are unique with regard to the redox state of thiols in other MBDs. Equivalent mutations in MBD4 and MBD6 were associated with conformational changes, but did not impact the redox status of other MBDs. Our data also shows susceptibility of N-ATP7B to irreversible oxidation, even in the presence of thioredoxin (Fig 2.5). It is thus imperative that the metal binding Cys residues remain reduced when not binding copper in order to maintain domain conformation and ability to receive copper from ATOX1. The demonstration that glutaredoxin interacts with N-ATP7B implies that a complex regulatory system may exist to maintain the proper redox state of Cu-ATPases (179). Given that ATOX1 itself can be glutathionylated (Lutsenko lab unpublished data), it is interesting to speculate that the chaperone itself may assist in maintaining the reduced state of MBDs under basal copper concentrations.

The ferredoxin-like fold shared by ATOX1 and the MBDs also suggests a role for self-regulated redox control. While these molecules have lost their ability to bind iron, they retain the ßαßßαß structure common to many ferro-proteins that catalyze electron transfer. It has recently been shown that the transfer of copper from the chaperone COX17 to SCO1 is coupled to the transfer of electrons, allowing copper to be transferred even if the metal binding Cys residues of SCO1 are oxidized in a disulfide (180). While a single molecule of Cu-ATOX1 may not be able to perform both transfer and reduction

reactions, a dimer of ATOX1 molecules centered around a single copper atom would have an unpaired Cys that could aid in this reaction. It would be useful to examine transfer experiments where ATOX1 is reconstituted in this ratio. As shown in Fig A.4, the inter-MBD loops of N-ATP7B are long enough to allow some non-metal binding Cys residues (from MBD3 or possibly MBD4) to come into proximity with the CxxC motif of MBD2. If these Cys residues are reduced, they may also aid in transfer and reduction reactions, forming temporary Cu-S clusters that allow directed transfer to MBD2 followed by domain rearrangement occurring in a cooperative fashion.

Cooperativity amongst MBDs has been previously reported (134), but there is also evidence showing that each individual MBD can receive copper from ATOX1 in the absence of other functional MBDs (150). Our data shows that some copper can be transferred to N-ATP7B when the CxxC motif of MBD2 is mutated and the reaction is performed in a reducing environment (Fig 2.2). The initial copper transferred shows the same concentration dependence as for wild type, but subsequent transfers require significantly higher concentrations of Cu-ATOX1. Transfers to wt N-ATP7B show noticeable cooperativity after the binding of 3 copper atoms (Figs 2.2.B, 3.2.A). Altering the concentration dependence of copper transfer from ATOX1 was also the most significant effect observed for the disease mutants G85V and G591D, suggesting these mutations might cause altered copper sensitivity.

Structure and function of inter-MBD loop regions

Previous CD data demonstrated that the most significant changes in secondary structure occur after the binding of 2 copper atoms to N-ATP7B (57). Since Cu-binding to individual MBDs does not significantly alter their structure, the cooperativity amongst MBDs is most likely achieved through structural changes that occur in the loops connecting the MBDs. These changes in N-ATP7B organization result in differential exposure of loop residues that are important for phosphorylation (146), inter-domain interactions (181), and as docking sites for the trafficking machinery (55). Our data shows copper transfer or mutation of the MBD2 CxxC motif to expose residues in the loops connecting MBD1-2 and MBD2-3 (Figs 2.3, 2.8). Rosetta models of MBD1-2 (fig 2.9) and MBD2-3 (fig A.4) show both loops having inherent α-helicity. The MBD1-2 loop is short (12 aa), but may allow interaction between the CxxC sites of MBDs 1 and 2. Our data suggest an altered exposure of Trp and Lys residues in the loop when the MBD2 CxxC residues are mutated to AxxA, although recent molecular dynamic simulations suggest that in the WT protein this loop may be fairly rigid(182). The altered exposure of the 1-2 loop could be due to changes in the overall fold of the N-terminal domain (N-ATP7B).

The MBD2-3 loop is much longer (42 aa) and likely to be more flexible than the MBD1-2 loop. This allows for a range of potential interactions between MBD2 and MBD3, resulting in proximity between the two metal binding loops, and/or between the CxxC of MBD2 and Cys305 located at the base of the α2 helix of MBD3 (one of six Cys residues

in N-ATP7B outside of the six metal-binding loops). Although these Cys residues do not have a tendency to form disulfide bonds (57), they may play a role in reducing the metal binding CxxC motifs. Alternatively, interaction between cysteines could enable cooperative changes by providing a stabilizing third ligand to copper. Earlier EXAFS data shows that the copper bound to N-ATP7B is capable of accepting a third exogenous ligand (132). By temporarily providing a third ligand, these Cys residues may play a role in facilitating conformational changes (Fig 2.8.D) and exposing other MBDs or key loop residues. While copper loaded N-ATP7B shows little to no Cys labeling (Fig 2.5.A), this lack of reactivity is probably due to limited exposure of Cys not involved in copper coordination rather than their oxidation, as some of these cysteines can be labeled when N-ATP7B is subject to limited proteolysis (data not shown). Likewise, there is residual Cys labeling in copper loaded N-ATP7A, presumably from the equivalent non-metal binding Cys residues (Figs 3.2.B, 3.7.A). These residues could also play a role in the coordination of other molecules, such as the chemotherapeutic drug cisplatin (Fig A.4).

Effects of ATOX1 mediated copper transfer to N-ATP7A and N-ATP7B

Both ATP7A and ATP7B obtain copper from ATOX1. We demonstrate that all six MBDs of N-ATP7A can be filled with copper in the presence of Cu-ATOX1, but that a higher concentration of the chaperone is necessary to achieve saturation than what is observed for N-ATP7B (Fig 3.2.A). In vitro, a 40-60 fold ratio of Cu-ATOX1 over N-ATP7A/B is necessary for six coppers to be transferred. However, it is not known whether this amount of the chaperone is present in cells; ATOX1 mRNA is 3-4 times

more abundant than ATP7B mRNA in hepatocytes (Lutsenko lab unpublished data). We show that when N-ATP7B is repeatedly presented with low concentrations of Cu-ATOX1 (10-fold over N-ATP7B) six copper molecules can be transferred (Fig 3.4). This phenomenon appears to require the complete removal of ATOX1 from solution, as ATOX1-MBD adducts may prevent additional transfer. When both N-ATP7A and N-ATP7B are present simultaneously, ATOX1 transfers copper to each with similar efficiency as observed when presented separately (Fig 3.7). ATP7B has been shown to undergo catalytic phosphorylation with greater sensitivity to free copper concentration (27). Our data suggest this trend holds for copper delivered by ATOX1, but it remains to be seen if there is a physiological difference in rates of ATOX1 mediated activation between the two Cu-ATPases. In cells that simultaneously express both Cu-ATPases, it seems likely that the distribution of copper between the two transporters (and their respective copper delivery pathways) would be determined by a combination of Cu-ATPase expression levels and their relative affinity for the copper-ATOX1 complex.

Much like for N-ATP7B, ATOX1 initially transfers copper to a specific MBD of ATP7A (Fig 3.6). N-ATP7A shows a distinct mobility shift upon copper acquisition (Fig 3.5), suggesting a copper-induced conformational change. Limited trypsinization did not reveal significant changes in the exposure of residues between MBD2 and 3 or MBD4 and 5 of N-ATP7A upon copper binding, suggesting the prominent conformational changes occur elsewhere in the domain. Although ATP7A and ATP7B have many similar properties, their differences in copper-dependent trafficking may involve interaction with different cytosolic proteins, thus requiring the exposure of a unique set of

residues in their N-Termini. However, the loop between MBDs 3 and 4 is subject to kinase-mediated phosphorylation in both proteins (59, 146) and thus must be considered a candidate for altered exposure in N-ATP7A.

Wilson's Disease causing mutations and domain-domain interactions within ATP7B

We observed that the Wilson's Disease causing mutations G85V and G591D have an effect on copper transfer from ATOX1 to N-ATP7B in that they eliminate the cooperativity described above. Aside from this, the G85V and G591D mutants behaved similar to WT N-ATP7B in regard to solubility, copper binding, oxidation and folding (Fig 4.2, 4.3, 4.4). We hypothesize that these mutations must exert their primary affects by altering the interactions between the N-Terminal domain and the other cytosolic domains of the protein. MBDs 5 and 6 (site of the G591D mutation) are likely to be in close proximity to the actuator domain (see Figs 1.3, 4.6.A). This interaction may be required for proper folding of the A-domain, for regulation of dephosphorylation, and for controlling access to the intra-membrane copper-binding site. MBDs 1-4 interact with the nucleotide-binding domain (181) (see Fig 1.3), and regulate catalytic phosphorylation. We hypothesize that the copper induced conformational changes to the N-Terminal domain described here reduce the affinity between the two domains, allowing for the catalytic cycle to proceed at a higher rate. Defining the key residues and sites of interaction between these domains will be important in better understanding of how copper regulates the ATPase activity. Dissecting the domain interface will also clarify how the ATP-binding domain may limit access to N-Terminal residues required

for proper trafficking and membrane targeting under basal copper conditions. The G85V mutation is situated in proximity to N-Terminal residues necessary for proper membrane targeting of ATP7B (fig 4.6.B). Altering the exposure of these amino acids may be sufficient to trigger protein mislocalization and cause a disease phenotype.

In summary, the research leading to this dissertation provides novel and significant data about the function of the N-Terminal domains of the human copper transporting ATPases ATP7A and ATP7B. Using an array of biochemical and computational techniques, we have shown that the N-Terminal domains function as a cooperative unit that uses copper binding as a means to regulate their conformation. In ATP7B, this is mediated by a close-packing of the metal binding domains, which may be dependent on the hydrogen bonding ability of the copper-coordinating cysteine residues. This ordered structure functions to maintain cysteine reduction and modulate interactions with the metallochaperone ATOX1. Copper transfer from ATOX1 remodels the network, allowing the N-terminal domain to proceed through a specific pathway of intermediate conformations, using the inter-MBD loops to amplify the structural effects of copper binding. Together, these data provide a mechanistic model of how the N-Terminal domain relays information about cytosolic copper concentrations to the rest of the ATPase in a regulatory manner. Our results lay groundwork for a further understanding of how ATP7A and ATP7B regulate cellular copper homeostasis, and how this regulation may be perturbed in Menkes and Wilson's Diseases.

Appendix I

Cisplatin binding by the N-Terminal metal binding domains of the Cu-ATPases

Portions of this Appendix have been published. Figure A.1 appears in Clinical Cancer Research as part of Mangala et al, 2009 (183). Some of the data in Figure A.3 is referenced in the Biochemical Journal as unpublished data in Dolgova et al, 2009 (184). Drs. Martina Ralle and Ujwal Shinde aided in data collection and compilation where noted.

Introduction

Although most of the research on ATP7A and ATP7B has centered on their function as essential copper transporters, there is a growing body of work exploring the role of the two ATPases in cancer, specifically in mediating resistance to the chemotherapeutic drug cisplatin. Numerous cisplatin resistant tumors, including ovarian carcinomas (185), squamous cell carcinomas (186), and esophageal carcinomas (187) show markedly increased expression of either ATP7A or ATP7B.

Cisplatin (as well as related molecules carboplatin and oxaliplatin) has been an indispensible drug for cancer treatment; testicular cancers, for example, are highly responsive. The drug acts by forming DNA adducts, leading to cell cycle arrest. Although treatment is effective for many types of cancer, acquired resistance to cisplatin often leads to recurrent tumors that defy chemotherapy. Many mechanisms have been implicated in leading to resistance, including enhanced DNA repair, altered cell signaling and cell cycle checkpoint evasion (188). As with many drugs, cells may alter expression of genes involved in uptake, efflux and detoxification. For cisplatin, several genes implicated in this response typically function in copper transport, including the cell surface transporters CTR1 and CTR2, as well as the cytosolic Cu-ATPases ATP7A and ATP7B.

Both CTR1 and CTR2 have been shown to be involved in cisplatin uptake (189, 190). Numerous studies have correlated CTR1 expression levels with amounts of cellular platinum accumulation (189, 191-193). Down regulation of CTR1 may be an additional

means of gaining cisplatin resistance. However, knockdown of CTR2 has been shown to increase cellular cisplatin uptake in cells lacking CTR1, suggesting complex regulation of cisplatin import. ATP7A and ATP7B remove excess copper by sequestering the ion in vesicles, which can then fuse to the plasma membrane facilitating excretion. The correlation between Cu-ATPase expression and cisplatin resistance has led to the hypothesis that the Cu-ATPases transport platinum facilitating its removal, thereby increasing cellular resistance.

In ovarian carcinoma cell lines, there is some evidence that ATP7A and ATP7B can localize to vesicles in response to cisplatin (194), though trafficking may not happen as rapidly as it does for copper (195). Fluorescent cisplatin analogs have been colocalized with ATP7A (196) and ATP7B (197) in vesicles. However, overexpression of ATP7A may not lead to enhanced cisplatin efflux (195), nor is it clear if ATP7B can transport cisplatin at a physiologically relevant rate (198). Given that copper and platinum have very different properties (even before the modifications made to platinum to form cisplatin), it would be surprising if the Cu-ATPases used an identical mechanism for transporting the two metals. Indeed, cisplatin does not impede copper transport by ATP7B, perhaps due to separate binding sites (199). This also appears to be true for CTR1, as different binding ligands have been identified for cisplatin and copper (200, 201).

Metallothioneins have also been shown to be upregulated in cisplatin resistant tumors (202), playing a role in detoxification through binding and sequestration of platinum.

The metallochaperone ATOX1 has also been implicated in cisplatin binding and pharmacology (203), with recent structural data providing a potential binding mechanism (204). We hypothesized that the observed intracellular colocalization of a fluorescent cisplatin analogue with the Cu-ATPases was due to the binding of cisplatin through their N-Terminal domains, which contain six metal-binding domains that bind copper through conserved CxxC motifs. Here we present evidence that N-ATP7A and N-ATP7B can bind cisplatin, in part using these metal-binding cysteines. However, our work supports recent findings suggesting that cisplatin is bound with different coordination than that described for copper.

Materials and Methods

Expression and Purification of Recombinant Proteins. N-ATP7A and N-ATP7B derived from human ATP7A and ATP7B, respectively, were expressed and purified as a fusion with Maltose-Binding Protein (MBP) as previously described (158). Further details are described in the Appendix.

Cysteine Protection Assays. Purified N-ATP7B and N-ATP7A were incubated with 100 μM TCEP, then dialyzed into buffer containing 25 mM $NaPO_4$ and 150 mM NaCl. 10 μg protein (1 nm) was used for each reaction. Stable aqueous Cisplatin-HCl (0.1% Cisplatin, 0.9% NaCl) was diluted into 0.9% NaCl, then added to purified protein in the dark at room temperature for 15 min. Cys reactivity was tested using CPM as described in Chapter 1. Samples were then separated on SDS-PAGE gels and CPM fluorescence and protein amounts were quantified by densitometry as described in Chapter 1. For copper binding, the same experiments were performed using $CuCl_2$ that was dissolved in 0.9% NaCl containing 100 μM Ascorbate.

Quantitation of Cisplatin Binding. Purified N-ATP7B and N-ATP7A were incubated with 100 μM TCEP, then dialyzed into buffer containing 25 mM $NaPO_4$ and 150 mM NaCl. 500 μg of protein (50 nm) was incubated with 5 μm of Cisplatin (diluted in 0.9% NaCl, as above). The solution was then dialyzed overnight into buffer containing 25 mM $NaPO_4$ and 150 mM NaCl. Final protein concentration was evaluated using the Lowry assay (165). Final platinum and copper concentrations were evaluated using inductively

coupled plasma mass spectrometry (ICP-MS) using a Perkin-Elmer Optima 2000 DV spectrometer.

Results

Despite clear evidence that ATP7A and ATP7B are upregulated in numerous cisplatin resistance tumors, it is not clear if the ATPases can transport platinum efficiently enough to detoxify cells. We hypothesized that the metal binding domains of N-ATP7A and N-ATP7B could bind cisplatin using the CxxC motifs in each MBD, thereby sequestering the drug, even if it is not removed from the cell with the same mechanism used for copper. To test whether the metal binding Cys residues were involved in cisplatin binding, we incubated purified N-Terminal Domain with cisplatin, then tested Cys availability by probing with the coumarin maleimide CPM, which fluoresces when bound to reduced sulfhydryls.

For N-ATP7B, there was a concentration dependent decrease in fluorescence per protein with increased concentrations of Cisplatin. This result suggested that cisplatin binds to N-ATP7B and directly (or indirectly via conformational change) protects Cys residues against the labeling. Some fluorescence (roughly 50% of untreated) was still detectable, even in with 60-fold molar excess of Cisplatin over protein (10-fold over each of six metal binding domains) (Fig A.1.A). In contrast, only 10 fold molar excess of Cu(I)-Ascorbate over protein was necessary to block labeling of nearly all cysteines (Fig A.1.B), in accordance with data demonstrating copper binding to N-ATP7B in a 6/1 ratio (158).

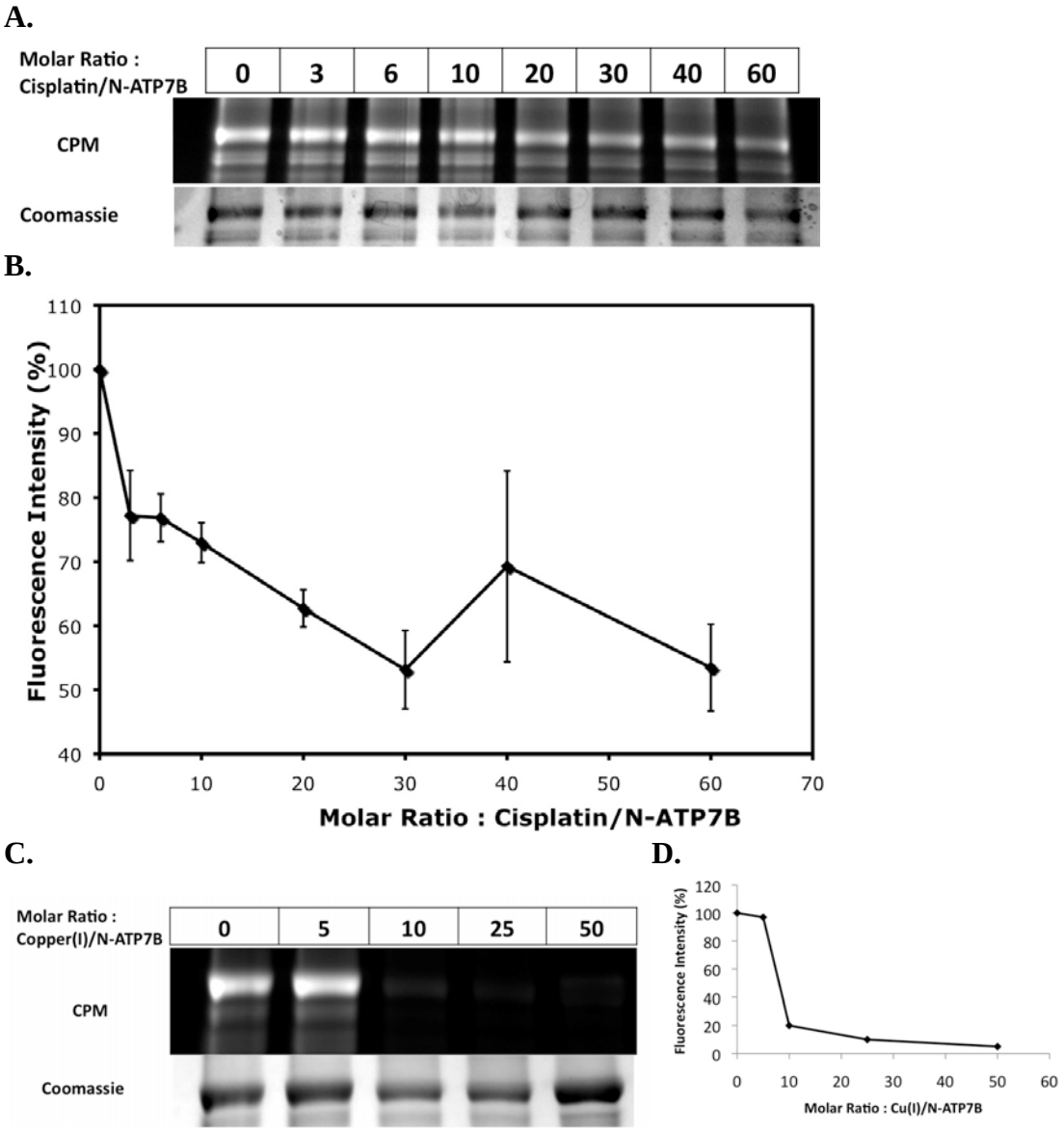

Figure A.1. Cisplatin protects cysteines in N-ATP7B against labeling with CPM. **A)** Fluorescence (top) and Coomassie (bottom) images of N-ATP7B that was incubated with the indicated molar ratios of Cisplatin per protein, then labeled with the Cys directed maleimide CPM. **B)** Graphic representation of data from **(A)**. Label per protein ratio for N-ATP7B that was not exposed to Cisplatin is defined as 100%. Error bars represent standard deviation across three experiments. **C)** Fluorescence (top) and Coomassie (bottom) images of N-ATP7B that was incubated with the indicated molar ratio of Cu-Ascorbate, then labeled with the Cys directed maleimide CPM. **D)** Graphic representation of data from **(C)**. This figure appears in Clinical Cancer Research as part of Mangala et al, 2009 (183).

Similar results were seen for N-ATP7A (Fig A.2). At 60-fold Cisplatin over protein, 40% of the initial fluorescence still remained, where 10-fold Cu(I)-Ascorbate over protein blocked nearly all CPM labeling. Also, protection by cisplatin reaches a plateau indicative of saturation of available binding sites From these data, it seemed clear that N-Terminal binding of Cisplatin did not follow the same binding mechanism as for copper, with each MBD capable of binding one copper between two cysteines. We hypothesized that the difference might be due to one of two reasons. Cisplatin could be bound to two cysteines from different MBDs, or could be bound in a motif involving one Cysteine and some other ligands. These two possibilities should yield different binding stoichiometries.

To evaluate the stoichiometry of Cisplatin binding to N-ATP7A and N-ATP7B, we incubated purified N-Terminal domain with a 100-fold excess of Cisplatin, then dialyzed the solution overnight and measured the amount of platinum that remain bound to the protein (Fig A.3). N-ATP7A and N-ATP7B retained 1.8 and 2.2 Pt/Protein. Both samples showed background copper binding as well (0.8 and 1.1 Cu/Protein respectively). These data suggest that cisplatin can be stably bound to N-ATP7A and N-ATP7B, but with fewer binding sites available than for copper.

A.

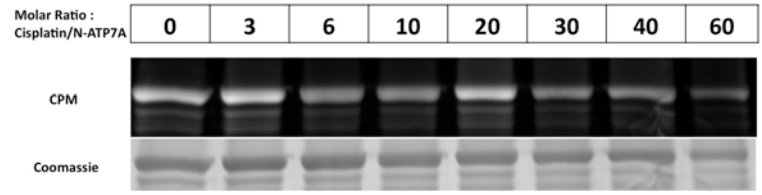

B.

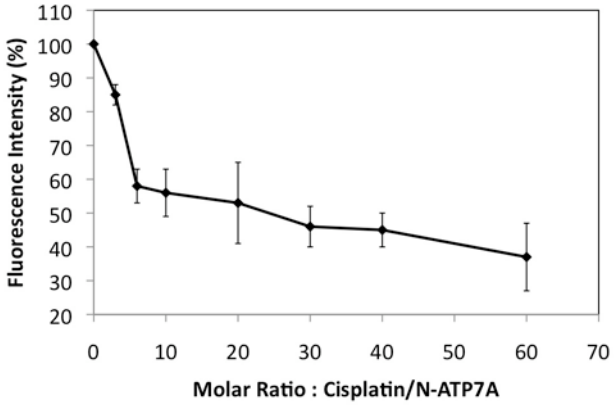

C.

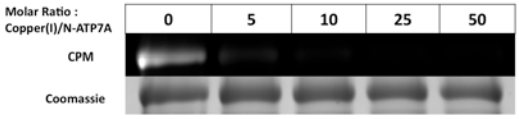

D.

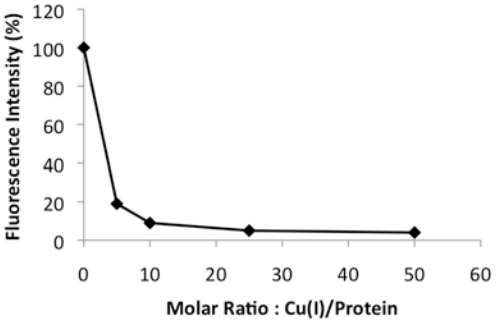

Figure A.2. Cisplatin protects cysteines in N-ATP7A against labeling with CPM. **A)** Fluorescence (top) and Coomassie (bottom) images of N-ATP7A that was incubated with the indicated molar ratio of Cisplatin, then labeled with the Cys directed maleimide CPM. **B)** Graphic representation of data from **(A)**. Label per protein ratio for N-ATP7A that was not exposed to Cisplatin defined as 100%. Error bars represent standard deviation across three experiments. **C)** Fluorescence (top) and Coomassie (bottom) images of N-ATP7A that was incubated with the indicated molar ratio of Cu-Ascorbate, then labeled with the Cys directed maleimide CPM. **D)** Graphic representation of data from **(C)**.

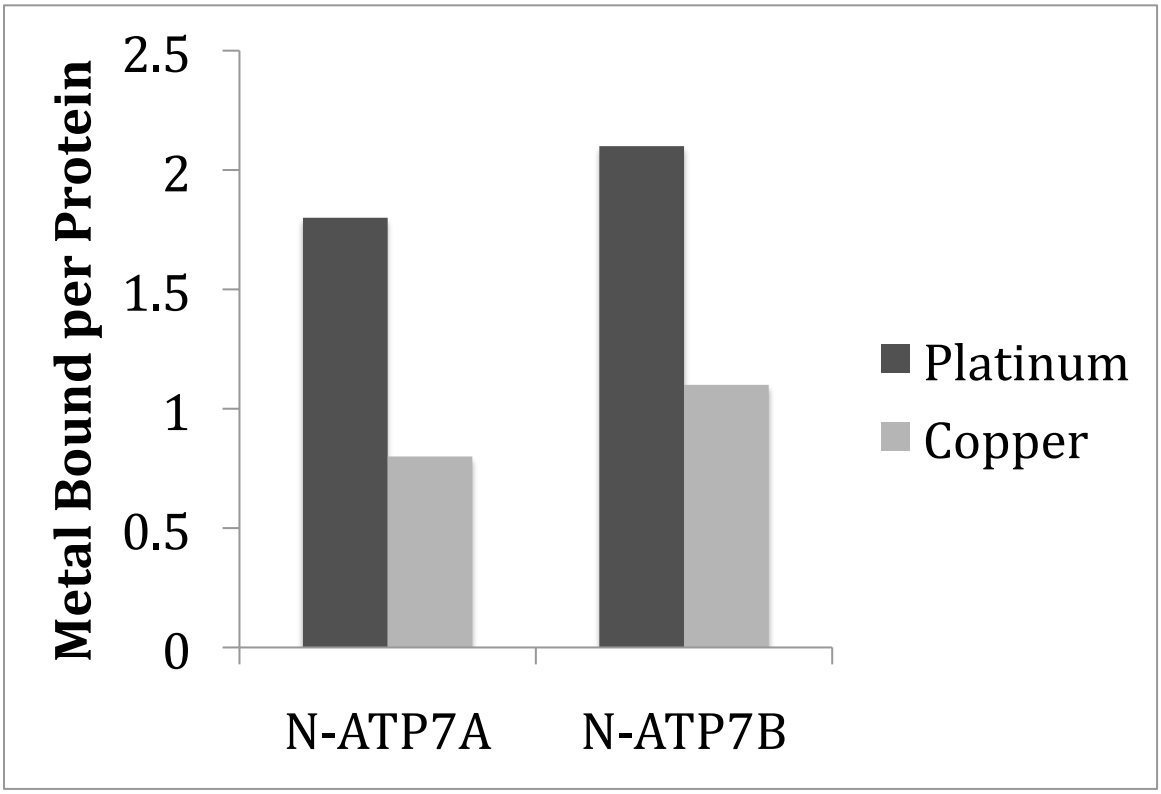

Figure A.3. Metal binding to N-ATP7A and N-ATP7B after dialysis. Platinum (Dark grey) and Copper (Light grey) per protein bound to N-ATP7A (left) and N-ATP7B (right) after incubation with 100x Cisplatin followed by overnight dialysis. Final ICP/MS measurements were taken by Dr. Martina Ralle. The ATP7B data was referenced as unpublished data in Dolgova et al, 2009 (184).

Discussion

The results of these experiments show that cisplatin binding to N-ATP7A or N-ATP7B protects against cysteine labeling by CPM, though not with the same efficacy as copper. 60 fold excess of cisplatin over protein (10-fold over metal binding sites) reduces Cys labeling by 50% in N-ATP7B and by 60% in N-ATP7A compared to >95% for copper.

After overnight dialysis, only 2.2 and 1.8 platinum molecules remain bound to N-ATP7B and N-ATP7A, respectively. The residual binding of copper may have reduced the overall cisplatin binding capability. It is clear that cisplatin can bind to the N-Terminal domains of the Cu-ATPases, but it appears to have lower affinity and perhaps a different binding motif than does copper.

In the time since this work was completed, other groups have further explored the mechanism and consequences of cisplatin binding to copper transport proteins, which support and give context to our results. Dolgova et al (184) showed the first four MBDs of N-ATP7B can bind up to three cisplatin molecules, and that this binding was sufficient to alter the tryptic digest pattern of the protein, particularly in the region of the CxxC motif of MBD2, but not MBD1 or 3, suggesting that some Cys residues, but perhaps not all, are involved in Cisplatin binding. The flexibility of the metal binding loops of MBD2 and MBD4 (discussed in Chapters 1 and 2) may allow for these domains to more readily form a potential binding site for cisplatin, as opposed to the more rigid MBD3.

Boal and Rozensweig (204) solved the crystal structure of the chaperone ATOX1 bound to cisplatin as both a monomer and a dimer. The monomer showed the metal binding Cys residues bound to a platinum ion with exogenous TCEP acting as a third ligand, and the amide nitrogen of the N-terminal Cys as a fourth. In the dimeric structure, the cisplatin molecule retained its ammine groups and was bound between one Cys of each molecule of ATOX1. Both structures show the platinum ion in a square planar conformation, as opposed to the linear conformation used to bind copper. This supports our hypothesis that the MBDs of N-ATP7A and N-ATP7B (which strongly resemble ATOX1) use a different binding mode for cisplatin than for copper. It is possible that multiple MBDs are bridged together around one cisplatin molecule (See Figure A.4.A for example), with each donating a Cys ligand. Alternatively, there are additional Cys residues in both N-Terminal domains that could provide an additional ligand to stabilize cisplatin binding (Fig A.4.B). The dimeric structure of ATOX1-cisplatin also suggests that cisplatin could form a bridge between the chaperone with an MBD. In vivo, an endogenous ligand like glutathione could provide stabilization for platinum bound to both Cys residues of an MBD. These situations could potentially increase the stoichiometry of cisplatin bound to the N-Terminus.

Leonhardt et al (199) showed that Cisplatin could stimulate phosphorylation of ATP7B, but could not out compete copper in transport assays. A truncation mutant removing the first 4 MBDs could not be activated by cisplatin, but a mutant with MBDs 1-5 inactivated could. They also found that cisplatin could not induce ATP7B trafficking in hepatocytes. It is possible that cisplatin binding to N-ATP7B would alter the conformation of the

domain enough to lower the binding affinity of the N-Terminal domain for the nucleotide binding domain and stimulate catalytic activity (181). However, if N-ATP7B uses different binding mechanisms for cisplatin, it may not adopt the conformation necessary for proper interaction with the trafficking machinery, or the proper exposure of the N-Terminal segment required for apical targeting (147).

Mangala et al (183) showed that expression of the N-Terminal domain of ATP7B alone in ovarian carcinoma cells was sufficient to affect a 2-fold increase in cisplatin resistance. Likewise, Dolgova et al showed increased cisplatin resistance in *E. coli* expressing MBD1-4 of ATP7B (184). It is possible that ATP7A and ATP7B are upregulated as part of a more general response to cisplatin toxicity and remain expressed at high levels due to their ability to sequester platinum, whether or not they are effective at removing the compound from the cell. Having a clear identification of which MBDs are involved with cisplatin binding, and how this binding affects the structure of the N-Terminal domain would provide a better understanding of how cisplatin stimulates ATPase activity, and under which conditions cisplatin may be able to induce trafficking.

A. **B.**

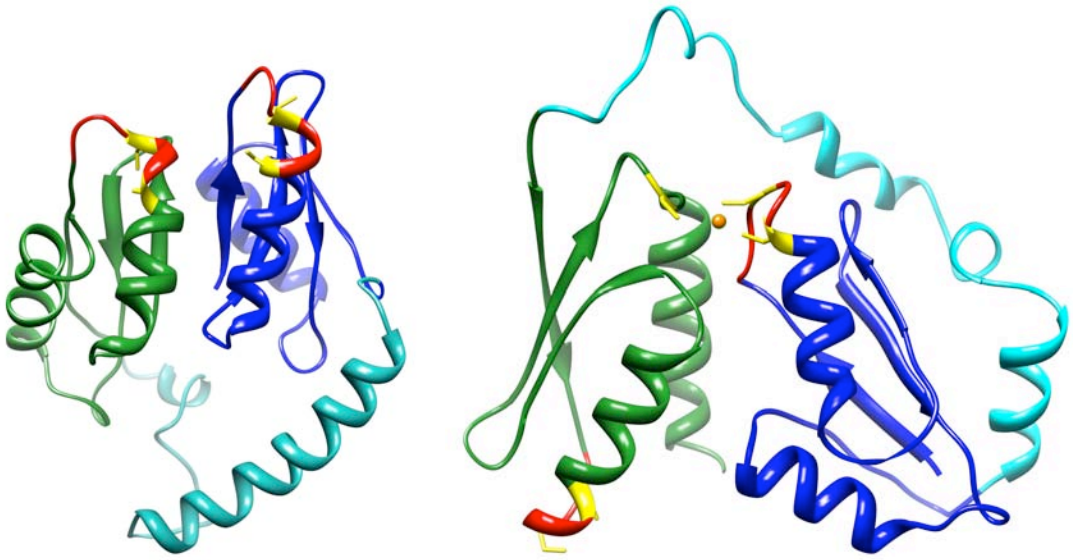

Figure 4. MBDs 2 and 3 of ATP7B could share coordination of a single cisplatin molecule. **A)** *Ab initio* Rosetta model of MBD2 and 3 of ATP7B. MBD2 shown in blue, MBD3 in green. GMxCxxC shown in red, metal binding Cys residues in yellow. The loop separating MBD2 and 3 (shown in teal) has the length (42 aa) and flexibility to allow the CxxC motifs to come close together. **B)** MBD3 also has a Cys residue outside of the CxxC motif that can come in close proximity to the CxxC of MBD2 as show in this *Ab initio* model. Cisplatin (pink) modeled into MBD2 using alignment with published structure of ATOX1-Cisplatin (Boal and Rosenzweig, 2009 (204) PDB Code : 3iwl). *Ab initio* models were compiled by Dr. Ujwal Shinde.

APPENDIX II

ADDITIONAL MATERIALS AND METHODS

Constructs & Sequences

N-ATP7B

N-ATB7B is based on the N-Terminal domain of the human ATP7B and is expressed as a fusion protein with the maltose-binding protein (MBP) as first described in Lutsenko et al, 1997 (158). Base pairs 64-1868 of the *ATP7B* cDNA have been inserted into the pMAL-c2 vector (New England Biolabs, Ipswitch, MA) at the 3' end of the coding sequence for MBP, fusing MBP to the N-Terminus of N-ATP7B. The first 21 residues have been truncated. These reside within the 56 aa N-Terminal segment C-terminal to MBD1. MBDs 1-5 and connecting loops are intact. The C-Terminal 12 residues of MBD6 (corresponding to the last ß-sheet) are also truncated. The fusion protein has a molecular weight of 108 kDa.

N-ATP7A

N-ATB7A is based on the N-Terminal domain of the human ATP7A and is expressed as a fusion protein with the maltose-binding protein (MBP) as first described in Lutsenko et al, 1997 (158). Base pairs 1-1836 of the *ATP7A* cDNA have been inserted into the pMAL-c2 vector (New England Biolabs, Ipswitch, MA) at the 3' end of the coding sequence for MBP, fusing MBP to the N-Terminus of N-ATP7A. MBDs 1-5 and connecting loops are intact. The C-Terminal 21 residues of MBD6 (corresponding to the last α-helix and ß-sheet) are truncated. The fusion protein has a molecular weight of 110 kDa.

ATOX1

The ATOX1 construct is based on the human ATOX1 protein and is expressed as a fusion protein with a chitin-binding protein (CBP) and intein tag as first described in Walker et al, 2002 (51). Base pairs 1-204 of the *ATOX1* cDNA have been inserted into the pTYB12 vector (New England Biolabs, Ipswitch, MA) at the 3' end of the coding sequence for the CBP/Intein. The CBP/Intein can be self-cleaved in the presence of a reducing thiol, and leaves a 3 aa tag (Ala-Gly-His) at the N-Terminus of ATOX1. The cleaved protein is 71 aa long and has a molecular weight of 7,667 Da.

Sequences and MBD boundaries

N-ATP7A and N-ATP7B contain six MBDs connected by loops of various lengths (see Fig 1.5). For consistency, we have defined the individual domains as 72 aa segments beginning 9 aa N-Terminal to the GMxCxxC motif of each MBD. Those divisions are printed below. GMxCxxC motifs are in Red, residues truncated from the constructs are in Blue.

N-ATP7B

N-Terminus (56)
MPEQERQITAREGASRKILSKLSLPTRAWEPAMKKSFAFDNVGYEGGLDGLGPSSQ

MBS1
VATSTVRILGMTCQSCVKSIEDRISNLKGIISMKVSLEQGSATVKYVPSVVCLQQVCHQIG
DMGFEASIAEG

Loop1-2 (13)
KAASWPSRSLPAQ

MBS2
EAVVKLRVEGMTCQSCVSSIEGKVRKLQGVVRVKVSLSNQEAVITYQPYLIQPEDLRDH
VNDMGFEAAIKSK

Loop2-3 (42)
VAPLSLGPIDIERLQSTNPKRPLSSANQNFNNSETLGHQGSH

MBS3
VVTLQLRIDGMHCKSCVLNIEENIGQLLGVQSIQVSLENKTAQVKYDPSCTSPVALQRAI
EALPPGNFKVSL

Loop3-4 (30)
PDGAEGSGTDHRSSSSHSPGSPPRNQVQGT

MBS4
CSTTLIAIAGMTCASCVHSIEGMISQLEGVQQISVSLAEGTATVLYNPSVISPEELRAAIED
MGFEASVVSE

Loop4-5 (57)
SCSTNPLGNHSAGNSMVQTTDGTPTSVQEVAPHTGRLPANHAPDILAKSPQ
STRAVA

MBS5
PQKCFLQIKGMTCASCVSNIERNLQKEAGVLSVLVALMAGKAEIKYDPEVIQPLEIAQFIQ
DLGFEAAVMED

Loop5-6 (4)
YAGS

MBS6
DGNIELTITGMTCASCVHNIESKLTRTNGITYASVALATSKALVKFDPEIIGPRDIIKIIEEIG
FHASLAQR

Loop6-Mem (14)
NPNAHHLDHKMEIK

N-ATP7A

N-Terminus (5)
MDPSM

MBS1
GVNSVTISVEGMTCNSCVWTIEQQIGKVNGVHHIKVSLEEKNATIIYDPKLQTPK
TLQEAIDDMGFDAVIHN

Loop1-2 (91)
PDPLPVLTDTLFLTVTASLTLPWDHIQSTLLKTKGVTDIKIYPQKRTVAVTIIPSIVNANQI
KELVPELSLDTGTLEKKSGACEDHSMAQA

MBS2
GEVVLKMKVEGMTCHSCTSTIEGKIGKLQGVQRIKVSLDNQEATIVYQPHLISVEEMKK
QIEAMGFPAFVKK

Loop2-3 (34)
QPKYLKLGAIDVERLKNTPVKSSEGSQQRSPSYT

MBS3
NDSTATFIIDGMHCKSCVSNIESTLSALQYVSSIVVSLENRSAIVKYNASSVTPESLRKAIE
AVSPGLYRVS

Loop3-4 (28)
ITSEVESTSNSPSSSSLQKIPLNVVSQP

MBS4
LTQETVINIDGMTCNSCVQSIEGVISKKPGVKSIRVSLANSNGTVEYDPLLTSPETLRGAIE
DMGFDATLSD

Loop4-5 (39)
TNEPLVVIAQPSSEMPLLTSTNEFYTKGMTPVQDKEEGK

MBS5
NSSKCYIQVTGMTCASCVANIERNLRREEGIYSILVALMAGKAEVRYNPAVIQPPMIAEFI
RELGFGATVIE

Loop5-6 (4)
NADE

MBS6
GDGVLELVVRGMTCASCVHKIESSLTKHRGILYCSVALATNKAHIKYDPEIIGPRDIIHTIE
SLGFEASLVK

Protein Expression and Purification

N-ATP7B and N-ATP7A

Expression : Both N-ATP7B-MBP and N-ATP7A-MBP (and all mutants thereof) are coexpressed with Thioredoxin (pThx) to reduce Cys residues and maintain protein solubility. All growth media and agar plates contain 100 μg/mL Ampicilin and 35 μg/mL Chloramphenicol. 10 mL overnight starter cultures from freshly streaked plates are added to 1.5 L of Luri Broth (LB) containing 0.2% glucose in a 2.8 L flask and grown at 37°C and 250 RPM until the OD_{600} is between 0.6 and 0.8. The culture is then cooled to 4°C for 30' and an additional 50 μg/mL of Ampicilin is added. If Cu-bound protein is being prepared, 250 μM $CuCl_2$ is also added to the culture. Expression is induced with 1mM IPTG and cultures are incubated at 25°C and 250 RPM for 3 hrs. Cells are harvested by centrifuging the culture in a JA-10 rotor for 15' at 5,000 RPM at 4°C. Cell pellets are resuspended in Lysis Buffer (25 mM NaH2PO4 pH 7.5 and 150 mM NaCl) containing Complete EDTA free protease inhibitors (Roche) using 15 mL of buffer per L equivalent of cells. The resuspended cells are then frozen at -20°C overnight.

Purification: Cells are thawed and lysed with two passes through a French press at 17,000 psi. The lysate is then cleared by centrifuging it in a JA-20 rotor for 30' at 17,000 RPM. The supernatant is taken and diluted in 5 volumes of lysis buffer and run 3 times over a gravity flow column containing 2 mL of Amylose resin (New England Biolabs) per L of culture. The resin is washed with 50x column volumes of lysis buffer followed by 20 volumes of 2x lysis buffer and then 25 volumes of 1x lysis buffer. The protein is

eluted by incubating with 0.5 column volumes of elution buffer (10 mM Maltose in 1x lysis buffer) for 15'. This is repeated 3x, with most of the protein residing in the 2nd and 3rd elutions. Maltose may be removed from the elution fractions by dialyzing against lysis buffer at 4°C overnight.

ATOX1

Expression: All growth media and agar plates contain 100 μg/mL Ampicilin. 10 mL overnight starter cultures from freshly streaked plates are added to 1.5 L of Luri Broth (LB) containing 0.2% glucose in a 2.8 L flask and grown at 37°C and 250 RPM until the OD_{600} is between 0.6 and 0.8. The culture is then cooled to 4°C for 30' and an additional 100 μg/mL of Ampicilin is added. Expression is induced with 500 μM IPTG and cultures are incubated at 16°C and 250 RPM for 16 hrs. Cells are harvested by centrifuging the culture in a JA-10 rotor for 15' at 5,000 RPM at 4°C. Cell pellets are resuspended in Lysis Buffer (25 mM NaH2PO4 pH 7.5 and 150 mM NaCl) containing Complete EDTA free protease inhibitors (Roche) using 15 mL of buffer per L equivalent of cells. The resuspended cells are then frozen at -20°C overnight.

Purification: Cells are thawed and lysed with two passes through a French press at 17,000 psi. The lysate is then cleared by centrifuging it in a JA-20 rotor for 30' at 17,000 RPM. The supernatant is taken and diluted in 5 volumes of lysis buffer and run 3 times over a gravity flow column containing 5 mL of Chitin resin (New England Biolabs) per L of culture. The resin is washed with 200x column volumes of lysis buffer. The protein is eluted by incubating with 5 column volumes of elution buffer (100 mM DTT in 1x lysis

buffer) for 36 h. Eluted protein is concentrated to 0.5 column volumes and then dialyzed overnight against lysis buffer at 4°C.

Copper Binding/Quantitation

Purified N-ATP7A or N-ATP7B that has bound copper either through E. coli loading or transfer from Cu-ATOX1 (as described in Chapters 2/3/4) is quantified with the Lowry assay (165), taking the average of three replicates. Proteins are separated on a 12% Laemmli gel and stained with Coomassie Blue to determine sample purity. For transfer experiments, the gels are silver stained (168) to detect any residual ATOX1. Pure samples (>90%) are diluted in 0.5% Nitric Acid to approximate a concentration between 2-10 ppb (generally between a 1:100 to 1:500 dilution factor, depending on protein concentration and copper bound). Samples are analyzed with atomic absorption spectroscopy (AA-6650G, Shimadzu; Columbia MO) using graphite furnace methods as recommended by the manufaturer. Spectra are collected using a hollow-cathode copper detection lamp with a 50 mm diameter, 0.7 nm slit and ~ 324.8 nm wavelength. Each sample is analyzed in triplicate and a copper/protein ratio is determined for each set.

***Ab initio* Structures**

The models shown in Figs 1.3b, 2.9b-d, 4.6 and A.4a&b were generated using *Ab initio* modeling using the Rosetta software program in an effort to predict possible structures of multiple MBD constructs. This was done by predicting the structures of neighboring pairs of MBDs (N-1, 1-2, 2-3 and 3-4) from ATP7B. Boundaries of these four constructs follow the MBD definitions as presented above. For N-MBD1 amino acids 1-128 were

modeled. MBD1-2 modeled amino acids 56-214, MBD2-3 modeled amino acids 142-328, and MBD3-4 modeled amino acids 257-340. Distance constraints were established for MBDs 3-4 using previously published structures (125). The structures for MBDs 1-2 have not been solved, so homology models were made using the Modeler software package (version 9.6) and distance constraints were based upon those models. Fragment libraries for the four constructs were generated using the Robetta online server. A large number of structures of similar proteins (Including ATOX1, other MBDs and homologs) have been solved, allowing for high-specificity fragments to be generated for these domains. Using these fragments and distance constraints, 10,000 structures were predicted using Rosetta software for each construct. The N-Terminus and loop regions were predicted without size constraints apart from bond lengths. These loop regions and five flanking residues from both adjacent MBDs were extracted from the total structure using the Multiscale Modeling Tools for Structural Biology (MMTSB) Tool Set software. The extracted fragments were subject to automated clustering analysis in Ensemble to group like predictions. The centers of 3-5 of the largest clusters (representing the most common predictions) were selected as the highest scoring predictions and used going forward. The clusters were then reintroduced to the constrained MBD models, using the extracted 5 aa MBD fragments as references. CHARMM27 force fields were used to minimize the final models. The CHARMM force field is a function for determining potential energy of macromolecules by taking into account all bond energy, bond angles, dihedrals, impropers (out of plane bond bending), harmonic potential (through the Urey-Bradley component), and nonbonded forces (van Der Waals energy and electrostatic energy of non-adjacent atoms) (205). The validities of the predicted structures were then

tested and confirmed using the ANOLEA (Atomic Non-local environment assessment) server to validate atomic mean-force potential, as well as distance dependent statistical potentials (206). To generate the N-1-4 model used in Fig 1.3b, overlapping pairs of MBDs (for example 1-2 and 2-3) were subject to molecular replacement modeling to "ligate" the pairs together into a three-MBD construct, repeating to add MBD 3-4 and N-MBD1 to generate a possibility for the relative orientation of the four N-Terminal MBDs.

Molecular Dynamics Simulations

The molecular dynamics data shown in figure 2.7 was generated through a 10.0 ns simulation performed with the NAMD software package. The published NMR structure of MBD2 from ATP7A (129) (PDB code: 1s6o) was used as the initial structural conformation. Solvent was simulated through the TIP3P explicit water model and the CHARMM27 force field. The TIP3P model is a 3-site model (H-O-H) that defines water as a rigid molecule with an OH distance of 0.957 Å and a HOH bond angle of 104.52° (207). The model provides for only non-bonded interactions: electrostatic interactions and dispersion and repulsion forces. All three atoms are assigned a fixed electrostatic potential, with the oxygen atom given Leonard-Jones parameters. The introduction of the CHARMM force field also assigns Leonard-Jones parameters to the hydrogen atoms (208). For this simulation, a field was defined around MBD2 such that the entire molecule was surrounded by at least 10 Å of water, along with counterions to balance the charge of the protein (such that the system pH = 7.0).

Prior to dynamic simulation, both the water and protein in the system had to be minimized. This was done using conjugate gradient energy minimization to provide stability and limit system divergence in the initial part of the simulation. This was accomplished by limiting the potential energy of the system so that the net force on each atom approached zero over time. Minimization was performed in two stages, first for the water with the protein given fixed coordinates, then for the entire system with the protein unfixed. Figure 2.S.6, the initial conformation of MBD2 is overlayed with the conformation at 200 ps into the simulation. The RMSD of these structures is ~1Å, demonstrating that the structure was stable and did not diverge in the initial part of the simulation, providing validity to the results of the entire time course.

The system was given additional parameters for the simulation to take into account heat and friction using a Langevin thermostat with a 5 ps^{-1} damping parameter. This models additional degrees of freedom that allow for random high-energy atomic collisions to occur during molecular movement without spiking the system temperature (in this case, set at 300 °K with a Berensden algorithm for re-scaling atomic velocities (209, 210)). This also serves to mimic the viscosity of the solvent (in this case, the TIP3P water model). Electorstatic and van Der Wals interactions were cutoff at 0.9 nm and bond angles and lengths further constrained by a SHAKE algorithm.

This system was subject to a 10.0 ns simulation with 2 fs time steps. Atom coordinates and velocities were recorded every 2 ps. At the end of the simulation, the coordinates

were plotted in NAMD, allowing us to calculate the backbone RMSD, and atom-atom distances for each 2 ps point that are plotted for the entire simulation in Fig 2.7.

Full-length ATP7B Model

The ATP7B structural model shown in Fig 1.3b is based on the model of CopA by Wu et al, 2008 (137) (PDB code : 2VOY) that aligns a low-resolution structure of CopA to higher resolution structures of the SERCA pump and individual structures of cytosolic CopA domains. We used molecular replacement modeling and molecular docking to create a model of ATP7B using known and *Ab initio* structures of the cytosolic domains of the protein. The N domain structure (119) (PDB code : 2arf) was placed using structural alignment and replacement modeling in PyMol. MBDs 5 and 6 (124) (PDB code 2ew9) were docked to the A domain of ATP7B (121) (unpublished structure) using the Patchdock web server (211). The top 20 docking solutions were further refined using the Firedock server (212). These structures were then placed into CopA using PyMol aligning with the A domain and MBD of CopA, eliminating structures that were sterically hindered by the protein or lipid bilayer or placed the C-Terminus of MBD6 at an improbable distance from the N-Terminus of TM1. MBDs 1-4 were derived from a set of Rosetta models compiled by Dr. Ujwal Shinde as described above. This structure was docked to the N-Domain using Patchdock followed by two sequential sets of refinement in Firedock. Final placements of MBDs 1-4 and 5-6 were chosen to eliminate steric hindrance and orient the C-Terminus of MBD4 within a feasible distance from the N-Terminus of MBD5 (given the 57 aa linker between the MBDs).

References

1. Aceruloplasminemia: molecular characterization of this disorder of iron metabolism. Harris, Z. L., Takahashi, Y., Miyajima, H., Serizawa, M., MacGillivray, R. T. and Gitlin, J. D. (1995) *Proc Natl Acad Sci U S A* **92**, 2539-2543

2. A mutation in the ceruloplasmin gene is associated with systemic hemosiderosis in humans. Yoshida, K., Furihata, K., Takeda, S., Nakamura, A., Yamamoto, K., Morita, H., Hiyamuta, S., Ikeda, S., Shimizu, N. and Yanagisawa, N. (1995) *Nat Genet* **9**, 267-272

3. The whole structure of the 13-subunit oxidized cytochrome c oxidase at 2.8 A. Tsukihara, T., Aoyama, H., Yamashita, E., Tomizaki, T., Yamaguchi, H., Shinzawa-Itoh, K., Nakashima, R., Yaono, R. and Yoshikawa, S. (1996) *Science* **272**, 1136-1144

4. 3,4-dihydroxyphenylethylamine beta-hydroxylase. Physical properties, copper content, and role of copper in the catalytic acttivity. Friedman, S. and Kaufman, S. (1965) *J Biol Chem* **240**, 4763-4773

5. Mammalian tyrosinase; the relationship of copper to enzymatic activity. LERNER, A. B., FITZPATRICK, T. B., CALKINS, E. and SUMMERSON, W. H. (1950) *J Biol Chem* **187**, 793-802

6. Copper and the synthesis of elastin and collagen. Harris, E. D., Rayton, J. K., Balthrop, J. E., DiSilvestro, R. A. and Garcia-de-Quevedo, M. (1980) *Ciba Found Symp* **79**, 163-182

7. Human Cu/Zn superoxide dismutase gene family: molecular structure and characterization of four Cu/Zn superoxide dismutase-related pseudogenes. Danciger, E., Dafni, N., Bernstein, Y., Laver-Rudich, Z., Neer, A. and Groner, Y. (1986) *Proc Natl Acad Sci U S A* **83**, 3619-3623

8. Congestive heart failure in copper-deficient mice. Elsherif, L., Ortines, R. V., Saari, J. T. and Kang, Y. J. (2003) *Exp Biol Med (Maywood)* **228**, 811-817

9. Regression of copper-deficient heart hypertrophy: reduction in the size of hypertrophic cardiomyocytes. Zhou, Z., Johnson, W. T. and Kang, Y. J. (2009) *J Nutr Biochem* **20**, 621-628

10. Menkes' disease and swayback. A comparative study of two copper deficiency syndromes. Tan, N. and Urich, H. (1983) *J Neurol Sci* **62**, 95-113

11. A sex-linked recessive disorder with retardation of growth, peculiar hair, and focal cerebral and cerebellar degeneration. MENKES, J. H., ALTER, M., STEIGLEDER, G. K., WEAKLEY, D. R. and SUNG, J. H. (1962) *Pediatrics* **29**, 764-779

12. Acquired copper deficiency: a potentially serious and preventable complication following gastric bypass surgery. Griffith, D. P., Liff, D. A., Ziegler, T. R., Esper, G. J. and Winton, E. F. (2009) *Obesity (Silver Spring)* **17**, 827-831

13. Wilson's disease: an update Das, S. K. and Ray, K. (2006) *Nat Clin Pract Neurol* **2**, 482-493

14. Copper homeostasis and neurodegenerative disorders (Alzheimer's, prion, and Parkinson's diseases and amyotrophic lateral sclerosis). Gaggelli, E., Kozlowski, H., Valensin, D. and Valensin, G. (2006) *Chem Rev* **106**, 1995-2044

15. The role of copper in neurodegenerative disease. Waggoner, D. J., Bartnikas, T. B. and Gitlin, J. D. (1999) *Neurobiol Dis* **6**, 221-230

16. Copper biochemistry and molecular biology. Linder, M. C. and Hazegh-Azam, M. (1996) *Am J Clin Nutr* **63**, 797S-811S

17. Copper exposure induces trafficking of the menkes protein in intestinal epithelium of ATP7A transgenic mice Monty, J. F., Llanos, R. M., Mercer, J. F. and Kramer, D. R. (2005) *J Nutr* **135**, 2762-2766

18. Copper transport Linder, M. C., Wooten, L., Cerveza, P., Cotton, S., Shulze, R. and Lomeli, N. (1998) *Am J Clin Nutr* **67**, 965S-971S

19. Ceruloplasmin metabolism and function. Hellman, N. E. and Gitlin, J. D. (2002) *Annu Rev Nutr* **22**, 439-458

20. Ceruloplasmin revisited: structural and functional roles of various metal cation-binding sites. Bento, I., Peixoto, C., Zaitsev, V. N. and Lindley, P. F. (2007) *Acta Crystallogr D Biol Crystallogr* **63**, 240-248

21. Origins of biliary copper. Kressner, M. S., Stockert, R. J., Morell, A. G. and Sternlieb, I. (1984) *Hepatology* **4**, 867-870

22. Wilson disease. Brewer, G. J. and Yuzbasiyan-Gurkan, V. (1992) *Medicine (Baltimore)* **71**, 139-164

23. Renal copper as an index of copper status in marginal deficiency. Saari, J. T. (2002) *Biol Trace Elem Res* **86**, 237-247

24.NGF promotes copper accumulation required for optimum neurite outgrowth and protein methylation. Birkaya, B. and Aletta, J. M. (2005) *J Neurobiol* **63**, 49-61

25. Copper deficiency and the central nervous system. Myelination in the rat: morphological and biochemical studies. Dipaolo, R. V., Kanfer, J. N. and Newberne, P. M. (1974) *J Neuropathol Exp Neurol* **33**, 226-236

26. Mutation analysis and expression of the mottled gene in the macular mouse model of Menkes disease. Murata, Y., Kodama, H., Abe, T., Ishida, N., Nishimura, M., Levinson, B., Gitschier, J. and Packman, S. (1997) *Pediatr Res* **42**, 436-442

27. The copper-transporting ATPases, menkes and wilson disease proteins, have distinct roles in adult and developing cerebellum Barnes, N., Tsivkovskii, R., Tsivkovskaia, N. and Lutsenko, S. (2005) *J Biol Chem* **280**, 9640-9645

28. Glycosylphosphatidylinositol-anchored ceruloplasmin is required for iron efflux from cells in the central nervous system. Jeong, S. Y. and David, S. (2003) *J Biol Chem* **278**, 27144-27148

29. The copper transporter CTR1 provides an essential function in mammalian embryonic development. Kuo, Y. M., Zhou, B., Cosco, D. and Gitschier, J. (2001) *Proc Natl Acad Sci U S A* **98**, 6836-6841

30. Undetectable intracellular free copper: the requirement of a copper chaperone for superoxide dismutase Rae, T. D., Schmidt, P. J., Pufahl, R. A., Culotta, V. C. and O'Halloran, T. V. (1999) *Science* **284**, 805-808

31. Biochemical characterization of the human copper transporter Ctr1. Lee, J., Pena, M. M., Nose, Y. and Thiele, D. J. (2002) *J Biol Chem* **277**, 4380-4387

32. Biochemical characterization and subcellular localization of human copper transporter 1 (hCTR1). Klomp, A. E., Tops, B. B., Van Denberg, I. E., Berger, R. and Klomp, L. W. (2002) *Biochem J* **364**, 497-505

33. Copper-stimulated endocytosis and degradation of the human copper transporter, hCtr1. Petris, M. J., Smith, K., Lee, J. and Thiele, D. J. (2003) *J Biol Chem* **278**, 9639-9646

34. Stable plasma membrane levels of hCTR1 mediate cellular copper uptake. Eisses, J. F., Chi, Y. and Kaplan, J. H. (2005) *J Biol Chem* **280**, 9635-9639

35. The N-terminus of the human copper transporter 1 (hCTR1) is localized extracellularly, and interacts with itself. Klomp, A. E., Juijn, J. A., van der Gun, L. T., van den Berg, I. E., Berger, R. and Klomp, L. W. (2003) *Biochem J* **370**, 881-889

36. Ctr2 is partially localized to the plasma membrane and stimulates copper uptake in COS-7 cells. Bertinato, J., Swist, E., Plouffe, L. J., Brooks, S. P. and L'abbe, M. R. (2008) *Biochem J* **409**, 731-740

37. Human copper transporter 2 is localized in late endosomes and lysosomes and facilitates cellular copper uptake. van den Berghe, P. V., Folmer, D. E., Malingre, H. E., van Beurden, E., Klomp, A. E., van de Sluis, B., Merkx, M., Berger, R. and Klomp, L. W. (2007) *Biochem J* **407**, 49-59

38. DMT1, a physiologically relevant apical Cu1+ transporter of intestinal cells. Arredondo, M., Munoz, P., Mura, C. V. and Nunez, M. T. (2003) *Am J Physiol Cell Physiol* **284**, C1525-30

39. Divalent metal transporter 1. Mims, M. P. and Prchal, J. T. (2005) *Hematology* **10**, 339-345

40. A C-terminal domain of the membrane copper pump Ctr1 exchanges copper(I) with the copper chaperone Atx1. Xiao, Z. and Wedd, A. G. (2002) *Chem Commun (Camb)* 588-589

41. The copper chaperone for superoxide dismutase. Culotta, V. C., Klomp, L. W., Strain, J., Casareno, R. L., Krems, B. and Gitlin, J. D. (1997) *J Biol Chem* **272**, 23469-23472

42. Mechanisms for activating Cu- and Zn-containing superoxide dismutase in the absence of the CCS Cu chaperone. Carroll, M. C., Girouard, J. B., Ulloa, J. L., Subramaniam, J. R., Wong, P. C., Valentine, J. S. and Culotta, V. C. (2004) *Proc Natl Acad Sci U S A* **101**, 5964-5969

43. Metallochaperones, an intracellular shuttle service for metal ions. O'Halloran, T. V. and Culotta, V. C. (2000) *J Biol Chem* **275**, 25057-25060

44. Mutagenesis reveals a specific role for Cox17p in copper transport to cytochrome oxidase. Punter, F. A. and Glerum, D. M. (2003) *J Biol Chem* **278**, 30875-30880

45. Knockdown of human COX17 affects assembly and supramolecular organization of cytochrome c oxidase. Oswald, C., Krause-Buchholz, U. and Rodel, G. (2009) *J Mol Biol* **389**, 470-479

46. Structural basis for copper transfer by the metallochaperone for the Menkes/Wilson disease proteins Wernimont, A. K., Huffman, D. L., Lamb, A. L., O'Halloran, T. V. and Rosenzweig, A. C. (2000) *Nat Struct Biol* **7**, 766-771

47. The metallochaperone Atox1 plays a critical role in perinatal copper homeostasis Hamza, I., Faisst, A., Prohaska, J., Chen, J., Gruss, P. and Gitlin, J. D. (2001) *Proc Natl Acad Sci U S A* **98**, 6848-6852

48. Novel role of antioxidant-1 (Atox1) as a copper-dependent transcription factor involved in cell proliferation. Itoh, S., Kim, H. W., Nakagawa, O., Ozumi, K., Lessner, S. M., Aoki, H., Akram, K., McKinney, R. D., Ushio-Fukai, M. and Fukai, T. (2008) *J Biol Chem* **283**, 9157-9167

49. The ATX1 gene of Saccharomyces cerevisiae encodes a small metal homeostasis factor that protects cells against reactive oxygen toxicity. Lin, S. J. and Culotta, V. C. (1995) *Proc Natl Acad Sci U S A* **92**, 3784-3788

50. Cellular multitasking: the dual role of human Cu-ATPases in cofactor delivery and intracellular copper balance. Lutsenko, S., Gupta, A., Burkhead, J. L. and Zuzel, V. (2008) *Arch Biochem Biophys* **476**, 22-32

51. Metallochaperone Atox1 transfers copper to the NH2-terminal domain of the Wilson's disease protein and regulates its catalytic activity. Walker, J. M., Tsivkovskii, R. and Lutsenko, S. (2002) *J Biol Chem* **277**, 27953-27959

52. The Menkes copper transporter is required for the activation of tyrosinase Petris, M. J., Strausak, D. and Mercer, J. F. (2000) *Hum Mol Genet* **9**, 2845-2851

53. Menkes protein contributes to the function of peptidylglycine alpha-amidating monooxygenase Steveson, T. C., Ciccotosto, G. D., Ma, X. M., Mueller, G. P., Mains, R. E. and Eipper, B. A. (2003) *Endocrinology* **144**, 188-200

54. Copper-induced trafficking of the cU-ATPases: a key mechanism for copper homeostasis. Mercer, J. F., Barnes, N., Stevenson, J., Strausak, D. and Llanos, R. M. (2003) *Biometals* **16**, 175-184

55. Copper-dependent interaction of dynactin subunit p62 with the N terminus of ATP7B but not ATP7A. Lim, C. M., Cater, M. A., Mercer, J. F. and La Fontaine, S. (2006) *J Biol Chem* **281**, 14006-14014

56. Distinct Wilson's disease mutations in ATP7B are associated with enhanced binding to COMMD1 and reduced stability of ATP7B. de Bie, P., van de Sluis, B., Burstein, E., van de Berghe, P. V., Muller, P., Berger, R., Gitlin, J. D., Wijmenga, C. and Klomp, L. W. (2007) *Gastroenterology* **133**, 1316-1326

57. Copper-induced conformational changes in the N-terminal domain of the Wilson disease copper-transporting ATPase DiDonato, M., Hsu, H. F., Narindrasorasak, S., Que, L. J. and Sarkar, B. (2000) *Biochemistry* **39**, 1890-1896

58. Copper specifically regulates intracellular phosphorylation of the Wilson's disease protein, a human copper-transporting ATPase. Vanderwerf, S. M., Cooper, M. J., Stetsenko, I. V. and Lutsenko, S. (2001) *J Biol Chem* **276**, 36289-36294

59. Phosphorylation regulates copper-responsive trafficking of the Menkes copper transporting P-type ATPase. Veldhuis, N. A., Valova, V. A., Gaeth, A. P., Palstra, N., Hannan, K. M., Michell, B. J., Kelly, L. E., Jennings, I., Kemp, B. E., Pearson, R. B., Robinson, P. J. and Camakaris, J. (2009) *Int J Biochem Cell Biol*

60. NMDA receptor activation mediates copper homeostasis in hippocampal neurons. Schlief, M. L., Craig, A. M. and Gitlin, J. D. (2005) *J Neurosci* **25**, 239-246

61. ATP7B expression in human breast epithelial cells is mediated by lactational hormones. Michalczyk, A., Bastow, E., Greenough, M., Camakaris, J., Freestone, D., Taylor, P., Linder, M., Mercer, J. and Ackland, M. L. (2008) *J Histochem Cytochem* **56**, 389-399

62. Hepatocyte-specific localization and copper-dependent trafficking of the Wilson's disease protein in the liver. Schaefer, M., Hopkins, R. G., Failla, M. L. and Gitlin, J. D. (1999) *Am J Physiol* **276**, G639-46

63. Cell-specific trafficking suggests a new role for renal ATP7B in the intracellular copper storage. Barnes, N., Bartee, M. Y., Braiterman, L., Gupta, A., Ustiyan, V., Zuzel, V., Kaplan, J. H., Hubbard, A. L. and Lutsenko, S. (2009) *Traffic* **10**, 767-779

64. NH2-terminal signals in ATP7B Cu-ATPase mediate its Cu-dependent anterograde traffic in polarized hepatic cells Guo, Y., Nyasae, L., Braiterman, L. T. and Hubbard, A. L. (2005) *Am J Physiol Gastrointest Liver Physiol* **289**, G904-16

65. Function, structure, and mechanism of intracellular copper trafficking proteins Huffman, D. L. and O'Halloran, T. V. (2001) *Annu Rev Biochem* **70**, 677-701

66. The Wilson disease gene is a copper transporting ATPase with homology to the Menkes disease gene. Tanzi, R. E., Petrukhin, K., Chernov, I., Pellequer, J. L., Wasco, W., Ross, B., Romano, D. M., Parano, E., Pavone, L., Brzustowicz, L. M. and et, a. (1993) *Nat Genet* **5**, 344-350

67. Characterization of the Wilson disease gene encoding a P-type copper transporting ATPase: genomic organization, alternative splicing, and structure/function predictions. Petrukhin, K., Lutsenko, S., Chernov, I., Ross, B. M., Kaplan, J. H. and Gilliam, T. C. (1994) *Hum Mol Genet* **3**, 1647-1656

68. Alternative Splicing of the Menkes Copper Atpase (Atp7a) Transcript in the Rat Intestinal Epithelium. Collins, J. F., Hua, P., Lu, Y. and Ranganathan, P. N. (2009) *Am J Physiol Gastrointest Liver Physiol*

69. A novel pineal night-specific ATPase encoded by the Wilson disease gene. Borjigin, J., Payne, A. S., Deng, J., Li, X., Wang, M. M., Ovodenko, B., Gitlin, J. D. and Snyder, S. H. (1999) *J Neurosci* **19**, 1018-1026

70. Developmental expression of the mouse mottled and toxic milk genes suggests distinct functions for the Menkes and Wilson disease copper transporters. Kuo, Y. M., Gitschier, J. and Packman, S. (1997) *Hum Mol Genet* **6**, 1043-1049

71. Localization of Menkes gene expression in the mouse brain; its association with neurological manifestations in Menkes model mice. Iwase, T., Nishimura, M., Sugimura, H., Igarashi, H., Ozawa, F., Shinmura, K., Suzuki, M., Tanaka, M. and Kino, I. (1996) *Acta Neuropathol* **91**, 482-488

72. Isolation of a candidate gene for Menkes disease and evidence that it encodes a copper-transporting ATPase. Vulpe, C., Levinson, B., Whitney, S., Packman, S. and Gitschier, J. (1993) *Nat Genet* **3**, 7-13

73. Incidence of Menkes disease. Tonnesen, T., Kleijer, W. J. and Horn, N. (1991) *Hum Genet* **86**, 408-410

74. Menkes's kinky hair syndrome. An inherited defect in copper absorption with widespread effects. Danks, D. M., Campbell, P. E., Stevens, B. J., Mayne, V. and Cartwright, E. (1972) *Pediatrics* **50**, 188-201

75. Molecular genetics and pathophysiology of Menkes disease Kodama, H. and Murata, Y. (1999) *Pediatr Int* **41**, 430-435

76. A comparison of the mutation spectra of Menkes disease and Wilson disease. Hsi, G. and Cox, D. W. (2004) *Hum Genet* **114**, 165-172

77. Copper-histidine therapy for Menkes disease. Sarkar, B., Lingertat-Walsh, K. and Clarke, J. T. (1993) *J Pediatr* **123**, 828-830

78. Late-onset treatment in Menkes disease: is there a correlation between genotype and response to therapy? Olivares, J. L., Bueno, I., Gallati, S. and Ramos, F. J. (2006) *Clin Genet* **69**, 363-366

79. Similar splicing mutations of the Menkes/mottled copper-transporting ATPase gene in occipital horn syndrome and the blotchy mouse. Das, S., Levinson, B., Vulpe, C., Whitney, S., Gitschier, J. and Packman, S. (1995) *Am J Hum Genet* **56**, 570-576

80. The mottled mouse as a model for human Menkes disease: identification of mutations in the Atp7a gene. Cecchi, C., Biasotto, M., Tosi, M. and Avner, P. (1997) *Hum Mol Genet* **6**, 425-433

81. Molecular basis of the brindled mouse mutant (Mo(br)): a murine model of Menkes disease. Grimes, A., Hearn, C. J., Lockhart, P., Newgreen, D. F. and Mercer, J. F. (1997) *Hum Mol Genet* **6**, 1037-1042

82. Intracellular localization and loss of copper responsiveness of Mnk, the murine homologue of the Menkes protein, in cells from blotchy (Mo blo) and brindled (Mo br) mouse mutants. La Fontaine, S., Firth, S. D., Lockhart, P. J., Brooks, H., Camakaris, J. and Mercer, J. F. (1999) *Hum Mol Genet* **8**, 1069-1075

83. Atp7a determines a hierarchy of copper metabolism essential for notochord development. Mendelsohn, B. A., Yin, C., Johnson, S. L., Wilm, T. P., Solnica-Krezel, L. and Gitlin, J. D. (2006) *Cell Metab* **4**, 155-162

84. Wilson's disease. Ala, A., Walker, A. P., Ashkan, K., Dooley, J. S. and Schilsky, M. L. (2007) *Lancet* **369**, 397-408

85. High incidence and allelic homogeneity of Wilson disease in 2 isolated populations: a prerequisite for efficient disease prevention programs. Zappu, A., Magli, O., Lepori, M. B., Dessi, V., Diana, S., Incollu, S., Kanavakis, E., Nicolaidou, P., Manolaki, N., Fretzayas, A., De Virgiliis, S., Cao, A. and Loudianos, G. (2008) *J Pediatr Gastroenterol Nutr* **47**, 334-338

86. Diagnosis of Wilson's disease: a comprehensive review. Mak, C. M. and Lam, C. W. (2008) *Crit Rev Clin Lab Sci* **45**, 263-290

87. History of Wilson's disease: 1912 to 2000. Walshe, J. M. (2006) *Mov Disord* **21**, 142-147

88. The Wilson's disease gene and phenotypic diversity. Riordan, S. M. and Williams, R. (2001) *J Hepatol* **34**, 165-171

89. The ophthalmologic manifestations of Wilson's disease. Wiebers, D. O., Hollenhorst, R. W. and Goldstein, N. P. (1977) *Mayo Clin Proc* **52**, 409-416

90. Wilson disease: findings at MR imaging and CT of the brain with clinical correlation. van Wassenaer-van Hall, H. N., van den Heuvel, A. G., Algra, A., Hoogenraad, T. U. and Mali, W. P. (1996) *Radiology* **198**, 531-536

91. Hypercalciuria and nephrolithiasis as a presenting sign in Wilson disease. Azizi, E., Eshel, G. and Aladjem, M. (1989) *Eur J Pediatr* **148**, 548-549

92. Wilson's disease: clinical management and therapy. Brewer, G. J. and Askari, F. K. (2005) *J Hepatol* **42 Suppl**, S13-21

93. Orthotopic liver transplantation for acute fulminant Wilson disease. Sokol, R. J., Francis, P. D., Gold, S. H., Ford, D. M., Lum, G. M. and Ambruso, D. R. (1985) *J Pediatr* **107**, 549-552

94. Reversal of severe neurological manifestations of Wilson's disease following orthotopic liver transplantation. Polson, R. J., Rolles, K., Calne, R. Y., Williams, R. and Marsden, D. (1987) *Q J Med* **64**, 685-691

95. No neurological improvement after liver transplantation for Wilson's disease. Guarino, M., Stracciari, A., D'Alessandro, R. and Pazzaglia, P. (1995) *Acta Neurol Scand* **92**, 405-408

96. The Wilson disease gene: spectrum of mutations and their consequences. Thomas, G. R., Forbes, J. R., Roberts, E. A., Walshe, J. M. and Cox, D. W. (1995) *Nat Genet* **9**, 210-217

97. Frameshift and nonsense mutations in the gene for ATPase7B are associated with severe impairment of copper metabolism and with an early clinical manifestation of Wilson's disease. Gromadzka, G., Schmidt, H. H., Genschel, J., Bochow, B., Rodo, M., Tarnacka, B., Litwin, T., Chabik, G. and Czlonkowska, A. (2005) *Clin Genet* **68**, 524-532

98. High copper selectively alters lipid metabolism and cell cycle machinery in the mouse model of Wilson disease. Huster, D., Purnat, T. D., Burkhead, J. L., Ralle, M., Fiehn, O., Stuckert, F., Olson, N. E., Teupser, D. and Lutsenko, S. (2007) *J Biol Chem* **282**, 8343-8355

99. Intracellular targeting of copper-transporting ATPase ATP7A in a normal and Atp7b-/- kidney. Linz, R., Barnes, N. L., Zimnicka, A. M., Kaplan, J. H., Eipper, B. and Lutsenko, S. (2008) *Am J Physiol Renal Physiol* **294**, F53-61

100. The LEC rat has a deletion in the copper transporting ATPase gene homologous to the Wilson disease gene. Wu, J., Forbes, J. R., Chen, H. S. and Cox, D. W. (1994) *Nat Genet* **7**, 541-545

101. The toxic milk mouse is a murine model of Wilson disease. Theophilos, M. B., Cox, D. W. and Mercer, J. F. (1996) *Hum Mol Genet* **5**, 1619-1624

102. Identification of a new copper metabolism gene by positional cloning in a purebred dog population. van De Sluis, B., Rothuizen, J., Pearson, P. L., van Oost, B. A. and Wijmenga, C. (2002) *Hum Mol Genet* **11**, 165-173

103. COMMD1 forms oligomeric complexes targeted to the endocytic membranes via specific interactions with phosphatidylinositol 4,5-bisphosphate. Burkhead, J. L., Morgan, C. T., Shinde, U., Haddock, G. and Lutsenko, S. (2009) *J Biol Chem* **284**, 696-707

104. The canine copper toxicosis gene MURR1 is not implicated in the pathogenesis of Wilson disease. Lovicu, M., Dessi, V., Lepori, M. B., Zappu, A., Zancan, L., Giacchino, R., Marazzi, M. G., Iorio, R., Vegnente, A., Vajro, P., Maggiore, G., Marcellini, M., Barbera, C., Kostic, V., Farci, A. M., Solinas, A., Altuntas, B., Yuce, A., Kocak, N., Tsezou, A., De Virgiliis, S., Cao, A. and Loudianos, G. (2006) *J Gastroenterol* **41**, 582-587

105. Mutation analysis of 218 Chinese patients with Wilson disease revealed no correlation between the canine copper toxicosis gene MURR1 and Wilson disease. Wu, Z. Y., Zhao, G. X., Chen, W. J., Wang, N., Wan, B., Lin, M. T., Murong, S. X. and Yu, L. (2006) *J Mol Med* **84**, 438-442

106. Role of copper in Indian childhood cirrhosis. Tanner, M. S. (1998) *Am J Clin Nutr* **67**, 1074S-1081S

107. Endemic Tyrolean infantile cirrhosis: an ecogenetic disorder. Muller, T., Feichtinger, H., Berger, H. and Muller, W. (1996) *Lancet* **347**, 877-880

108. Idiopathic copper toxicosis. Muller, T., Muller, W. and Feichtinger, H. (1998) *Am J Clin Nutr* **67**, 1082S-1086S

109. Endemic Tyrolean infantile cirrhosis is not an allelic variant of Wilson's disease. Wijmenga, C., Muller, T., Murli, I. S., Brunt, T., Feichtinger, H., Schonitzer, D., Houwen, R. H., Muller, W., Sandkuijl, L. A. and Pearson, P. L. (1998) *Eur J Hum Genet* **6**, 624-628

110. The canine copper toxicosis gene MURR1 does not cause non-Wilsonian hepatic copper toxicosis. Muller, T., van de Sluis, B., Zhernakova, A., van Binsbergen, E., Janecke, A. R., Bavdekar, A., Pandit, A., Weirich-Schwaiger, H., Witt, H., Ellemunter, H., Deutsch, J., Denk, H., Muller, W., Sternlieb, I., Tanner, M. S. and Wijmenga, C. (2003) *J Hepatol* **38**, 164-168

111. MR imaging of CNS involvement in children affected by chronic liver disease. Genovese, E., Maghnie, M., Maggiore, G., Tinelli, C., Lizzoli, F., De Giacomo, C., Pozza, S. and Campani, R. (2000) *AJNR Am J Neuroradiol* **21**, 845-851

112. Large scale SOD1 mutation screening provides evidence for genetic heterogeneity in amyotrophic lateral sclerosis. van Es, M. A., Dahlberg, C., Birve, A., Veldink, J. H., van den Berg, L. H. and Andersen, P. M. (2009) *J Neurol Neurosurg Psychiatry*

113. Cupric-amyloid beta peptide complex stimulates oxidation of ascorbate and generation of hydroxyl radical. Dikalov, S. I., Vitek, M. P. and Mason, R. P. (2004) *Free Radic Biol Med* **36**, 340-347

114. Prion protein selectively binds copper(II) ions. Stockel, J., Safar, J., Wallace, A. C., Cohen, F. E. and Prusiner, S. B. (1998) *Biochemistry* **37**, 7185-7193

115. The structure and function of heavy metal transport P(1B)-ATPases Arguello, J. M., Eren, E. and Gonzalez-Guerrero, M. (2007) *Biometals*

116. Biochemical basis of regulation of human copper-transporting ATPases. Lutsenko, S., LeShane, E. S. and Shinde, U. (2007) *Arch Biochem Biophys* **463**, 134-148

117. Structure of the ATP binding domain from the Archaeoglobus fulgidus Cu+-ATPase Sazinsky, M. H., Mandal, A. K., Arguello, J. M. and Rosenzweig, A. C. (2006) *J Biol Chem* **281**, 11161-11166

118. Crystal structures of Ca2+-ATPase in various physiological states. Toyoshima, C., Nomura, H. and Sugita, Y. (2003) *Ann N Y Acad Sci* **986**, 1-8

119. Solution structure of the N-domain of Wilson disease protein: distinct nucleotide-binding environment and effects of disease mutations Dmitriev, O., Tsivkovskii, R., Abildgaard, F., Morgan, C. T., Markley, J. L. and Lutsenko, S. (2006) *Proc Natl Acad Sci U S A* **103**, 5302-5307

120. The binding mode of ATP revealed by the solution structure of the N-domain of human ATP7A. Banci, L., Bertini, I., Cantini, F., Inagaki, S., Migliardi, M. and Rosato, A. (2010) *J Biol Chem* **285**, 2537-2544

121. Solution Structures of the Actuator Domain of ATP7A and ATP7B, the Menkes and Wilson Disease Proteins. Banci, L., Bertini, I., Cantini, F., Migliardi, M., Natile, G., Nushi, F. and Rosato, A. (2009) *Biochemistry*

122. Copper-regulated trafficking of the Menkes disease copper ATPase is associated with formation of a phosphorylated catalytic intermediate Petris, M. J., Voskoboinik, I., Cater, M., Smith, K., Kim, B. E., Llanos, R. M., Strausak, D., Camakaris, J. and Mercer, J. F. (2002) *J Biol Chem* **277**, 46736-46742

123. Identification of the transmembrane metal binding site in Cu+-transporting PIB-type ATPases Mandal, A. K., Yang, Y., Kertesz, T. M. and Arguello, J. M. (2004) *J Biol Chem* **279**, 54802-54807

124. Structure of human Wilson protein domains 5 and 6 and their interplay with domain 4 and the copper chaperone HAH1 in copper uptake Achila, D., Banci, L., Bertini, I., Bunce, J., Ciofi-Baffoni, S. and Huffman, D. L. (2006) *Proc Natl Acad Sci U S A* **103**, 5729-5734

125. Metal binding domains 3 and 4 of the Wilson disease protein: solution structure and interaction with the copper(I) chaperone HAH1. Banci, L., Bertini, I., Cantini, F., Rosenzweig, A. C. and Yatsunyk, L. A. (2008) *Biochemistry* **47**, 7423-7429

126. Solution structure and intermolecular interactions of the third metal-binding domain of ATP7A, the Menkes disease protein Banci, L., Bertini, I., Cantini, F., DellaMalva, N., Herrmann, T., Rosato, A. and Wuthrich, K. (2006) *J Biol Chem* **281**, 29141-29147

127. An atomic-level investigation of the disease-causing A629P mutant of the Menkes protein, ATP7A Banci, L., Bertini, I., Cantini, F., Migliardi, M., Rosato, A. and Wang, S. (2005) *J Mol Biol* **352**, 409-417

128. An NMR study of the interaction between the human copper(I) chaperone and the second and fifth metal-binding domains of the Menkes protein Banci, L., Bertini, I., Ciofi-Baffoni, S., Chasapis, C. T., Hadjiliadis, N. and Rosato, A. (2005) *Febs J* **272**, 865-871

129. Solution structure and backbone dynamics of the Cu(I) and apo forms of the second metal-binding domain of the Menkes protein ATP7A Banci, L., Bertini, I., Del Conte, R., D'Onofrio, M. and Rosato, A. (2004) *Biochemistry* **43**, 3396-3403

130. Solution structures of the reduced and Cu(I) bound forms of the first metal binding sequence of ATP7A associated with Menkes disease DeSilva, T. M., Veglia, G. and Opella, S. J. (2005) *Proteins* **61**, 1038-1049

131. Solution structure of the fourth metal-binding domain from the Menkes copper-transporting ATPase Gitschier, J., Moffat, B., Reilly, D., Wood, W. I. and Fairbrother, W. J. (1998) *Nat Struct Biol* **5**, 47-54

132. Copper transfer to the N-terminal domain of the Wilson disease protein (ATP7B): X-ray absorption spectroscopy of reconstituted and chaperone-loaded metal binding domains and their interaction with exogenous ligands Ralle, M., Lutsenko, S. and Blackburn, N. J. (2004) *J Inorg Biochem* **98**, 765-774

133. The regulation of catalytic activity of the menkes copper-translocating P-type ATPase. Role of high affinity copper-binding sites. Voskoboinik, I., Mar, J., Strausak, D. and Camakaris, J. (2001) *J Biol Chem* **276**, 28620-28627

134. Role of the copper-binding domain in the copper transport function of ATP7B, the P-type ATPase defective in Wilson disease Forbes, J. R., Hsi, G. and Cox, D. W. (1999) *J Biol Chem* **274**, 12408-12413

135. The distinct roles of the N-terminal copper-binding sites in regulation of catalytic activity of the Wilson's disease protein Huster, D. and Lutsenko, S. (2003) *J Biol Chem* **278**, 32212-32218

136. Intracellular trafficking of the human Wilson protein: the role of the six N-terminal metal-binding sites Cater, M. A., Forbes, J., La Fontaine, S., Cox, D. and Mercer, J. F. (2004) *Biochem J* **380**, 805-813

137. Structure of a copper pump suggests a regulatory role for its metal-binding domain. Wu, C. C., Rice, W. J. and Stokes, D. L. (2008) *Structure* **16**, 976-985

138. The role of GMXCXXC metal binding sites in the copper-induced redistribution of the Menkes protein Strausak, D., La Fontaine, S., Hill, J., Firth, S. D., Lockhart, P. J. and Mercer, J. F. (1999) *J Biol Chem* **274**, 11170-11177

139. The Lys1010-Lys1325 fragment of the Wilson's disease protein binds nucleotides and interacts with the N-terminal domain of this protein in a copper-dependent manner. Tsivkovskii, R., MacArthur, B. C. and Lutsenko, S. (2001) *J Biol Chem* **276**, 2234-2242

140. The N-terminal metal-binding site 2 of the Wilson's Disease Protein plays a key role in the transfer of copper from Atox1 Walker, J. M., Huster, D., Ralle, M., Morgan, C. T., Blackburn, N. J. and Lutsenko, S. (2004) *J Biol Chem* **279**, 15376-15384

141. Structure and metal binding studies of the second copper binding domain of the Menkes ATPase Lim, C. M., Cater, M. A., Mercer, J. F. and La Fontaine, S. (2003) *Journal of Structural Biology* **143**, 209-218

142. Binding of copper(I) by the Wilson disease protein and its copper chaperone Wernimont, A. K., Yatsunyk, L. A. and Rosenzweig, A. C. (2004) *J Biol Chem* **279**, 12269-12276

143. Conformational dynamics of metal-binding domains in Wilson disease protein: molecular insights into selective copper transfer. Rodriguez-Granillo, A., Crespo, A. and Wittung-Stafshede, P. (2009) *Biochemistry* **48**, 5849-5863

144. Structure and dynamics of Cu(I) binding in copper chaperones Atox1 and CopZ: a computer simulation study. Rodriguez-Granillo, A. and Wittung-Stafshede, P. (2008) *J Phys Chem B* **112**, 4583-4593

145. Copper transport and its defect in Wilson disease: characterization of the copper-binding domain of Wilson disease ATPase Sarkar, B. (2000) *J Inorg Biochem* **79**, 187-191

146. The loop connecting metal-binding domains 3 and 4 of ATP7B is a target of a kinase-mediated phosphorylation. Bartee, M. Y., Ralle, M. and Lutsenko, S. (2009) *Biochemistry* **48**, 5573-5581

147. Apical targeting and Golgi retention signals reside within a 9-amino acid sequence in the copper-ATPase, ATP7B. Braiterman, L., Nyasae, L., Guo, Y., Bustos, R., Lutsenko, S. and Hubbard, A. (2009) *Am J Physiol Gastrointest Liver Physiol* **296**, G433-44

148. X-ray absorption spectroscopy of the copper chaperone HAH1 reveals a linear two-coordinate Cu(I) center capable of adduct formation with exogenous thiols and phosphines Ralle, M., Lutsenko, S. and Blackburn, N. J. (2003) *J Biol Chem* **278**, 23163-23170

149. A novel role for the immunophilin FKBP52 in copper transport Sanokawa-Akakura, R., Dai, H., Akakura, S., Weinstein, D., Fajardo, J. E., Lang, S. E., Wadsworth, S., Siekierka, J. and Birge, R. B. (2004) *J Biol Chem* **279**, 27845-27848

150. Cu(I) binding and transfer by the N terminus of the Wilson disease protein. Yatsunyk, L. A. and Rosenzweig, A. C. (2007) *J Biol Chem* **282**, 8622-8631

151. An NMR study of the interaction of the N-terminal cytoplasmic tail of the Wilson disease protein with copper(I)-Hah1. Banci, L., Bertini, I., Cantini, F., Massagni, C., Migliardi, M. and Rosato, A. (2009) *J Biol Chem*

152. The different intermolecular interactions of the soluble copper-binding domains of the menkes protein, ATP7A Banci, L., Bertini, I., Cantini, F., Della-Malva, N., Migliardi, M. and Rosato, A. (2007) *Journal of Biological Chemistry* **282**, 23140

153. A NMR study of the interaction of a three-domain construct of ATP7A with copper(I) and copper(I)-HAH1: the interplay of domains Banci, L., Bertini, I., Cantini, F., Chasapis, C. T., Hadjiliadis, N. and Rosato, A. (2005) *J Biol Chem* **280**, 38259-38263

154. Protein kinase-dependent phosphorylation of the Menkes copper P-type ATPase. Voskoboinik, I., Fernando, R., Veldhuis, N., Hannan, K. M., Marmy-Conus, N., Pearson, R. B. and Camakaris, J. (2003) *Biochem Biophys Res Commun* **303**, 337-342

155. The copper toxicosis gene product Murr1 directly interacts with the Wilson disease protein. Tao, T. Y., Liu, F., Klomp, L., Wijmenga, C. and Gitlin, J. D. (2003) *J Biol Chem* **278**, 41593-41596

156. Characterization of COMMD protein-protein interactions in NF-kappaB signalling. de Bie, P., van de Sluis, B., Burstein, E., Duran, K. J., Berger, R., Duckett, C. S., Wijmenga, C. and Klomp, L. W. (2006) *Biochem J* **398**, 63-71

157. Copper-induced translocation of the Wilson disease protein ATP7B independent of Murr1/COMMD1 and Rab7. Weiss, K. H., Lozoya, J. C., Tuma, S., Gotthardt, D., Reichert, J., Ehehalt, R., Stremmel, W. and Fullekrug, J. (2008) *Am J Pathol* **173**, 1783-1794

158. N-terminal domains of human copper-transporting adenosine triphosphatases (the Wilson's and Menkes disease proteins) bind copper selectively in vivo and in vitro with stoichiometry of one copper per metal-binding repeat Lutsenko, S., Petrukhin, K., Cooper, M. J., Gilliam, C. T. and Kaplan, J. H. (1997) *J Biol Chem* **272**, 18939-18944

159. Evidence that translation reinitiation leads to a partially functional Menkes protein containing two copper-binding sites. Paulsen, M., Lund, C., Akram, Z., Winther, J. R., Horn, N. and Moller, L. B. (2006) *Am J Hum Genet* **79**, 214-229

160. Differences in ATP7A gene expression underlie intrafamilial variability in Menkes disease/occipital horn syndrome. Donsante, A., Tang, J., Godwin, S. C., Holmes, C. S., Goldstein, D. S., Bassuk, A. and Kaler, S. G. (2007) *J Med Genet* **44**, 492-497

161. Interaction of the copper chaperone HAH1 with the Wilson disease protein is essential for copper homeostasis Hamza, I., Schaefer, M., Klomp, L. W. and Gitlin, J. D. (1999) *Proc Natl Acad Sci U S A* **96**, 13363-13368

162. Reduced expression of ATP7B affected by Wilson disease-causing mutations is rescued by pharmacological folding chaperones 4-phenylbutyrate and curcumin. van den Berghe, P. V., Stapelbroek, J. M., Krieger, E., de Bie, P., van de Graaf, S. F., de Groot, R. E., van Beurden, E., Spijker, E., Houwen, R. H., Berger, R. and Klomp, L. W. (2009) *Hepatology* **50**, 1783-1795

163. Interactions between copper-binding sites determine the redox status and conformation of the regulatory N-terminal domain of ATP7B. Leshane, E. S., Shinde, U., Walker, J. M., Barry, A. N., Blackburn, N. J., Ralle, M. and Lutsenko, S. (2009) *J Biol Chem*

164. Menkes disease. Bertini, I. and Rosato, A. (2008) *Cell Mol Life Sci* **65**, 89-91

165. Protein measurement with the Folin phenol reagent. LOWRY, O. H., ROSEBROUGH, N. J., FARR, A. L. and RANDALL, R. J. (1951) *J Biol Chem* **193**, 265-275

166. A selenocysteine variant of the human copper chaperone for superoxide dismutase. A Se-XAS probe of cluster composition at the domain 3-domain 3 dimer interface. Barry, A. N. and Blackburn, N. J. (2008) *Biochemistry* **47**, 4916-4928

167. A colorimetric method for determining low concentrations of mercaptans. ELLMAN, G. L. (1958) *Arch Biochem Biophys* **74**, 443-450

168. Mass spectrometric sequencing of proteins silver-stained polyacrylamide gels. Shevchenko, A., Wilm, M., Vorm, O. and Mann, M. (1996) *Anal Chem* **68**, 850-858

169. Positive selection dictates the choice between kinetic and thermodynamic protein folding and stability in subtilases. Subbian, E., Yabuta, Y. and Shinde, U. (2004) *Biochemistry* **43**, 14348-14360

170. High yield heterologous expression of wild-type and mutant Cu+-ATPase (ATP7B, Wilson disease protein) for functional characterization of catalytic activity and serine residues undergoing copper-dependent phosphorylation. Pilankatta, R., Lewis, D., Adams, C. M. and Inesi, G. (2009) *J Biol Chem* **284**, 21307-21316

171. Oxidative modification to cysteine sulfonic acid of Cys111 in human copper-zinc superoxide dismutase. Fujiwara, N., Nakano, M., Kato, S., Yoshihara, D., Ookawara, T., Eguchi, H., Taniguchi, N. and Suzuki, K. (2007) *J Biol Chem* **282**, 35933-35944

172. Copper-dependent interaction of glutaredoxin with the N termini of the copper-ATPases (ATP7A and ATP7B) defective in Menkes and Wilson diseases. Lim, C. M., Cater, M. A., Mercer, J. F. and La Fontaine, S. (2006) *Biochem Biophys Res Commun* **348**, 428-436

173. Menkes disease: underlying genetic defect and new diagnostic possibilities Tumer, Z. and Horn, N. (1998) *J Inherit Metab Dis* **21**, 604-612

174. Wilson's Disease. Pfeiffer, R. F. (2007) *Semin Neurol* **27**, 123-132

175. Kinetic analysis of the interaction of the copper chaperone Atox1 with the metal binding sites of the Menkes protein Strausak, D., Howie, M. K., Firth, S. D., Schlicksupp, A., Pipkorn, R., Multhaup, G. and Mercer, J. F. (2003) *J Biol Chem* **278**, 20821-20827

176. Essential role for Atox1 in the copper-mediated intracellular trafficking of the Menkes ATPase Hamza, I., Prohaska, J. and Gitlin, J. D. (2003) *Proc Natl Acad Sci U S A* **100**, 1215-1220

177. Copper-dependent protein-protein interactions studied by yeast two-hybrid analysis. van Dongen, E. M., Klomp, L. W. and Merkx, M. (2004) *Biochem Biophys Res Commun* **323**, 789-795

178. Copper in disorders with neurological symptoms: Alzheimer's, Menkes, and Wilson diseases. Strausak, D., Mercer, J. F., Dieter, H. H., Stremmel, W. and Multhaup, G. (2001) *Brain Res Bull* **55**, 175-185

179. Copper-dependent interaction of glutaredoxin with the N termini of the copper-ATPases (ATP7A and ATP7B) defective in Menkes and Wilson diseases Lim, C. M., Cater, M. A., Mercer, J. F. and La Fontaine, S. (2006) *Biochem Biophys Res Commun* **348**, 428-436

180. Mitochondrial copper(I) transfer from Cox17 to Sco1 is coupled to electron transfer. Banci, L., Bertini, I., Ciofi-Baffoni, S., Hadjiloi, T., Martinelli, M. and Palumaa, P. (2008) *Proc Natl Acad Sci U S A* **105**, 6803-6808

181. The distinct functional properties of the nucleotide-binding domain of ATP7B, the human copper-transporting ATPase: analysis of the Wilson disease mutations E1064A, H1069Q, R1151H, and C1104F. Morgan, C. T., Tsivkovskii, R., Kosinsky, Y. A., Efremov, R. G. and Lutsenko, S. (2004) *J Biol Chem* **279**, 36363-36371

182. Interdomain Interactions Modulate Collective Dynamics of the Metal-Binding Domains in the Wilson Disease Protein. Rodriguez-Granillo, A., Crespo, A. and Wittung-Stafshede, P. (2010) *J Phys Chem B*

183. Therapeutic Targeting of ATP7B in Ovarian Carcinoma. Mangala, L. S., Zuzel, V., Schmandt, R., Leshane, E. S., Halder, J. B., Armaiz-Pena, G. N., Spannuth, W. A., Tanaka, T., Shahzad, M. M., Lin, Y. G., Nick, A. M., Danes, C. G., Lee, J. W., Jennings, N. B., Vivas-Mejia, P. E., Wolf, J. K., Coleman, R. L., Siddik, Z. H., Lopez-Berestein, G., Lutsenko, S. and Sood, A. K. (2009) *Clin Cancer Res* **15**, 3770-3780

184. The soluble metal-binding domain of the copper transporter ATP7B binds and detoxifies cisplatin. Dolgova, N. V., Olson, D., Lutsenko, S. and Dmitriev, O. Y. (2009) *Biochem J* **419**, 51-6, 3 p following 56

185. Increase in expression of the copper transporter ATP7A during platinum drug-based treatment is associated with poor survival in ovarian cancer patients. Samimi, G., Varki, N. M., Wilczynski, S., Safaei, R., Alberts, D. S. and Howell, S. B. (2003) *Clin Cancer Res* **9**, 5853-5859

186. Copper efflux transporter (ATP7B) contributes to the acquisition of cisplatin-resistance in human oral squamous cell lines. Yoshizawa, K., Nozaki, S., Kitahara, H., Ohara, T., Kato, K., Kawashiri, S. and Yamamoto, E. (2007) *Oncol Rep* **18**, 987-991

187. Expression of copper-transporting P-type adenosine triphosphatase in human esophageal carcinoma. Higashimoto, M., Kanzaki, A., Shimakawa, T., Konno, S., Naritaka, Y., Nitta, Y., Mori, S., Shirata, S., Yoshida, A., Terada, K., Sugiyama, T., Ogawa, K. and Takebayashi, Y. (2003) *Int J Mol Med* **11**, 337-341

188. Mechanisms of resistance to cisplatin and carboplatin. Stewart, D. J. (2007) *Crit Rev Oncol Hematol* **63**, 12-31

189. Contribution of the major copper influx transporter CTR1 to the cellular accumulation of cisplatin, carboplatin, and oxaliplatin. Holzer, A. K., Manorek, G. H. and Howell, S. B. (2006) *Mol Pharmacol* **70**, 1390-1394

190. Copper transporter 2 regulates the cellular accumulation and cytotoxicity of Cisplatin and Carboplatin. Blair, B. G., Larson, C. A., Safaei, R. and Howell, S. B. (2009) *Clin Cancer Res* **15**, 4312-4321

191. Role of human copper transporter Ctr1 in the transport of platinum-based antitumor agents in cisplatin-sensitive and cisplatin-resistant cells. Song, I. S., Savaraj, N., Siddik, Z. H., Liu, P., Wei, Y., Wu, C. J. and Kuo, M. T. (2004) *Mol Cancer Ther* **3**, 1543-1549

192. The role of the mammalian copper transporter 1 in the cellular accumulation of platinum-based drugs. Larson, C. A., Blair, B. G., Safaei, R. and Howell, S. B. (2009) *Mol Pharmacol* **75**, 324-330

193. The copper transporter Ctr1 contributes to cisplatin uptake by renal tubular cells during cisplatin nephrotoxicity. Pabla, N., Murphy, R. F., Liu, K. and Dong, Z. (2009) *Am J Physiol Renal Physiol* **296**, F505-11

194. Altered localisation of the copper efflux transporters ATP7A and ATP7B associated with cisplatin resistance in human ovarian carcinoma cells. Kalayda, G. V., Wagner, C. H., Buss, I., Reedijk, J. and Jaehde, U. (2008) *BMC Cancer* **8**, 175

195. Increased expression of the copper efflux transporter ATP7A mediates resistance to cisplatin, carboplatin, and oxaliplatin in ovarian cancer cells. Samimi, G., Safaei, R., Katano, K., Holzer, A. K., Rochdi, M., Tomioka, M., Goodman, M. and Howell, S. B. (2004) *Clin Cancer Res* **10**, 4661-4669

196. Intracellular localization and trafficking of fluorescein-labeled cisplatin in human ovarian carcinoma cells. Safaei, R., Katano, K., Larson, B. J., Samimi, G., Holzer, A. K., Naerdemann, W., Tomioka, M., Goodman, M. and Howell, S. B. (2005) *Clin Cancer Res* **11**, 756-767

197. Confocal microscopic analysis of the interaction between cisplatin and the copper transporter ATP7B in human ovarian carcinoma cells. Katano, K., Safaei, R., Samimi, G., Holzer, A., Tomioka, M., Goodman, M. and Howell, S. B. (2004) *Clin Cancer Res* **10**, 4578-4588

198. Transport of cisplatin by the copper efflux transporter ATP7B. Safaei, R., Otani, S., Larson, B. J., Rasmussen, M. L. and Howell, S. B. (2008) *Mol Pharmacol* **73**, 461-468

199. Functional interactions of Cu-ATPase ATP7B with cisplatin and the role of ATP7B in the resistance of cells to the drug. Leonhardt, K., Gebhardt, R., Mossner, J., Lutsenko, S. and Huster, D. (2009) *J Biol Chem* **284**, 7793-7802

200. Distinct mechanisms for Ctr1-mediated copper and cisplatin transport. Sinani, D., Adle, D. J., Kim, H. and Lee, J. (2007) *J Biol Chem* **282**, 26775-26785

201. Interaction of cisplatin and analogues with a Met-rich protein site. Sze, C. M., Khairallah, G. N., Xiao, Z., Donnelly, P. S., O'Hair, R. A. and Wedd, A. G. (2009) *J Biol Inorg Chem* **14**, 163-165

202. Metallothioneins and platinum(II) anti-tumor compounds. Knipp, M. (2009) *Curr Med Chem* **16**, 522-537

203. Effects of the loss of Atox1 on the cellular pharmacology of cisplatin. Safaei, R., Maktabi, M. H., Blair, B. G., Larson, C. A. and Howell, S. B. (2009) *J Inorg Biochem* **103**, 333-341

204. Crystal structures of cisplatin bound to a human copper chaperone. Boal, A. K. and Rosenzweig, A. C. (2009) *J Am Chem Soc* **131**, 14196-14197

205. An improved empirical potential energy function for molecular simulations of phospholipids Feller, S. E. and MacKerell, A. D. (2000) *JOURNAL OF PHYSICAL CHEMISTRY A* **104**, 7510-7515

206. ANOLEA: a www server to assess protein structures Melo, F., Devos, D., Depiereux, E. and Feytmans, E. (1997) *Proc. Int. Conf. Intell. Syst. Mol. Biol* **5**, 187-190

207. Comparison of simple potential functions for simulating liquid water Jorgensen, W. L., Chandrasekhar, J., Madura, J. D., Impey, R. W. and Klein, M. L. (1983) *The Journal of Chemical Physics* **79**, 926

208. All-atom empirical potential for molecular modeling and dynamics studies of proteins MacKerell Jr, A. D., Bashford, D., Bellott, M., Dunbrack Jr, R. L., Evanseck, J. D., Field, M. J., Fischer, S., Gao, J., Guo, H. and Ha, S. (1998) *Journal of Physical Chemistry B-Condensed Phase* **102**, 3586-3616

209. Molecular dynamics with coupling to an external bath Berendsen, H. J. C., Postma, J. P. M., Van Gunsteren, W. F., DiNola, A. and Haak, J. R. (1984) *The Journal of Chemical Physics* **81**, 3684

210. Schlick, T. (2002) *Molecular modeling and simulation*, Springer New York,

211. PatchDock and SymmDock: servers for rigid and symmetric docking. Schneidman-Duhovny, D., Inbar, Y., Nussinov, R. and Wolfson, H. J. (2005) *Nucleic Acids Res* **33**, W363-7

212. FireDock: fast interaction refinement in molecular docking. Andrusier, N., Nussinov, R. and Wolfson, H. J. (2007) *Proteins* **69**, 139-159